UNIVERSITE DE YAHIA FARES DE MEDEA

Faculté de la Technologie

Département de Génie Electrique

THESE DE DOCTORAT

en Génie Electrique

Option:

Automatique des Systèmes

CONTRIBUTION TO THE DEVELOPMENT OF A ROBUST CHARGE CONTROLLER OF A STATIONARY BATTERY FOR PHOTOVOLTAIC APPLICATIONS

Par :

BLAIFI SID-ALI

Devant le jury composé de :

O. Bouchhida	**Professeur, Université de Médéa**	**Président**
D. Boudana	**MCA, Université de Médéa**	**Examinateur**
H. Bentarzi	**Professeur, Université de Boumerdès**	**Examinateur**
L. Hadjout	**Professeur, USTHB, Alger**	**Examinateur**
R. Mellah	**Professeur, Université de Tizi Ouzou**	**Examinateur**
S. Moulahoum	**Professeur, Université de Médéa**	**Directeur de thèse**

ACKNOWLEDGMENT

Je remercie Dieu le compassion et le miséricordieux de m'avoir aidé et donné patience et courage pour accomplir ce modeste travail. Je tiens à exprimer ma reconnaissance à mon directeur de thèse, le professeur Samir Moulahoum, qui m'a donné courage et motivation à aller jusqu'au bout du chemin et je suis reconnaissant pour sa présence à mes côtés aux moments de doutes, pour ses précieux conseils, aide et soutient.

Mes appréciations sont également étendues au professeur Ilhami Çolak de l'université de Nişantaşı à Istanbul pour ses précieuses observations, suggestions et toutes les corrections qu'il a apportées à mes articles.

Je remercie également Monsieur Walid Merrouche du centre de recherche CDER pour toutes ses observations et ses suggestions durant la préparation de cette thèse.

Je remercie vivement aussi les docteurs Houssine Hamza et Nadir Kabache pour tout l'aide qui m'ont donné durant tout le cycle doctorat

Je tiens aussi a remercié mes collègues et mes amis Aissa Oualid, Benkercha Rabah, Benyamina Abderrahmen, Mouhamedi Amine, Saim Abdelhakim, Garrodja Elyes, Islem Belarbi, Boukenoui Rachid et Derbal Abdeladhim pour leurs aides et pour l'atmosphère de fraternité et le confort que j'ai senti durant mes travaux.

Je remercie tout le staff et toute l'équipe du laboratoire de recherche en électrotechnique et en Automatique LREA.

A la fin, je remercie mes parents, ainsi que toute ma famille, pour leur amour, soutient et encouragement. Ils m'ont toujours donné confiance en soi et m'ont motivé pour toujours marcher en avant.

ABSTRACT

Due to the large demand of the electrical energy in the world, the photovoltaic systems take increasingly an important aspect as a new energy source. From this context, it has been interested recently by several scientific researches in the purpose to improve its efficiency, decrease its cost and extend its lifetime. Particularly, our interest is on the stand-alone photovoltaic systems where the aim of this thesis is to give an optimal management to these systems. The optimization of these systems can be divided into two main ways: the first way is the optimization in the solar panel level that can be done through the maximum power point tracker (MPPT). The second way is passes by management of the energy storage systems, especially the battery. The good prediction and the modelling can play an important role in our purpose. Hence, we have proposed an enhancement of the CIEMAT battery model by the automatic extraction parameters using both Levenberg-Marquardt and genetic algorithm. The improvement presents good results compared to the real measurements. Moreover, a monitoring interface of the battery using LabVIEW has been proposed that can be used for many applications such as the monitoring and the fault detection. A new fast MPPT algorithm has been proposed also in this thesis. A new modelling of the fuzzy logic algorithm by using the M5P model tree is proposed. This new algorithm presents a good agreement with the former fuzzy algorithm with providing of a simple if/else code which will be easy to be implemented. Furthermore, we have proposed a new robust battery charge regulator that is based on the estimation of the battery stat of charge (SOC) mathematically. The new MPPT algorithm is also integrated in this regulator.

RESUME

En raison de l'évolution exponentielle des besoins énergétiques mondiaux, les sources d'énergies renouvelables (notamment l'énergie solaire photovoltaïque) commencent à devenir de plus en plus un acteur incontournable pour répondre à ces besoins en énergie. Dans ce sens, la communauté scientifique de par le monde affiche un intérêt particulier pour le suivi de cette évolution en proposant un ensemble de mesures visant à améliorer l'efficacité de ces structures. Notre projet de thèse s'inscrit dans cette démarche et concerne essentiellement les systèmes photovoltaïques (PV) autonomes avec comme objectif, la gestion optimale de ces installations. Cet objectif est atteint de deux façons: la première concerne l'optimisation du fonctionnement du générateur photovoltaïque par le développement d'une stratégie de suivi du point maximale de puissance (MPPT : Maximum Power Point Tracker). Le deuxième point est consacré à la gestion optimale du système de stockage d'énergie (Batterie). Toutefois, pour atteindre ces objectifs, il est primordial de passer par une modélisation précise des phénomènes, fortement non linéaires, qui régissent le fonctionnement de ces applications. A partir de cela, nous avons proposé d'améliorer le model de la batterie CIEMAT en passant par l'identification des paramètres liés à son fonctionnement en utilisant deux algorithmes : Levenberg-Marquardt et l'algorithme Génétique. Les résultats obtenus de la comparaison avec des mesures réelles confortent l'efficacité des algorithmes proposés. De plus, une interface LABVIEW dédiée à la surveillance et au diagnostic des défauts de l'installation (en particulier la batterie) a été proposée. Une nouvelle stratégie de suivi du point maximale de puissance est aussi proposée. Celle-ci consiste en la modélisation de l'algorithme réalisé en logique floue en utilisant un modèle d'arbre de décisions M5P. Ce nouvel algorithme nécessite une charge de calcul insignifiante et corrobore parfaitement avec l'algorithme réalisé en logique floue. Au final, un régulateur de charge de la batterie est construit sur la base de l'estimation de l'état de charge (SOC : State Of Charge) de cette dernière.

ملخص

في ظل الطلب المتزايد على الطاقة الكهربائية في العالم, بدأت النظم الكهروضوئية تأخذ حيزا هاما كمصدر جديد للطاقة. من هذا السياق لطالما كانت موضوع إهتمام من طرف العديد من الباحثين لهدف تطوير مردودها, التقليل من كلفتها و كذلك تمديد عمرها لأطول مدة ممكنة. بصفة خاصة مجال اهتمامنا يكمن في تطوير النظم الكهروضوئية القائمة بذاتها إذ أن المبتغى من هذا العمل هو توفير تسيير مثالى لهذه النظم. الإستفادة المثلى لهذه النظم تمر عبر طريقين: الأول على مستوى اللوح الشمسي و الذي يتم عبر تطوير خوارزمية تتبع نقطة الطاقة القصوى (MPPT). أما الطريق الثاني فيتم عبر الإدارة الجيدة لنظام تخزين الطاقة بصفة خاصة البطارية. إضافة إلى هذا, توفير نموذج تنبأ جيد لهذه النظم من شأنه أن يلعب دور هام في هذا الهدف. من هذا المنطلق, إقترحنا في هذا العمل تطوير جديد لنموذج تنبأ البطارية CIEMAT عبراستخراج المعلمات بطريقة آلية باستعمال الخوارزميتين Levenberg-Marquardt و Genetic algorithm. هذا التطوير أعطى نتائج جيدة من حيث التناسب مع القياسات الحقيقية. علاوة على هذا, واجهة مراقبة للبطارية قد طورت باستعمال LabVIEW التي يمكن أن تستعمل في عدة تطبيقات المراقبة و الكشف عن الأعطال في البطارية. بالإضافة إلى هذا, خوارزمية جديدة و سريعة من أجل تتبع نقطة الطاقة القصوى (MPPT) قد طورت في هذا العمل نمذجة جديدة للخوارزمية المبنية على Fuzzy logic باستعمال نموذج الشجرة M5P. هذه الخوارزمية أعطت نتائج جيدة من حيث التطابق مع خوارزمية Fuzzy logic و من حيث سرعة استجابتها تحت التغير السريع للأشعة الشمسية مع أنها تعطي برنامج جد بسيط و سهل للتطبيق مبني على <if/else>. و في النهاية نقترح مراقب جديد لشحن البطارية مبني على التنبأ بحالة شحن الطاقة (SOC) و الذي يحتوي أيضا على خوارزمية تتبع نقطة الطاقة القصوى المطورة مسبقا.

CONTENTS

ACKNOWLEDGMENT……...1

ABSTRACT……... 2

CONTENTS……... 5

LIST OF FIGURES……...9

LIST OF TABLES……12

LIST OF SYMBOLS…… 13

INTRODUCTION…….115

CHAPTER I
BACKGROUND IN THE STORAGE SYSTEMES AND THE STORAGE IN PHOTOVOLTAIC ENERGY

1. 1 Introduction…… 21

1. 2 Overview in the storage devices……..... 21

1.2.1 Pumped hydro storage (PHS)……..… 21

1.2.2 Compressed air……..…… 22

1.2.3 Flywheels……. 23

1.2.4 Capacitor and Supercapacitors……..……..……23

1.2.5 Superconducting Magnetic Energy Storage (SMES)…..…….…….... 24

1.2.6 Hydrogen storage and fuel cell……..…….. 25

1.2.7 Electrochemical storage…….…….... 25

1. 3 Lead-acid Batteries……...28

1.3.1 Lead-acid cell design……...…… 28

1.3.2 Lead-acid batteries construction types and technology…..…… 30

1.3.2.1 Modification in the electrodes……..…..……. 30

1.3.2.2 Modification in the internal design…….…….. **31**

1.3.2.3 Modification in the external design……..**32**

1.3.3 The temperature effect……..…….……... **33**

1. 4 The photovoltaic systems and storage……...…… **34**

1.4.1 Modeling and characterization of the PV array……..**34**

1.4.2 The photovoltaic systems type……...……**36**

1.4.3 The storage in photovoltaic systems……...…….. **37**

1. 5 Battery charging modes and charge controller types……**38**

1.5.1 Battery charging modes……...…….. **38**

1.5.1.1 On-of charging mode……...…….... **39**

1.5.1.2 Constant current charging……...……... **39**

1.5.1.3 Constant voltage charging…….……..……..... **40**

1.5.2 Battery charge regulators and their technology…….. **41**

1.5.2.1 Series type regulators……... **42**

1.5.2.2 Shunt type regulators……... **42**

1.5.2.3 PWM regulators……...……..... **43**

1.6 Conclusion……. **44**

CHAPTER II

LEAD ACID BATTERY MODELING AND EXTRACTION PARAMETERS

2. 1 Introduction…….……..... **46**

2. 2 Lead-acid battery modeling……..... **46**

2.2.1 Battery internal resistance……..……..…….... **47**

2.2.2 Battery state of charge and level of energy…….…..…….. **47**

2.2.3 Terminal voltage and working zones variation……..…… **48**

2.2.3.1 Charge, Overcharge and Saturation zone……..……... **49**

2.2.3.2 Discharge zone, Overdischarge zone and Exhaustion zone…...……... **50**

2.2.3.3 Transition voltage…….……..…….…… **51**

2.2.4 Static simulation…… **52**
2.3 Parameters extraction ……..……...…….. **52**
2.3.1 Model parameters extraction by Levenberg-Marquardt algorithm ……. **53**
2.3.1.1 Algorithm process……..……..……...……. **54**
2.3.1.2 Results……...……. **54**
2.3.2 Extraction of battery's parameters using the Genetic algorithm…….…… **55**
2.3.2.1 Generation of initial population……...….....……... **58**
2.3.2.2 Fitness…….……...…… **58**
2.3.2.3 Selection……...……...…… **58**
2.3.2.4 Crossover……...……... **59**
2.3.2.5 Mutation…….…...……..... **59**
2.3.2.6 Simulation results ……...…… **62**
2.4 Extraction of gassing and saturation voltage parameters…… **67**
2.5 Conclusion…….…….. **68**

CHAPITRE III
BATTERY MONITORING, MANAGEMENT AND REAL TIME ACQUISITION

3.1 Introduction…….…... **70**
3.2 System description and test bench…….……...……. **70**
3.2.1 Measurement and acquisition……...…...…….……... **70**
3.2.2 The sensors……...……...…… **72**
3.2.2.1. Current measuring…….. **72**
3.2.2.2. Voltage measuring……... **73**
3.2.2.3 Temperature measuring..... **74**
3.2.3 Supply circuit……...……..……. **75**
3.2.3 Acquisition…… **76**

3.2.3.1 Acquisition and calibration in LabVIEW language…..……..…….. **77**

3.2.3.2 Model implementation in LabVIEW……...…….…….. **77**

3.3 Model validation…….……..... **77**

3.4 Monitoring and Simulation LabVIEW interface…….……..…… **80**

3.5Conclusion…….……... **81**

CHAPTER IV

DEVELOPMENT OF NOVEL MPPT AND BATTERY CHARGE CONTROLLER

4.1 Introduction……...…….……..….. **84**

4.2 The proposed algorithm for the MPPT……..…….…… **84**

4.2.1 Fuzzy MPPT algorithm…… **86**

4.2.2 M5P model tree……..…..…….. **88**

4.2.2.1 Decision tree……...…….. **88**

4.2.2.2 Multi-linear regression model (MLR)……...…… **92**

4.3 Training model results…….…….…… **94**

4.3.1 Modeling results……...…… **94**

4.3.2 Modeling robustness results……...…….. **96**

4.4 Simulation results and discussion……...…….. **97**

4.5 The battery charge controller…….……...……... **106**

4.6 Conclusion…….……...…… **110**

GENERALE CONLUSION ………...…… **112**

REFERENCES…….…… **115**

PUBLICATIONS AND CONFERENCES…… **122**

LIST OF FIGURES

Figure 1.1: pumped hydro Layout…….……..…….... **22**
Figure 1.2: Compressed air system schematic diagram……..…….…… **22**
Figure 1.3: Flywheel energy storage system…….…….…….…….... **23**
Figure 1.4: Super capacitors schematic diagram……..…..…….……..… **24**
Figure 1.5: The diagram of the SMES system……...…..…….……..…… **24**
Figure 1.6: The diagram of hydrogen storage and fuel cell……..…...…….……..…… **25**
Figure 1.7: lead-acid battery design ……..……...…..…… **28**
Figure 1.8: the conduction in the negative electrode.…….……..…….. **29**
Figure 1.9: the conduction in the positive electrode……..……....…… **30**
Figure 1.10: Manchex lead-acid batteries type design……..…….……..…… **31**
Figure 1.11: Tubular lead-acid batteries type design……..……..…….. **32**
Figure 1.12: Pasted Plate lead-acid design……...……...…… **32**
Figure 1.13: The opened lead-acid batteries design……..…….. **33**
Figure 1.14: VRLA lead-acid batteries design…….……..…….…… **33**
Figure 1.15: One diode equivalent circuit……..……..…… **34**
Figures 1.16: PV panel characteristic for different irradiation and temperature…….…… **36**
Figure 1.17: Grid-connected system design…….……..…….. **37**
Figure 1.18: Stand-alone system design……..……..…….. **37**
Figure 1.19: Battery position in the PV system……..……..…….. **38**
Figure 1.20: On-off charging……..……..…….. **40**
Figure 1.21: Constant current charging…….……....…… **41**
Figure 1.22: Modified constant voltage charging……..……..…..…… **41**
Figure 1.23: Series type regulator……...……....…… **42**
Figure 1.24: Shunt type regulator…….…….…….. **43**
Figure 1.25: PWM regulator……..……....…… **43**

Figure 2.1: Equivalent circuit for the battery……..……..…..……. **46**
Figure 2.2: Voltage areas variation……..……..…….…… **48**
Figures 2.3: (a) the battery' current for charge and discharge. (b) Variation of voltage as

functions temperature. (c) Variation of SOC as functions temperature. (d) Variation of LOE as functions temperature……..……..……...… **53**
Figure 2.4: Control and estimation tools manager…….……...…….……. **56**
Figures 2.5: Battery input measurements. (a) The battery current. (b) The ambient temperature……...…….…….…… **56**
Figures 2.6: Battery output: (a) battery voltage. (b) Battery state of charge…….……. **57**
Figure 2.7: Genetic algorithm steps……...……..... **60**
Figure 2.8: Flowchart of GA applied for parameters extraction process…..…..……..…….. **61**
Figure 2.9: Parameters extraction process by GA……..……...……..….. **63**
Figure 2.10: Simulation and experimental results…….……..… **64**
Figure 2.11: Battery current and ambient temperature measurements provided by PV modules……...…….... **65**
Figures 2.12: Battery voltage measurements of three experiments and simulation results obtained by genetic algorithm extracted parameters and by former parameters……..… **66**
Figures 2.13: battery gassing and saturation level……..… **67**

Figure 3.1: -a- System description. –b- The test bench……..... **71**
Figure 3.2: PV system and data acquisition……...……. **71**
Figures 3.3: ACS712 sensor: -a- the sensor design. -b- the sensor pinout……. **72**
Figure 3.4: Input output characteristic……...……..…...… **73**
Figures 3.5: LEM LV 25-P sensor. -a- the sensor design. -b- the sensor pinout..…..……. **73**
Figure 3.6: The differential amplifier……...……...…..... **74**
Figures 3.7: -a- the LM335 design. -b- the LM335 broaching used……..…. **75**
Figure 3.8: Supply circuit design……..……..…...…... **75**
Figure 3.9: Measurements and power supply boards……..……..……..…...…. **76**
Figure 3.10: NI-USB 6008 multiplexer data acquisition……..……..……..….. **76**
Figures 3.11: -a- DAQ assistant tool windows. -b- VI diagram for acquisition……....… **78**
Figures 3.12: -a- VI diagram for the model implementation. -b- Synoptic Diagram of Simulation process……..……..... **79**

Figures 3.13: -a- Measured vs Simulated voltage and representation of gassing voltage. -b- Absolute error of measured vs simulated voltage……..……. **80**
Figure 3.14: LabVIEW monitoring interface……...……...…… **81**
Figure 3.15: LabVIEW monitoring experimental curves……...……...……...…… **82**
Figure 4.1: The dataset stocked for modelling……..……..……...…. **85**
Figure 4.2: The diagram block of the system……..……..…….. **85**
Figure 4.3: Fuzzy logic algorithm steps…….....… **87**
Figures 4.4: (a) Error membership; (b) Variation of error membership; (c) Duty cycle membership……. **87**
Figure 4.5: decision tree…….....…… **91**
Figure 4.6: Example illustrates the linear regression……..…… **92**
Figures 4.7: Training model results: (a) Target as function the Error *E*, (b) Target as function the variation of Error *ΔE*…… **95**
Figure 4.8: The model tree for MPPT obtained by the M5P algorithm……..……...… **95**
Figures 4.9: Power obtained from fuzzy algorithm VS Power obtained the new model: (a) fuzzy algorithm VS new model. (b) The error between fuzzy algorithm and new model…….. **96**
Figures 4.10: Results obtained from fuzzy algorithm VS Power obtained the new model: ….. **97**
Figures 4.11: Results for irradiation 1000 W/m^2……..….. **98**
Figures 4.12: Results for irradiation 900 W/m^2……..… **99**
Figures 4.13: Results for irradiation 800 W/m^2……...……... **100**
Figures 4.14: Results for irradiation 700 W/m^2……...……... **101**
Figures 4.15: Results for irradiation 600 W/m^2…….……...……..… **102**
Figures 4.16: Results for irradiation 400 W/m^2……...…..…. **103**
Figures 4.17: Results for irradiation 300 W/m^2……..…… **104**
Figures 4.18: Results for irradiation variation from…….……..……... **105**
Figure 4.19 : The control system description…….. **106**
Figures 4.20: realized DC/DC buck converter……..... **107**
Figure 4.21: TLP 250 driver……... **108**
Figure 4.22: STM32F407 kit……..… **108**
Figure 4.23: The MPPT and the charge regulation control program in Matlab/Simulink……. **109**
Figure 4.24: Charging mode progress……. **109**

LIST OF TABLES

Table 1-1: Properties comparison between the batteries types…….…….…… **27**

Table 2.1: Battery working zone extremities…….…….…….…… **51**
Table 2.2: Values of the CIEMAT model parameters…….…….…….…… **51**
Table 2.3: PV module, battery and the load characteristics…….…….. **57**
Table 2.4: Extracted parameter values by Levenberg–Marquardt algorithm…….…….…… **57**
Table 2.5: The GA parameters taken in program…….…….. **61**
Table 2.6: Extracted Temperature Independent Parameters……..…….. **62**
Table 2.7: Extracted Temperature Dependent Parameters……..…….…… **62**
Table 2.8: Mean error simulated vs measured voltage……..…….. **63**
Table 2.9: Extracted parameters of overcharge area……..…….. **68**

Table 4.1: PV module characteristics……...…… **85**
Table 4.2: DC/DC boost converter parameters……...……. **86**
Table 4.3: Inference table……..…….. **88**
Table 4.4: example of the dataset ……..…….……..…..……... **90**
Table 4.5: Attribute 1 and Target……..…….. **90**
Table 4.6: Attribute 2 and Target……..…….. **96**
Table 4.7: Result of training and testing of the final model……..…….. **107**

LIST OF SYMBOLS AND ABBREVIATIONS

PVS	Photovoltaic systems
GA :	Genetic Algorithm
SOC :	State of charge
LOE :	Level of energy
V_{bat} **:**	Battery voltage
R_b **:**	Battery internal resistance
C :	Battery capacity
$C_{nominal}$ **:**	Nominal capacity
C_n **:**	Battery maximum capacity
V_c **:**	Charging voltage
V_{dc}**:**	Discharging voltage
V_g **:**	Gassing voltage
V_{ec} **:**	Saturation voltage
η ***c :***	Coulomb efficiency
V_{oc} **:**	Open circuit voltage
Isc :	Short-circuit current
MPPT :	Maximum power point tracking
P_{mpp} **:**	Power at maximum power point
V_{mpp} **:**	Voltage at maximum power point
I_{mpp} **:**	Current at maximum power point
MPP :	Maximum power point
ANN :	Artificial Neural Network
P&O :	Perturb and observe
FL :	Fuzzy logic
n :	Diode ideality factor
q :	Charge of electron
Rs :	Series resistance
Rsh :	Parallel resistance
T :	Temperature
T_{ref} **:**	Temperature of reference
K :	Boltzmann constant

INTRODUCTION

INTRODUCTION

In the last years, the needs of energy increase dramatically with the requirements of the biggest industries and other uses in the world. Consequently, large emissions caused by the several kinds of energy stations which cause environmental pollution. For this reason, it's necessary to thinking to find an environmentally friendly and clean energy source. The photovoltaic (PV) energy can be the alternative energy that responses to the new challenges and ensures the energy abundance in the word. The PV cell is composed of two semiconductors doped positively and negatively; if the two semiconductors receives a sufficient gape of light energy, the electrons are liberated from the valence band to the conduction band that creates a potential difference between the two semiconductors [1]. However, in addition to its low energy conversion efficiency, the PV module in any configuration presents a nonlinear power characteristic depending strongly to the continuous change of irradiation and temperature, where the load must be adapted in which the module working in the maximum power point (MPP) [2-4]. From there, many research works have been proposed in the literature based on the introduction of dynamic load by using DC/DC converter. Perturb and Observe (P&O) is the basic and the classical method used to track the MPP. It based on the introduction of a perturbation of specific step in some control variable as voltage, current and duty cycle, and observes the power obtained until fall in the MPP [5]. The Hill Climbing (HC) method used in the P&O by the perturbation in the duty cycle [6-7] when the P&O use typically the perturbation of the voltage [8]. The both algorithms are similar in which combine information in the direction of the power variation. They are the commonly used technical result to the facility of implementation, the simplicity and the low cost [9-11]. The disadvantage of these approaches is the slow convergence. In other hand, with the bad choice of the step size perturbation the algorithms present oscillation in the steady-state regime [7, 8, 10, 12]. The incremental conductance (IncCond) is another conventional technic based on the camper of the variation of the both voltage and the current by calculating of the derivation up to fall in the MPP. While the IncCond is principally share with P&O the operating bases, is considered as implementation of P&O by different way. By consequence, the IncCond presents the same disadvantages including speed and the oscillations in the steady-state [13]. The Artificial Neural Network (ANN) MPPT approach is an intelligence technique that provides a non-parametrical model. The training of this

model is based on the environmental condition data. More the experimental data are significant, more the model is robust. The Fuzzy logic technical is another intelligence MPPT technique that uses Fuzzy Logic approach [14-15]. Two inference models for the fuzzy logic are applied for the MPPT: Mamdani and Sakagi-Sugino. Sakagi Sugino inference model is the most popular because it minimizes rules and the ease of implementation in the real time systems 16]. The fuzzy logic technique can provide a high accuracy by the introduction of more number of membership functions; however, also the trade-off between the accuracy and the convergence speed appears. In this context, we propose a new fast MPPT algorithm by modeling of the fuzzy logic MPPT using machine learning technique namely M5P model tree. The M5P model tree is a reconstruction of Quinlan's M5 algorithm [17] that is based on the conventional decision tree with introducing of linear regression function at the leaves nodes. The decision tree is a representation of the algorithms by a tree form trained through a data to form nodes. The nodes constituting the decision tree are divided into three types: The root nodes, internal nodes and the leaves nodes. Each node is interconnected with each other by branches until reaches the leaves [18-19]. This simple, high speed and low cost algorithm gives good results in terms of accuracy, where the model algorithm was trained for an irradiation of 500 W/m^2 and tested with different other irradiations. Moreover, the algorithm is easy to be implemented for real time MPPT.

In the photovoltaic systems especially the stand-alone systems, the storage is still the major problem in order to store the electrical energy to be released in case of lack of the sun. A several storage devices systems have been used in the history such as pumped hydro [20], compressed air [21], flywheel [22], super capacitors [23] and also electrochemical storage [24]. However, the electrochemical storage namely storage using the battery is still the most used in the photovoltaic application. Because of its low cost, the lead-acid battery is the most used in the photovoltaic systems and it takes a largest part in the scientific research. In addition to its electrochemical complexity, the lead-acid battery in the photovoltaic applications is subject to a random working related to the continuous changes of the solar irradiation and the temperature besides to its limited cycle lifetime. Therefore, it still plays a critical role in different work in order to achieve a deep understanding of its behavior. Consequently, many approximates models of battery have been proposed in literature based on practical tests varying in the method that has been taken for obtaining the equations which expresses the battery' behavior. Several models were proposed to predict the batteries characteristics behavior from different bases such as electrochemical,

analytical and electrical. Based on electrochemical approach Ryan Ahmed et al. [25, 26] have given an improved model for battery by parameters identification of reduced-order electrochemical model. This proposed enhancement can to estimate the state of charge (SOC) and voltage for old and healthy batteries. Woosuk Sung et al [27] have proposed also an electrochemical model for the automotive battery management systems. This model is able to predict the battery voltage as function of the current density, solid-phase potential, electronic and ionic resistances. The validation of this model for constant current presents good results compared to the real measurements. From the analytical approach, Jingzhi Xun et al [28] introduced thermal behavior prediction for lithium ion battery. This model takes into consideration the heat and temperature variation according to battery volume. From the electric approach for which we are interested, Ziyad M. Salameh et al [29] have developed an electrical model through modification of Thevenin model by adding nonlinear components. After that, J.B Copetti et al [30-31] proposed an empirical electrical model for PVS application called CIEMAT model. This model presents good dynamic performances and takes into account Battery output variation as a function of current and temperature. Whereas, the disadvantage of this model is the large number of parameters that taken as constants; therefore, this model is not adaptable with any types of batteries. Another improvement is given by D. Guasch and S. Silvestre et al. [32] by the identification of 11 parameters of Copetti model using Levenberg–Marquardt algorithm and the addition of the State of health factor (SOH). For the stand-alone PVS system simulation, Rafael Illanes et al [33] have introduced a modification in CIEMAT model by adding linear components in the battery electrical circuit with keeping the former model parameters. Later on, Wladislaw Waag et al [34] have proposed an online estimation of battery state of charge (SOC) and capacity based on the open circuit voltage after stabilization time. Static validation has been given in this work. In other application of electric vehicle, Guangming Liu et al [35] have given a predictive-adaptive model from electrical equivalent circuit for the estimation of the energy stored in the battery. The validation of this model shows good matching with the real measurements. Robert L. Fares et al [36] have, proposed a dynamic model based on electrical circuit formed of open circuit battery voltage source varying as function state of charge and constant voltage drop due to the battery internal resistance. In another improvement of Thevenin model, Massimo et al. [37] have given electrical battery equivalent circuit by adding components of n order. This model presents good matching with the real measurement from the validation

given in [38]. Wenhua H et al. [39], have proposed a simpli ed equivalent circuit model that can predict both the voltage and the impedance of the Battery. In this context, we are interested in the CIEMAT model, where we propose in the first step, an enhancement of this model by the extraction of its parameters using Levenberg-Marquardt. After that, we propose an improvement of 21 parameters by using the genetic algorithm. Furthermore, we propose an improvement also of 4 parameters for the estimation approximately of the gassing and the saturation areas by new static method using genetic algorithm (GA). This was done relying on static measurements when the battery has been charged by different current.

The GA can be a suitable algorithm for the parameters extraction of this model in terms of its complexity and the large number of its parameters. This algorithm is a stochastic method that is used to solve mathematical optimization problems [40]. Basically, four principal steps constituting this algorithm, that start through the generation of initial population; in this step, the algorithm generates a population of chromosomes that represent the information holder namely the genes. By analogy, the genes are the parameters extracted of the cost function to be optimized [41]. In the second step, the algorithm selects the chromosomes that participate as parents in the next process (crossover and mutation) after the evaluation of the fitness for each one. The chromosomes that have a good fitness obtain a better chance to be selected [42-43]. After that, the selected chromosomes play a role of the parents by the crossover two by two for generation of children. Finally, in the Mutation process the children generated in the previous step are randomly subjected to a change of some characters [44-45].

Moreover, a real time validation of the improved model has been carried out by the acquisition of real battery measurements (Current, temperature and voltage) taken as input and output of the model for a real time validation using LABVIEW Language. Also, we propose battery monitoring and simulation using the improved model with the parameters extracted on off-line.

The management of the lead-acid battery is very important in terms of extending its lifetime and the maximum benefit to its capacity. Therefore, the name of the battery in the photovoltaic systems is usually related with the charge regulator. Several method of charge existing varying according to the application such as: off-on, constant current and constant voltage method. From this context, we propose a new and robust charge regulator based on the estimation of the battery

state of charge (SOC) with the application of a constant voltage when the battery achieves the full charge. Moreover, a new developed MPPT is integrated in this regulator based on the modeling using M5P model tree.

The content of the thesis is organized as follows:

As a first chapter, we provide briefly a background and history about the storage systems with more details about the storage in photovoltaic systems specially the stand-alone systems. While the battery is widely used in these systems, this chapter highlights the batteries types especially the lead-acid type. The management and the charging modes of the lead-acid battery are also highlighted. Furthermore, the technology and the types of the battery charge regulator are discussed in this chapter. In the second chapter, the lead-acid battery modeling is given with an enhancement by the parameters extraction using Levenberg-Marquardt and genetic algorithm. In the third chapter we give more details about the battery monitoring systems and the realization of the real time acquisition. Finely, the new proposed MPPT algorithm and the charge regulator are highlighted in the fourth chapter.

CHAPTER I

BACKGROUND IN THE STORAGE SYSTEMES AND STORAGE IN PHOTOVOLTAIC ENERGY

CHAPTER I

BACKGROUND IN THE STORAGE SYSTEMES AND STORAGE IN PHOTOVOLTAIC ENERGY

1. 1 Introduction

The generation of the electrical energy increases around the world to meet the large demand due to the expansion of industry and the public requirements. In the case of lack in electrical energy supply, the storage systems play the role to ensure certain autonomy by saving the extras electricity for using when it is needed. According to the suitability with different applications, various storage system technologies have been developed such as pumped hydro, compressed air, flywheel, Supercapacitors and electrochemical storage. Where, almost all of them pass by the conversion to another form of energy. This chapter provides a brief overview on the stationary storage with more details for battery technology and its application in stand-alone photovoltaic systems. Furthermore, the battery charging modes and charge regulator types are highlighted in this chapter.

1.2 Overview in the storage devices

1.2.1 Pumped hydro storage (PHS)

Pumped hydro storage is the most common storage method used in large scale electrical stations. These systems represent more than 99% of worldwide bulk storage capacity and have been used since 1929 [20, 46]. As the Figure (1.1) shows, this technique is based on the movement of water from the higher to the lower basin through hydraulic turbine that turns the electrical generator during the peak periods.

The pumped hydro can be coupled with renewable energy source such as wind or solar for grid connected or micro-grid applications in order to adopt the renewable energy source in the networks [47].

1.2.2 Compressed air

Compressed air is a pneumatic energy storage technique based on the keep of compressed air under certain pressure that can be released to a generator during the peak demand [21]. In

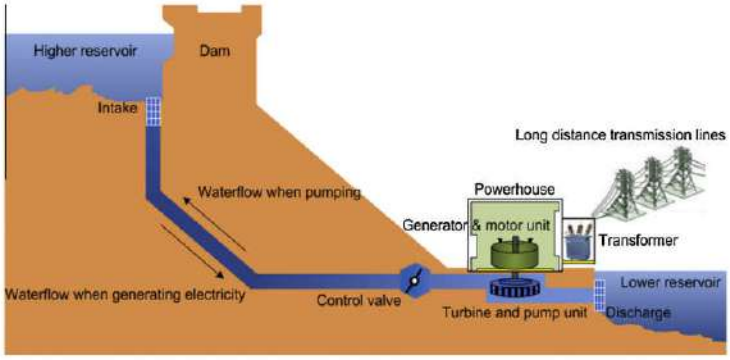


Figure 1.1 pumped hydro Layout

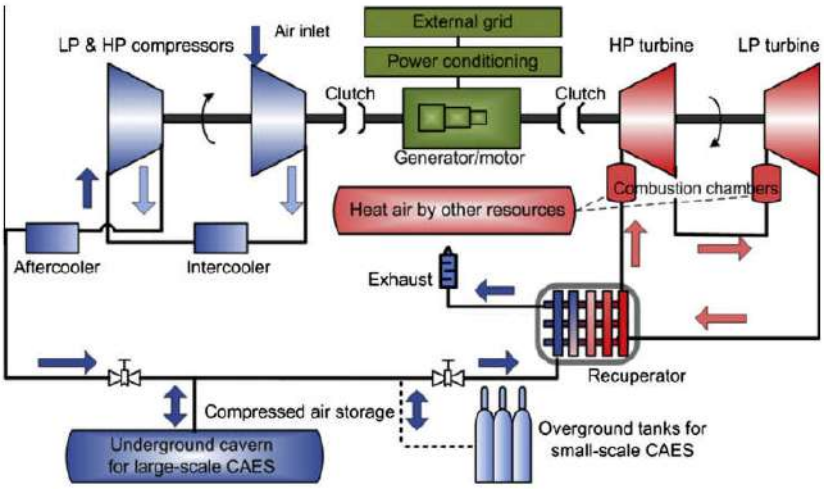


Figure 1.2 Compressed air system schematic diagram

the case when the network have a low load power demand, the surplus electricity drives a reversible motor/generator unit in turn to run the chain of compressors for injecting air into a storage vessel. The figure (1.2) shows the process of this technique.

The first compressed air energy storage facility was used the E.ON-Kraftwerk's 290MW plant built in Huntorf, Germany in 1978 [48]. Compressed air system can be built to have small or large scale of capacities. The most common practical use are the compressed air systems involve grid applications for load shifting, peak demand, frequency and voltage control [49].

Also, the Liquid air energy storage is another technical developed principally similar to the compressed air [50].

1.2.3 Flywheels

Flywheels are a mechanical storage device that can store the kinetic energy of a rotation movement from inertia. This technique can be very effective storage method for the short duration cycle [22]. This energy stored can be used for the rotation of turbines to produce electrical energy. The Figure (1.3) shows the simplified structure of flywheels energy storage system.

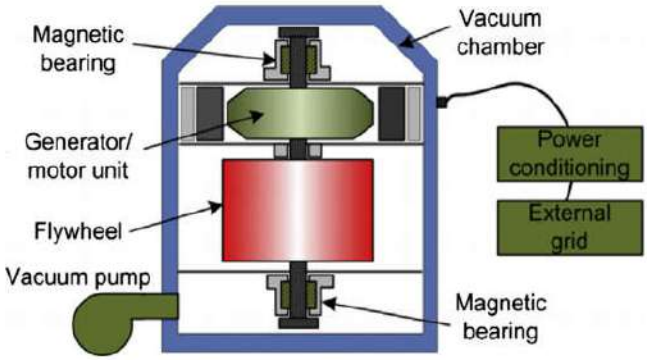


Figure 1.3 Flywheel energy storage system

In order to increase the rotation speed that improves the efficiency of the system, new developed researches include the use of new materials in the flywheel to reduce energy loss caused by air resistance and the friction [51].

1.2.4 Capacitor and Supercapacitors

The capacitor is a component that contains two electrical positive and negative conductors separated by a dielectric. The capacitor saves electrical energy in the dielectric on an electrostatic field form. When it is charged, a positive charge is gathered in one conductor and a negative charge is gathered in the other [23].

Supercapacitor is a storage device with high electrical capacity that contains double-layer capacitors. As shown in Figure (1.4), the supecapacitor is composed to electrodes, an electrolyte and a porous membrane separator [52]. This device can provide a high flow of energy whereas it is not a stationary device. In another meaning it cannot provide energy for a long duration comparing with the conventional batteries. This device is commonly used in motors start-up for electrical cars application, where the motor needs a high energy for starting [53].

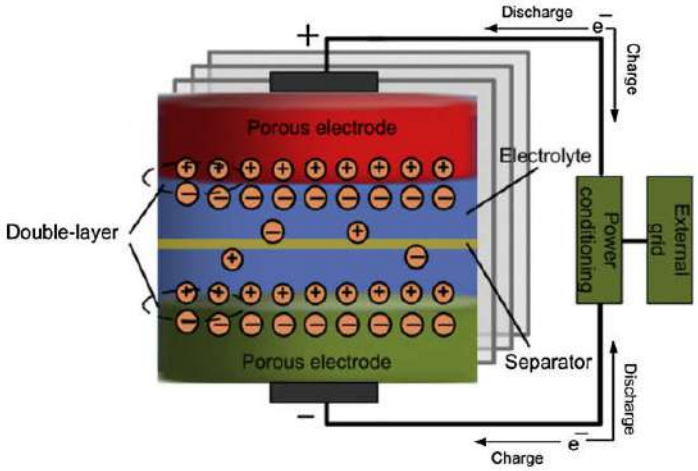


Figure 1.4 Supercapacitors schematic diagram

1.2.5 Superconducting Magnetic Energy Storage (SMES)

The superconducting magnetic energy storage is a technical based on the superconductors properties. The SMES system saves electrical energy in the magnetic field created by Direct Current (DC) in the superconducting coil which has been cooled to temperature below its superconducting critical temperature. [54]. Basically, the SMES systems is composed to a vessel that include superconducting coil and cooling material such as helium or nitrogen. The passage of the cooling material through the superconducting coil creates an electrical energy in the magnetic field. The figure (1.5) describes briefly the SMES system.

Superconducting coil can be classified into two principal categories: the first is the coil of low critical temperature which works near to 5 K; the second is of high critical temperature which works at temperature nearly to 70 K. This technique is used for relatively high scale energy storage and increasingly it becomes more mature [55].

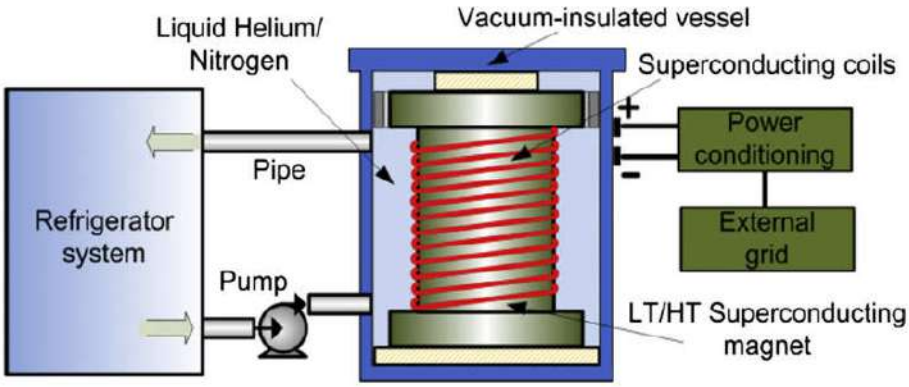


Figure 1.5 The diagram of the SMES system.

1.2.6 Hydrogen storage and fuel cell

This technique is composed of two main processes; the first is the produce of hydrogen which is done by water electrolysis unit. This unit produces the hydrogen from water by receiving electricity. Hence, the obtained hydrogen will be stored in containers with high pressure for use when needed. In the second process, the hydrogen saved is transmitted to the fuel cell by a pipeline which will be converted from chemical to electrical energy. With the same principle of conventional batteries, the fuel cells have positive cathode and negative anode that contain oxygen and generated hydrogen respectively. The both are separated by an electrolyte [56]. According to the nature of the electrolyte, it exists various types of fuel cells. The figure (1.6) describes briefly the process of this technique.

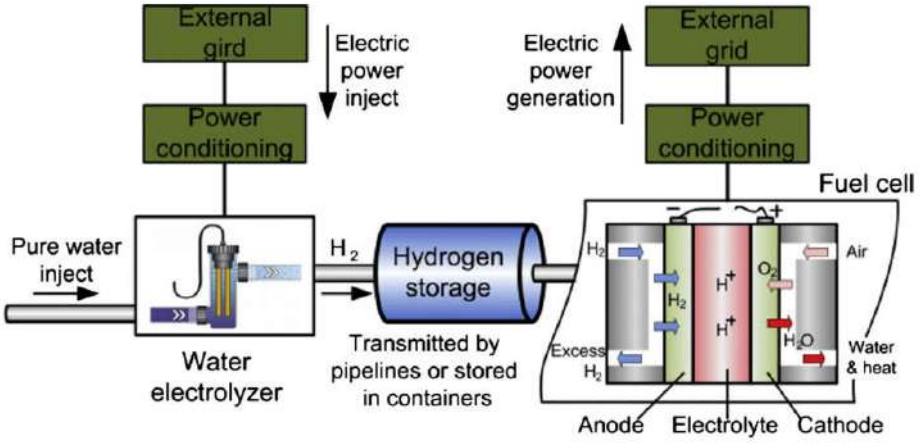


Figure 1.6 The diagram of hydrogen storage and fuel cell.

This technique presents many advantages in terms of the efficiency, less pollution and quieter [57]. Moreover, the fuel cell combined with hydrogen production can provide high capacity for stationary power distribution. The hydrogen storage and fuel cell technique is used also for renewable energy storage such as solar and wind energy.

1.2.7 Electrochemical storage

The electrochemical storage, that we are interested in, is based on the keep of electrical energy on electrochemical form and providing it when it is needed. Basically, these storage systems are composed of positive and negative cathode and anode respectively separated by an electrolyte [24]. The rechargeable batteries are the most common electrochemical storage systems used for the storage of electricity. The battery is composed of one or more

electrochemical cells; each cell contains two electrodes (anode and cathode) with the electrolyte that can be liquid, solid or other states. The battery cell is a reversible system that can be charged or discharged. It converts the electrochemical to electrical energy in the discharge process. In this process, the electrons are provided from the anode and collected at the cathode through the external load. In the charge process, the electrochemical cell can convert the electrical energy to electrochemical energy when it is supplied by an external source. In this process, the inverse reaction is happen. According to the desired voltage and current, the cells are collected in series and parallel. However, the battery devise presents two main drawbacks that somewhat obstructed its progress, the first is its complex electrical behavior due to its electrochemical interaction that makes the battery difficult to be modeled. Thus, the batteries are still a major problem for the stand-alone systems. Due to electrochemical effects and its internal variation, the second drawback of the battery is the capacity degradation, in which the battery can be unqualified after its lifetime finished. The recent researches are devoted to cope with the aforementioned problems in order to extend, predict and optimize the batteries lifetime. Based on the material included in electrodes and the electrolyte, many types of batteries have been designed such as Sodium–sulfur, Nickel–cadmium, nickel hydride, Lithium-ion and lead-acid battery [58].

Nickel–cadmium (NiCd): This rechargeable battery type contains electrodes of nickel hydroxide and metallic cadmium and the aqueous alkali solution as an electrolyte. This type presents a good robustness and low maintenance. However, cadmium and nickel are toxic metals; hence the NiCd batteries are not environmentally friendly. Moreover, their capacity can be decreased rapidly if they are repeatedly recharged after partial discharge that called the "memory effect". In addition NiCd batteries have a high self-discharge current. These batteries are commercially used for the starter systems and standby service [59, 60].

Nickel-metal hydride (NiMH): This type is similar with Nickel–cadmium type in terms of size, cell voltage and design. Whereas, the NiMH based batteries contain hydrogen-absorbing alloy in the negative electrode instead cadmium to avoid its toxic effect which make them friendlier for the environment. Furthermore, the NiMH batteries present other advantages such as low internal resistance and relatively high cycle durability. However, the NiMH like the

NiCd batteries have a high self-discharge current rate, also the memory effect still appears in NiMH batteries type [59, 60].

Lithium-ion (Li-ion): For this batteries type the cathode is made of lithium metal oxide such as $LiCoO_2$ and $LiMO_2$, whereas the anode is made of graphitic carbon. The electrolyte is composed of dissolved lithium salts such as $LiClO_4$. The Li-ion batteries occupy a large use in many applications especially the electronic applications such as smart phones, camera, laptop…etc. This batteries type has many attractive performance advantages that make them in the good ranking according to the other types. The first advantage is that the Li-ion batteries possess a high energy density. Also, they have deepest discharge and lowest self-discharge current compared with the other types. Their electrolyte is not liquid that means that they are immune from leaking. However, the Li-ion based batteries are very affected by high depth of discharge (DOD) cycle that accelerates their lifetime degradation. Added to this, the Li-ion batteries pack requires an electronic on-board monitoring that make them relatively costly [59, 60].

Type	Voltage cell (V)	Energy Density (Wh/kg)	Power Density (W/kg)	Self-Discharge rate	Cycle Durability
Nickel-Cadmium	**1.2**	**40-60**	**150**	**20%**	**1500**
Nickel-Metal Hydride	**1.2**	**30-80**	**250-1000**	**20%**	**1000**
Lithium-ion	**3.6**	**160**	**1800**	**5%-10%**	**1000- 1200**

Table 1-1: Properties comparison among the batteries types [60]

1.3 Lead-acid Batteries

Because of their low cost, the rechargeable lead-acid batteries are the most widely used type for many stationary and large scale applications. The cathode and the anode of these batteries are made of lead dioxide (PbO_2) and of lead (Pb) respectively, while, their electrolyte is composed of sulfuric acid. The advantage of this design is that the electrolyte takes part in the reaction of the both electrodes and vice versa. The lead-acid batteries type can accept deep discharge and have lower self-discharge current rate. Added to this, the lead-acid based batteries have no problem of memory effect phenomena comparing with nickel batteries type. However, as any batteries type the lead-acid batteries have a limited lifetime inconvenience and their capacity decreases with the time due to the internal interactions. Moreover, the lead-acid batteries must be recycled as the active material "lead" is toxic to the environment [60].

1.3.1 Lead-acid cell design

As shown in figure (1.7), the lead-acid cell is composed of active materials. The positive plate (positive electrode) is made of lead dioxide (PbO_2) and the negative plate (negative electrode) is made of sponge lead (Pb). These two electrodes are dipped in a solution composed of sulfuric acid (H_2SO_4) and water. The reaction during charge and discharge of the lead-acid cell is given in the following chemical equation:

$$PbO_2 + Pb + 2H_2SO_4 \underset{discharge}{\overset{charge}{\rightleftarrows}} 2PbSO_4 + 2H_2O \qquad (1.1)$$

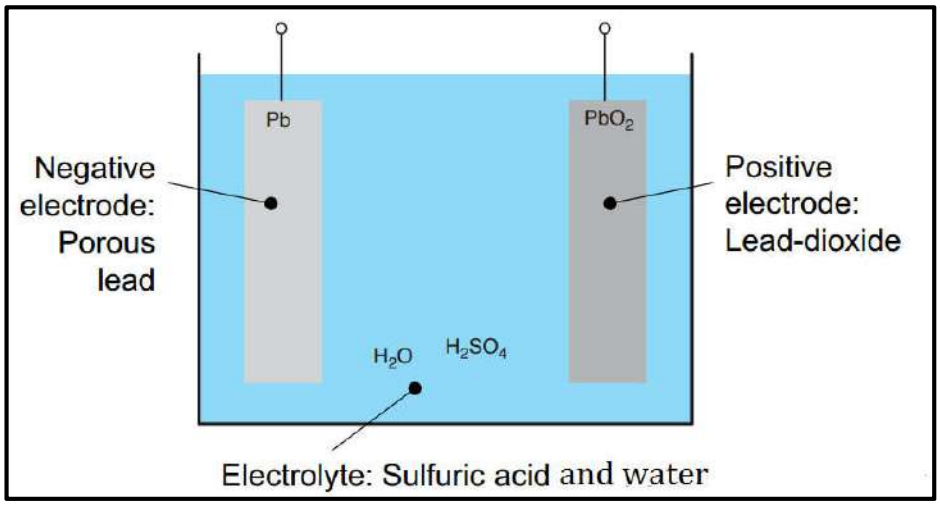


Figure 1.7 lead-acid battery design

The lead and lead-dioxide materials have a good electrical conduction, where the conduction is done via the jumping of electrons between the atoms. The conduction within the electrolyte is done via the ions transport and diffusion. At the negative electrode that is composed of lead, the charged sulfate ions are approaching to the uncharged lead atoms and stabilize at the surface of the negative electrode. Therefore, the lead atoms become ionized and form an ionic bond with the sulfate ions. In this case, two electrons are liberated at the lead atom as given in the equation of the chemical reaction (1.2). The figure (1.8) shows the reaction process at the negative electrode.

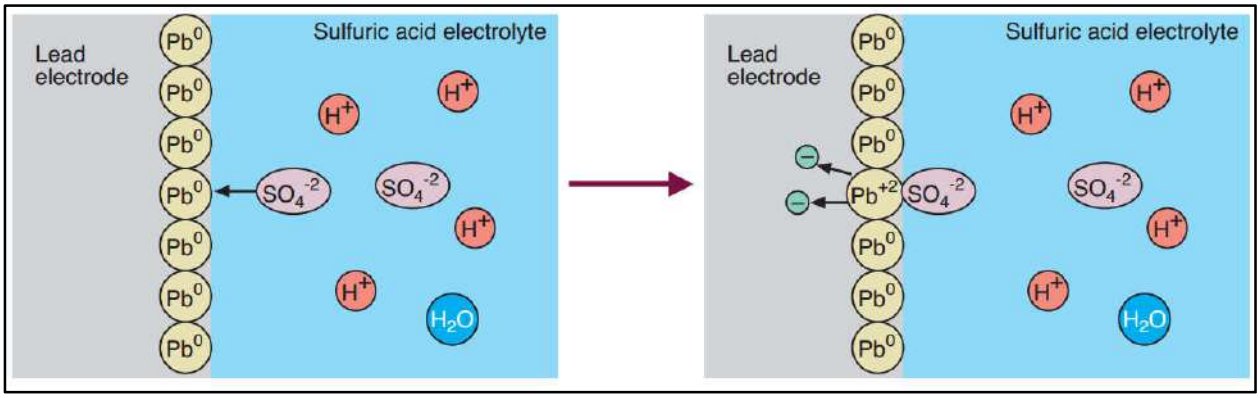


Figure 1.8 the conduction at the negative electrode

$$\underset{Solid}{Pb} + \underset{aqueous}{SO_4^{-2}} \rightarrow \underset{Solid}{PbSO_4} + \underset{Conduction}{2e^-} \qquad (1.2)$$

At the positive electrode composed of lead-dioxide, the charged sulfate and hydrogen ions are approaching to the ear-dioxide molecule and stabilize at the surface of the positive electrode. Lead-dioxide atom becomes ionized and forms ionic bond with sulfate ion. Two electrons are removed from conduction band at the electrode. The reaction is expressed in the equation (1.3). The figure (1.9) shows the reaction process at the positive electrode.

$$\underset{solid}{PbO_4} + \underset{aqueous}{SO_4^{-2}} + \underset{aqueous}{4H^+} + \underset{Condution}{2e^-} \rightarrow \underset{Solid}{PbSO_4} + \underset{liquid}{2H_2O} \qquad (1.3)$$

When the battery cell is discharging, the negative electrode behaves as anode and the positive electrode behaves as cathode. The connection between the two electrodes by an external wire or load leads to a movement of excess electrons in form of current from the anode to the cathode.

When the battery is subjected of an external source namely in charging process, the electrons are forced backwards against the electrodes potential and the reaction is driven backwards. In this case, the negative electrode behaves as cathode and the positive electrode behaves as anode [58-60].

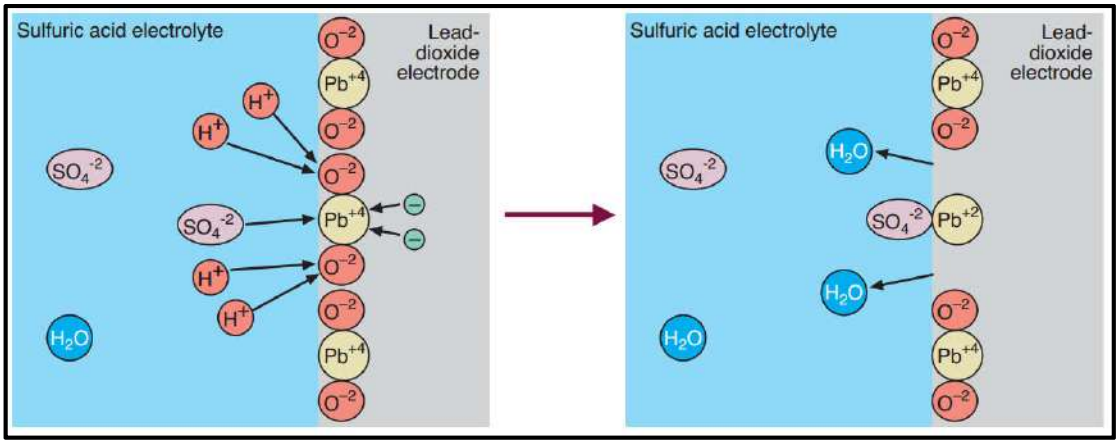


Figure 1.9 the conduction at the positive electrode

1.3.2 Lead-acid batteries design types and technologies

To improve the advantages of lead-acid batteries, several designs have been manufactured either by addition of other materials in the plats such as lead-calcium and Lead-antimony batteries or by the internal design modification such as Manchex, tubular and pasted flat plate. Furthermore, other external design technologies exist such as Valve Regulated Lead-Acid (VRLA) and Vented Lead-Acid Batteries [58-60].

1.3.2.1 Modification in the electrodes

In order to develop and optimize various aspects of lead-acid batteries performances, there are two main modifications: introduction of calcium and the antimony additives.

Lead-Calcium Battery cells: the addition of calcium to the electrodes lead provides several advantages: the battery becomes more resistant to corrosion, overcharging, gassing, water usage and self-discharge. Furthermore, the battery obtains large electrolyte reserve area above the plates. The Lead-Calcium Batteries are recommended for applications that require deep discharge cycling [58-60].

Lead-Antimony Battery cells: in addition to their low cost, the batteries modified with Antimony addition present also several advantages. The first advantage is the reduction of heat and water loss at the gassing working zone. Moreover, the Lead-Antimony batteries have longer lifetime comparing with the Lead-Calcium type. The main disadvantage of these batteries kind is a higher self-discharge comparing with Lead-Calcium model [58-60]. Lead-antimony cells are recommended for applications requiring very long lifetime under cycling discharge depths greater than 20% of their rated capacity.

1.3.2.2 Modification in the internal design

To obtain more advantages for lead-acid battery type, Manchex, tubular and pasted flat plate are three main internal designs existing. Each form gives more benefits according to the applications use.

Manchex type: As shown in figure (1.10), the Manchex batteries are formed of a grid casted with low antimony lead alloy**.** The buttons pressed into the grid holes are obtained by the winding of pure lead ribbon into a spiral form. These are. All are soaked in the sulfuric acid. Due to the heavyweights of grid, these batteries give long lifetime that can reach 25 years with a good management.

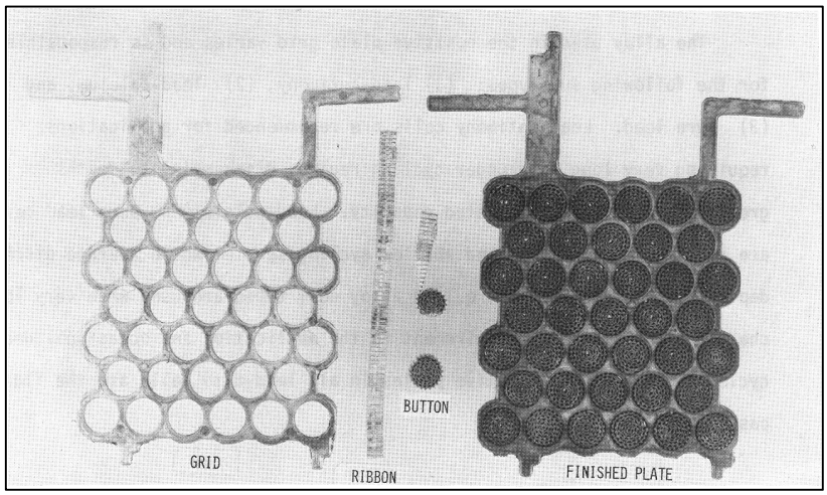


Figure 1.10 Manchex lead-acid battery design

Tubular type: as shown in the figure (1.11), the tubular batteries are composed of a grid that contains series of low antimony lead spines**.** Pipes of plastic or glass are centered on each spine where the active material is situated. These batteries are used for applications that require deep

discharge in the average of 70 to 80 % such as lift truck and material handling. This type is used also for the starting of diesel central. Tubular batteries lifetime can reach ten years for applications requiring 80% deep discharge.

Pasted flat plate: figure (1.12) shows that the grid of the pasted plate type is formed of pure lead, lead-calcium or lead-antimony depending on the size of the plate and application. The active material is situated in the grid holes. The grid plate is wrapped by glass mats and perforated plastic to minimize the loss of active material. This wrap has a similar role of tubes used in tubular plate type. According to the application, the pasted plates are made of thin or thick grids. The thin grids design is used for applications which require high current in a short time such as car starter application. Whereas, the thick grids are used for the applications where the current is relatively low and for long time such as photovoltaic applications.

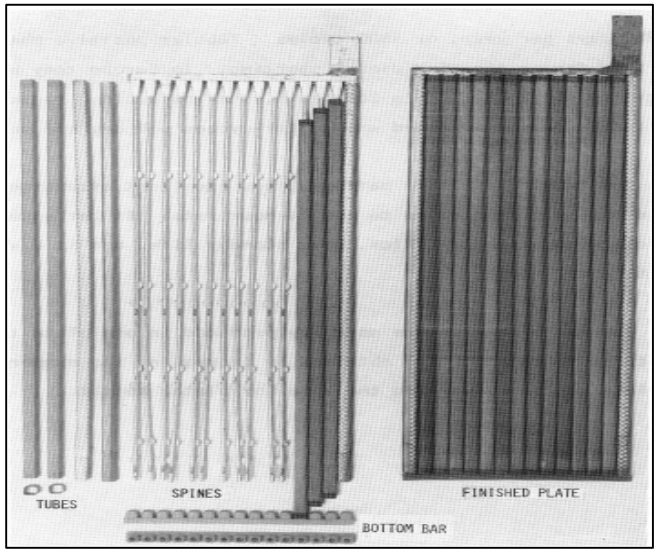


Figure 1.11 Pasted Plate lead-acid design

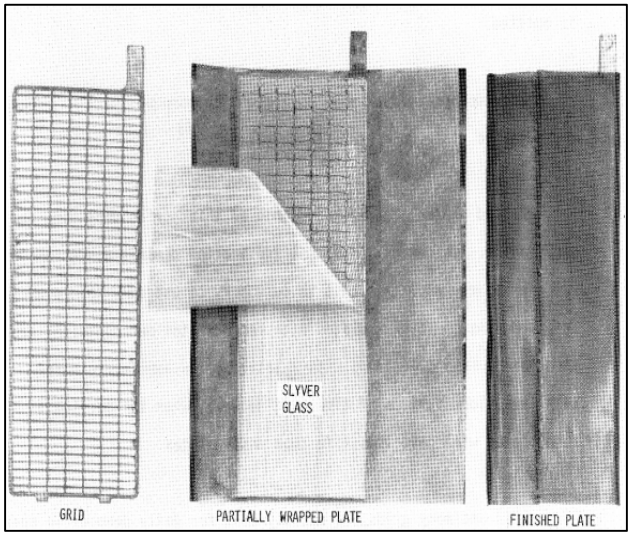


Figure 1.12 Tubular lead-acid batteries design

1.3.2.3 Modification in the external design

For more advantages, two main external modification design types exist: the open lead-acid battery type and the Valve Regulated Lead-Acid battery (VRLA) type.

Open Lead-Acid Battery: due to its low cost and easy maintenance, **Open or vented Lead-Acid Battery** type is the most used. The term open is because the battery can be open for the

addition of lost water. These batteries have several advantages: the first advantage is the possibility of water addition in maintenance; the second is the easy tests and faults diagnostic by measuring of electrolyte density. However, the loss of water in this battery type accelerates considerably its capacity degradation. Figure (1.13) shows the design form of an open lead-acid battery.

Valve Regulated Lead-Acid (VRLA) battery: called also "sealed" lead-acid battery; this type is popular in several applications such as motor cycles. These batteries have low water electrolyte evaporation comparing with the vented types. The loss of electrolyte is largely avoided thus the lifetime is prolonged considerably. The VRLA battery contains regulated valve used for water liberation if the battery reach overcharge level. The electrolyte is designed to be immobilized as gel materials, so it will not leak if the battery is inverted, pierced or broken. For this, VRLA batteries can be installed in any orientation position. The use of this battery type leads to maintenance free (no water addition). Figure (1.14) shows the design shape of this battery type.



Figure 1.13 Open lead-acid batteries design



Figure 1.14 VRLA lead-acid batteries design

1.3.3 Temperature effect

The working temperature of lead-acid battery must be taken into account as an important factor in terms of lifetime or characteristics variation such as capacity and voltage. Theoretically, the lead-acid battery voltage decreases by 5 millivolt per cell if the electrolyte temperature increases by 1 $^{\circ}$C. Moreover, the electrolyte temperature increases if the battery charge reaches the overcharge zone which causes liberation of hydrogen that affects

considerably its lifetime. A typical approximation is that for every 10 °C of temperature increment, the useful lifetime of the battery decreases by half (rule of thumb). Therefore, a cooling system must be installed in the working environment.

1.4 Photovoltaic systems and storage

The photovoltaic (PV) energy can be the alternative energy that responses to new challenges and ensures the energy abundance in the word. The PV cell is composed of two semiconductors doped positively and negatively; if the two semiconductors receive sufficient gape of light energy, the electrons are liberated from the valence band to the conduction band which create a potential difference between the two semiconductors [1].

1.4.1 Modeling and characterization of the PV array

In the most common equivalent circuit of one diode, the PV cell is represented by:

- source of current, that represents the current intensity generated by the cell,
- in parallel with diode,
- and both serial and parallel resistances taking into account the losses in cell.

Figure (1.15) shows the cell equivalent circuit [61].

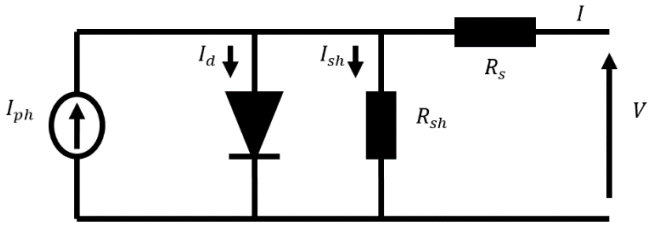


Figure 1.15 One diode equivalent circuit

From the electrical representation aforementioned, the current of cell I is the sum of I_{ph} and I_{sh} that represent the photo-generation and shunt current respectively. Equations (1.4)-(1.7) describe the evolution of cell current and voltage. Where, K is the constant of Boltzmann, q is the electrical charge, T_c is the temperature of the cell, n is the factor of ideality of the diode and I_0 is the saturation of current due to diffusion and recombination.

$$I = I_{ph} - I_d - I_{sh} \tag{1.4}$$

$$I = I_0\left[\exp\left(\frac{q\left(V+R_sI\right)}{nKT_c}\right)-1\right] \tag{1.5}$$

$$I_{sh} = \frac{V + R_sI}{R_{sh}} \tag{1.6}$$

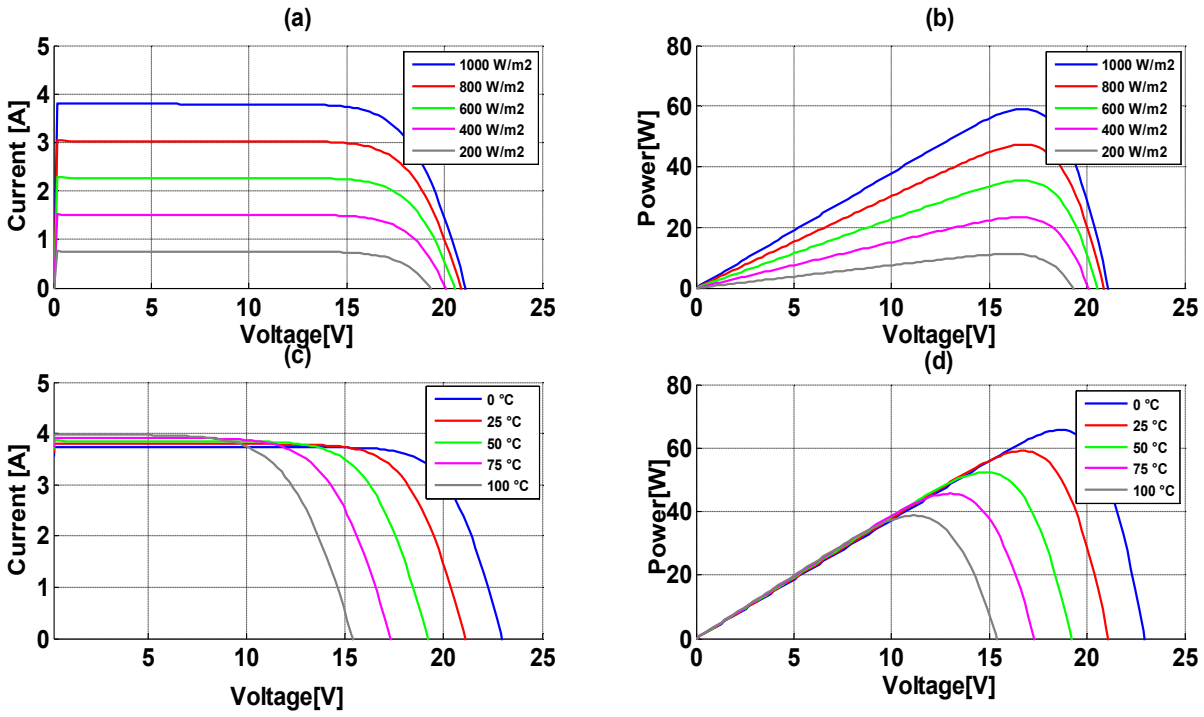
By replacing the equations (1.5) and (1.6) in equation (1.4), we obtain the following equation:

$$I = I_{ph} - I_0\left[\exp\left(\frac{q\left(V + R_sI\right)}{nKT_c}\right)-1\right] - \frac{V + R_sI}{R_{sh}} \tag{1.7}$$

I_{ph}, I_0, R_s, R_{sh} and n are parameters of the model given previously that will be identified.

By varying the load from short-circuit to open circuit states; the PV module in any configuration presents a nonlinear I-V characteristic. It represents the variation of current as function of voltage that depends strongly to the irradiation and temperature. Consequently, the PV array for certain irradiation and temperature possesses an optimum point in which a maximum of power can be extracted [62]. Figures (1.16) show characteristics for different irradiations and temperatures. Where, Figure (1.16) (a) and (1.16) (b) show the I(V) and P(V) characteristics respectively according to the variation of irradiation; Figure (1.16) (c) and (1.16) (d) show the influence of the temperature in the characteristics I(V) and P(V) respectively.

In order to extract the maximum power that the PV module can provide in any case, it is necessary to adapt the load in the maximum power point MPP. Therefore, a dynamic equivalent resistance must be introduced to keeping the working point in the MPP. The DC/DC converter controlled by algorithm may be used to find and track the MPP by dynamically. It enables us to avoid any loss of energy caused by the continuous change of the working irradiation and temperature.



Figures 1.16 PV panel characteristic for different irradiations and temperatures.

1.4.2 The photovoltaic systems type

Two main systems of photovoltaic exist according to the path of the energy from the source until the load:

a) **Grid-connected PV systems**: they are designed for providing the energy to the distribution network during the peak demand and get absorb the energy from the network when it is needed. These systems do not rely strongly on the storage unless for the compensation in the case of a hollow in the energy provided. The most important part in these systems is the inverter that consists of the conversion of DC energy generated by the PV to the AC energy needed by the line. Figure (1.17) shows that the grid-connected system is composed of PV array, DC/AC converter and automatic isolation [63].

b) **Stand-alone PV systems**: they are the most popular which provide energy even in the case of lack of solar irradiation. The stand-alone PV systems rely completely on the storage system. The solar energy is stored and released when it is needed to the load. The simple configuration of these systems is described briefly in the figure (1.18).

Where we can see that PV generator connected to the storage system, this connection may include conditioner and protection device. DC/AC converter is connected to the load for AC case. For the case of DC load, the storage system is connected directly. The stand-alone systems are widely used in water pumping application in the isolated areas. However, the storage of energy is still the major problem for these systems [63].

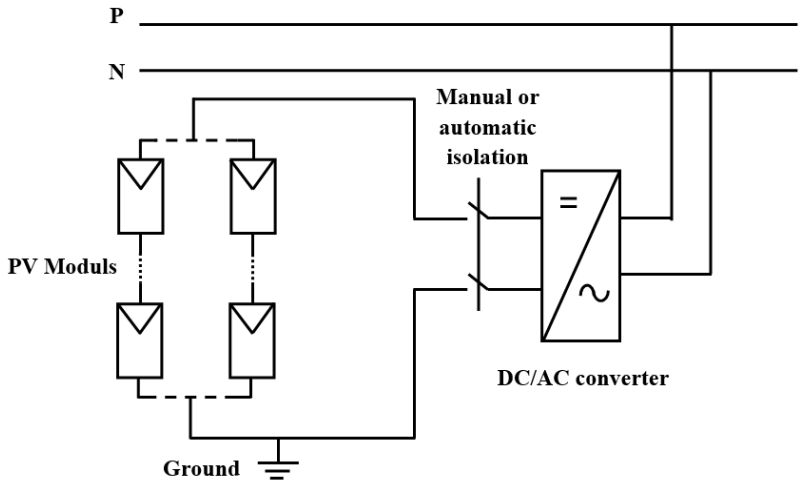


Figure 1.17 Grid-connected system design

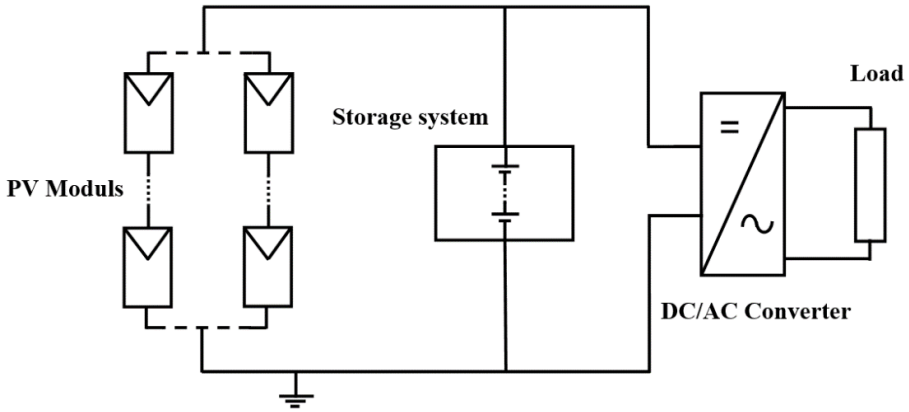


Figure 1.18 Stand-alone system design

1.4.3 The storage in photovoltaic systems

As aforementioned in the previous section, the PV storage is still a major issue for the recent searches as the PV energy is provided only in the day. Especially, in the isolated areas this problem is widely faced. Hence, many storage systems have been used in the PV systems more precisely in the stand-alone systems such as hydrogen storage, fuel cells and the

Supercapacitors. However, the stationary batteries are still taking a large place in the PV storage because of their low cost, their ease of maintenance and relatively their high capacity. Where the battery can provide the energy to the load in case of lack of radiation, and behave as a load when the PV power is available as is described in figure (1.19). The lead-acid battery is the most popular in the PV systems due to the aforementioned advantages [63].

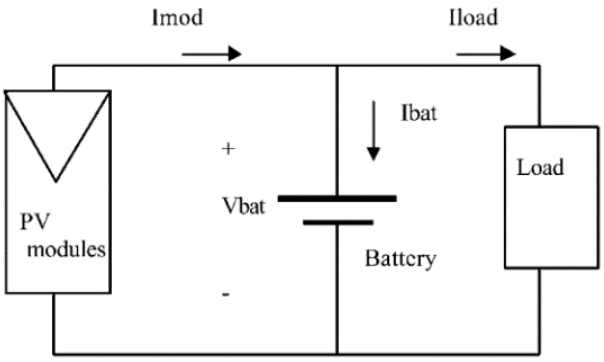


Figure 1.19 Battery position in the PV system

Despite this, in addition to its complex electrochemical behavior, the lead-acid battery in PV systems is subjected of random working condition due to the continuous change of solar irradiation and temperature. This makes its modeling or prediction more complex. Moreover, the lead-acid battery has a limited lifetime caused by the capacity degradation. However, good management and control of battery energy flow can extend its lifetime. Hence, the name of the battery in stand-alone systems has been associated with the charge controller. Further to the effective management and optimization of energy flow advantage, a robust charge controller can prolong considerably the lifetime of the battery.

1.5 Battery charging modes and charge controller types

According to applications, there is several lead-acid batteries charging modes such as on-off, constant current, constant voltage and pulsed charge modes. This enables us to prolong the lifetime and benefit of the maximum use of capacity. Therefore, various batteries charge controller have been introduced.

1.5.1 Battery charging modes

In order to obtain better management, good performance and optimal lifetime, specific conditions should be respected for charging lead-acid batteries. Mainly, the working conditions are:

- The charge current should not exceed the value that overheats the battery (C/4).
- The good estimation of the safe working zones to avoid the dangerous one: Overcharge and over discharge.
- The good estimation of battery state of charge.

Furthermore, the good PV system sizing plays an important role for an effective management of battery energy and optimization of stand-alone PV system power. For this end, several charging modes of batteries have been introduced in the literature for the purpose to response to the aforementioned conditions. Mainly, the most common modes are: on-off, constant current and constant voltage charging mode [64].

1.5.1.1 On-off charging mode

This charging type is parameterized by four voltage thresholds controlled as hysteresis. In the charge step, the source is disconnected at the gassing voltage level called also “end of charge”. The source is reconnected at the recharge voltage level when the battery can be recharged again. In the discharge step, the load must be disconnected at the level of end of discharge voltage and reconnected when the battery can provide energy to the load. Figure (1.20) describes the on-off mode evolution [64].

This charging mode is recommended for the systems of high storage capacity when the current is less than C/20 (where C is the battery capacity). However, in the case of high charging current, this current multiplied by the internal resistance creates voltages higher than the commutation thresholds. Therefore the charge stops before the battery full charge. If the voltage threshold of end of charge is increased the battery exceeds the gassing level. Moreover, the choice of discharge thresholds is another major problem in term of the maximum extraction of battery capacity [64].

1.5.1.2 Constant current charging

This charge method is applied to the control systems that ensure a constant charge current. It can be applied to different controlled levels of charging current. In the first charging step, the voltage starts to increase rapidly. When the battery is near to its charge voltage threshold, if the charge current is low we can consider that the state of charge is near to 100%. Then, it is

recommended to stop the charge by a low current near to C/100. Figure (1.21) describes both the current and voltage evolutions for this charging method [64].

1.5.1.3 Constant voltage charging

In this charging mode, the voltage is maintained at the same value almost throughout the process of the charge. This charging mode provides an important initial current due to the difference of the voltage between the discharged battery and the source. Thus, the battery charge increases until 70% at 30 minutes. For the systems of high charging current according to the storage capacity, it is recommended to use the constant voltage charging. However, in photovoltaic systems the current is unpredictable, then modified methods of the constant voltage is called in order to limit the current either in the start or in the end of the battery charging process as described in figure (1.22). These exists methods are:

- Modified charging of constant voltage with a constant current in the start of charging process.
- Modified charging of constant voltage with a constant current in final phase.
- Modified charging of constant voltage with a constant current in the start and the end of charging process.

These types use a PWM controller's technology based on DC/DC converter for the maintaining of the voltage or the current at a constant value. The PWM controllers enable us to integrate the MPPT for PV systems [64].

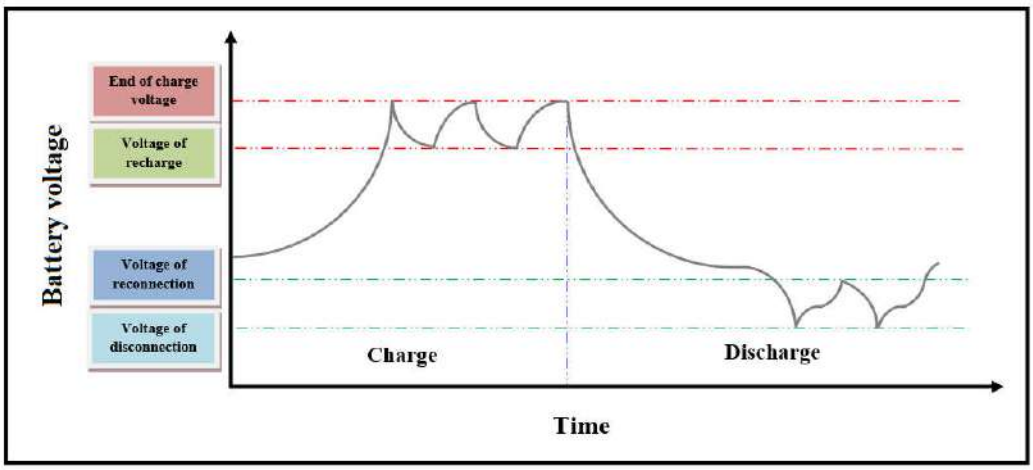


Figure 1.20 On-off charging

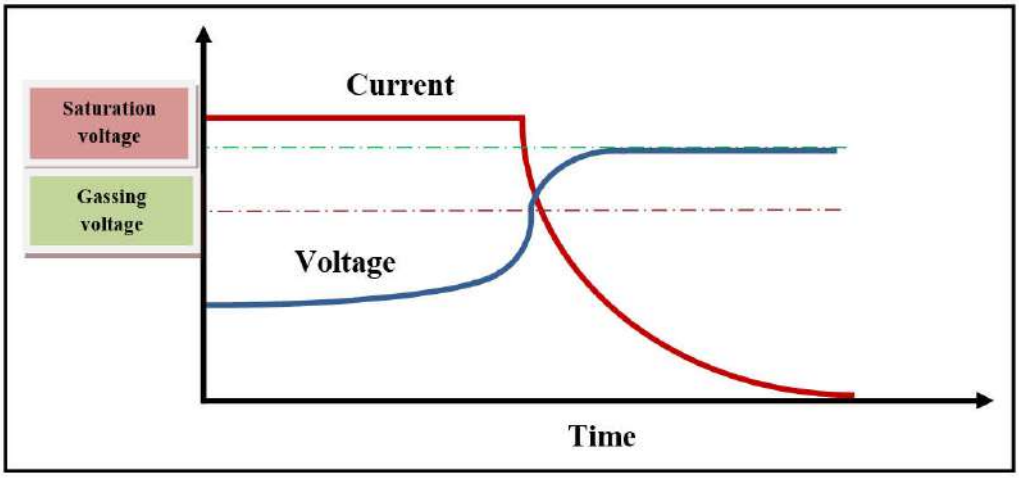


Figure 1.21: Constant current charging and discharging

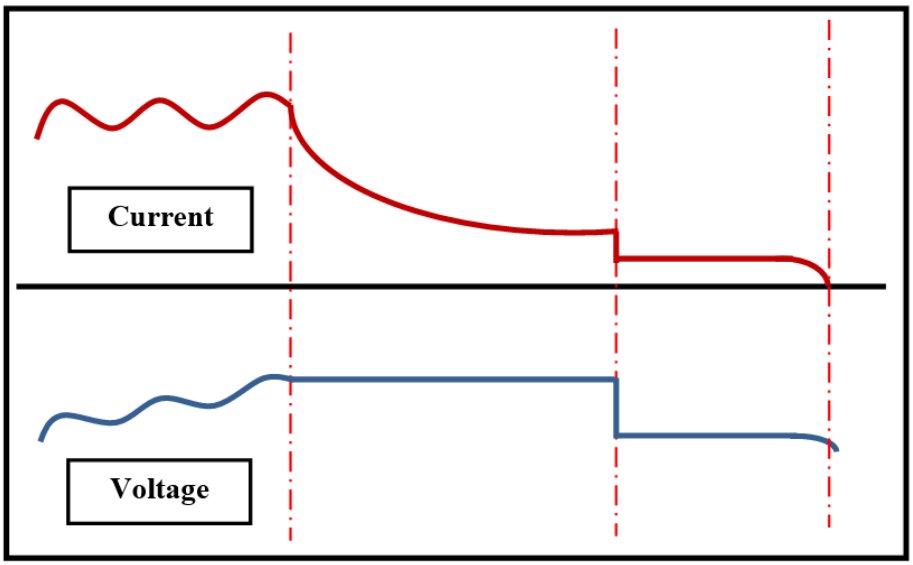


Figure 1.22: Modified constant voltage charging

1.5.2 Battery charge controllers and their technologies

At the beginning of use of photovoltaic energy systems, mainly two types of battery charge controller have been used: serial and shunt models. These models have commonly used the battery voltage characterization to determine the state of charge and thus reduce or stop the charging process. Although the wide enhancements of the calculators and the appearance of new technics to manage the battery energy flow using other battery characteristics. The PWM- MPPT charge controllers provide fast and effective solutions for an optimum battery charge and discharge mode and ensure good performances for solar applications [64].

1.5.2.1 Series type regulators

Figure (1.23) shows that the switch in this type is integrated in series with source. It is opened when the battery full charge is achieved. Another switch is integrated after the battery to control the load current. According to the size of the photovoltaic installation, one or multiple relays can be used. Hence, for the systems using output currents higher than 50 amperes, the controller should include more than one relay. The opening and closing of the relay is performed according to the predetermined maximum and minimum voltage thresholds.

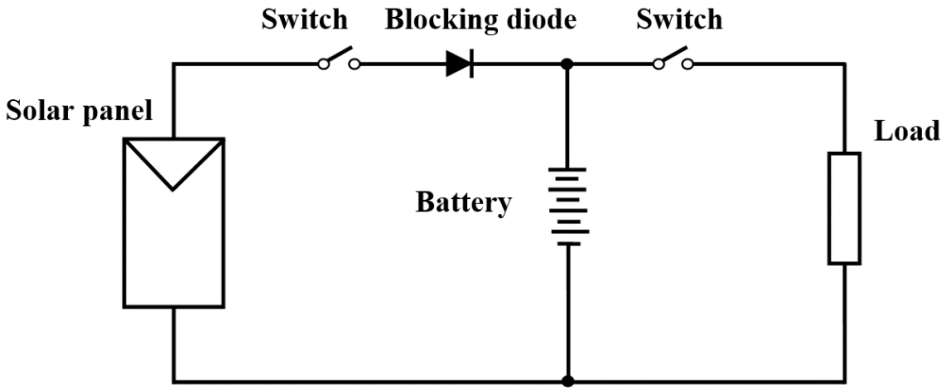


Figure 1.23: Series type controller.

Practically, stationary batteries that work in the fixed position may risk losing the homogeneity of charge in the electrolyte. The charge concentration may be situated in the bottom of the battery. Therefore, the regulator, every month, should overcharge the battery at the equalization voltage threshold to create gasification that homogenizes the electrolyte. This is an automatic Homogenization manner without moving the battery. At this end, another controlled switch can be added in parallel with the serial switch [64].

1.5.2.2 Shunt type regulators

This type is the most widely used due to its easy realization in which the switch is placed in parallel with the solar panel and the battery. Where, the current is provided from the panel through the diode in the charge process. When the battery is full charged, the parallel switch is closed to disconnect the source. For the discharge process, the second switch is closed in order to provide the current to the load. Figure (1.24) describes briefly the principle of this regulator type [64].

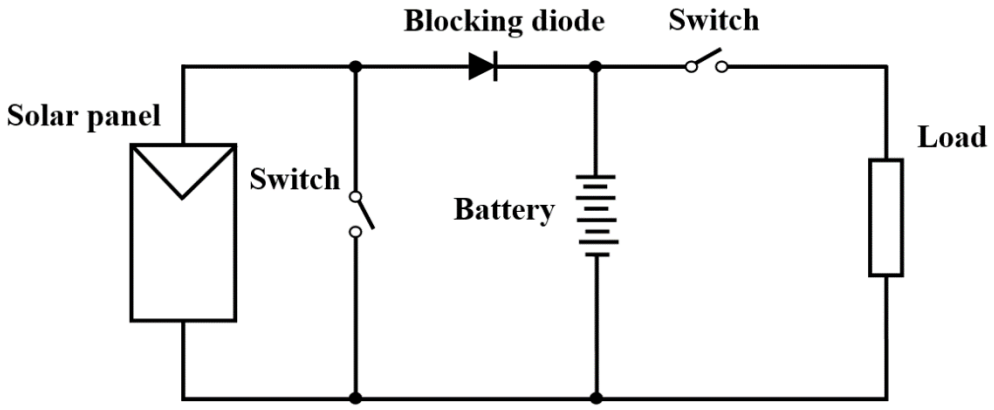


Figure 1.24: Shunt type regulator.

Among the shunt type controllers, there is the linear shunt controller type. This model maintains the battery in a constant voltage when its full charge is achieved. The linear shunt controller ensures the full charge of the battery. However, the unused power of the panel, when the battery is full charged, may be dissipated in a parallel transistor (switch). For this dissipation, this type of controller is limited for small currents [64].

1.5.2.3 PWM controller

Using the Pulse Width Modulation feature, PWM controllers benefit to the advantages of the two previous techniques. It is a DC/DC converter that uses MOSFETs or power transistors operating at high frequencies in order to generate the specific pulses which control the battery voltage. The PWM controllers have an excellent charging characteristic for PV systems in which the battery full charge can be rapidly achieved. However, the commutation with high frequencies can cause a power loss at the switches. Figure (1.25) shows the PWM regulator design.

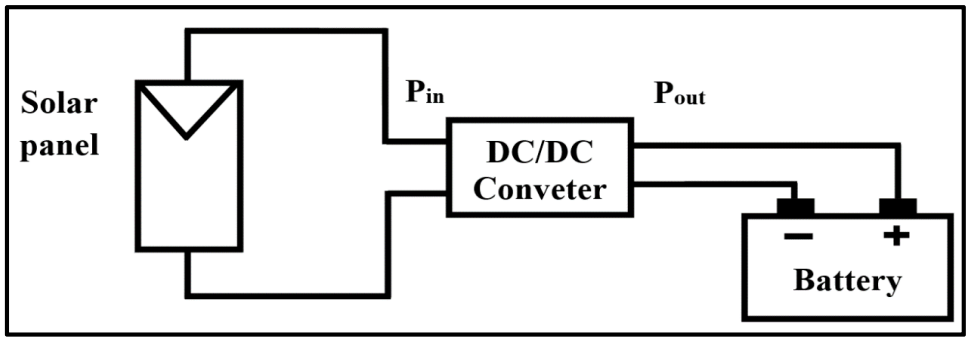


Figure 1.25: PWM regulator

Among the advantages of PWM regulator is that it can maintain the battery voltage in constant value to achieve the full charge. Furthermore, these regulators can integrate the maximum power point tracker by using the same DC/DC converter. This ensures that the maximum energy provided by the solar panel is recovered [64].

1.6 Conclusion

In this chapter, we give a background about the energy storage techniques such as: pumped hydro, compressed air, flywheel, Supercapacitors and electrochemical storage. While our interest focuses on the storage in the photovoltaic systems, the lead-acid battery type was taken an important part of this chapter because of its wide use in this domain. For an optimal use of battery energy and prolonged lifetime in photovoltaic systems the integration of controller is required. For this end, the battery charging modes and charge controller types have been also highlighted.

CHAPTER II
LEAD ACID BATTERY MODELING AND PARAMETERS EXTRACTION

CHAPTER II

LEAD ACID BATTERY MODELING AND PARAMETERS EXTRACTION

2.1 Introduction

In Photovoltaic Systems (PVS), particularly in stand-alone systems, the battery remains one of the most important components for energy storage. In addition to its complexity due to the electrochemical behavior, the battery in PVS is subjected to dynamic state caused by continuous change in irradiation and temperature. Therefore, the battery is considered as a major problem in PVS and it has been interested in by several researches in order to achieve a deep comprehension of its interaction. To obtain a best prediction, which gives a good agreement with real battery behavior, it is necessary to establish an accurate battery model. Several models have been proposed in the literature based on the electrical approach and other different approaches like electrochemical, analytical and stochastic models. The electrical approach allows us to have a profound comprehension for behavior analysis. In this chapter, we propose the modeling and the improvement of CIEMAT electrical model by the extraction of its parameters using genetic algorithm and Levenberg-Maquart algorithm.

2.2 Lead-acid battery modeling

The equivalent electrical circuit of a lead acid battery is illustrated in Figure (2.1) [31-32, 65, 66]. The battery is represented by an open circuit voltage V_{oc}, which models the electromotive force resulting from electrochemical activities of the solution and an internal resistance R_b that represents all losses during charge/discharge process.

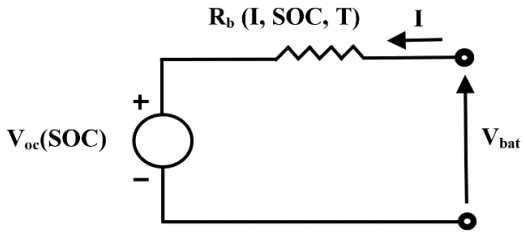


Figure 2.1. Equivalent circuit for the battery

The voltage at the output terminals can be expressed by the following expression:

$$V_{bat} = V_{oc} \pm I.R_b \tag{2.1}$$

I is the charge/discharge current. This current is positive during charge process and negative during discharge process.

2.2.1 Battery internal resistance

Due to the internal behavior inside the battery, the internal resistance term appears as one of its characteristics that expresses the energy losses in different mode (charge, discharge). It is mainly caused by the electrolyte, the electrode resistance and the material constituting the battery and varies strongly according to the temperature. There are many methods for measurement of this resistance as the current pulse, the period of rest and the milliohm-meter method. An empirical relationship has been established by Copetti et al which represents the battery resistance for both charge and discharge mode as shown in expression (2.2) [31-32, 65-67].

$$R_b = \left(\frac{P_1}{1 + I(t)^{P_2}} + \frac{P_3}{\left(1 - SOC(t)\right)^{P_4}} + P_5 \right) \left(1 - \alpha_T \left(T - T_{ref}\right)\right) \tag{2.2}$$

Where: P_1 to P_5 and α_T are empirical parameters that will be identified for the enhancement of this model, I is the current that pass from and to the battery, SOC is the battery state of charge, T is the electrolyte temperature and T_{ref} is the reference temperature of 25 °C.

2.2.2 Battery state of charge and level of energy

The battery state of charge (SOC) is an indicator that describes the charge storage in the battery as a percentage varied in the range 0 < SOC < 1. It is obtained by calculating the sum of amperes that pass through the battery according to its instantaneous capacity and initial state of charge (SOC_0). In the same concept, the level of energy (LOE) expresses the energy storage in the battery according to the maximal capacity for I equals to 0 and temperature in the range [-40, +40]. Equations (2.3) to (2.7) describe the evolution of both SOC and LOE [31,32, 68].

$$SOC(t) = SOC_0 + \frac{1}{C(t)} \int_0^t \eta_c(t) I(t) \partial t \tag{2.3}$$

$$C(t) = \frac{C_{nominal}.C_{tcoef}}{1 + A_{cap} \left(\frac{|I(t)|}{I_{nominal}} \right)^{B_{cap}}} \left(1 + \alpha_c \Delta T + \beta_c \Delta T^2\right) \tag{2.4}$$

$$I_{nominal} = \frac{C_{nominal}}{n} \tag{2.5}$$

$$LOE(t) = LOE_0 + \frac{1}{C_n}\int_0^t \eta_c(t)\, I(t)\, \partial t \tag{2.6}$$

$$C_n = \max(C)\Big|_{\substack{I=0 \\ T=[-40,+40]}} \tag{2.7}$$

Where, C_{tcoef}, A_{cap}, B_{cap}, α_c, β_c are parameters that will be identified for the development of this model, $C_{nominal}$ is the nominal capacity, η_c is the coulomb efficiency and C_n is the maximal capacity for current equals to 0 and temperature in the range [-40, +40]. For reducing the number of parameters, we assume that the capacity varies linearly with the temperature therefore β_c is equal to 0 [31, 68].

2.2.3 Terminal voltage and working zones variation

Battery voltage exhibits different behavior depending on its operating mode (charge or discharge mode). In charge mode, there are three operating zones: charge zone, overcharge zone and saturation zone. While in discharge mode; the output voltage transits through transition zone, over-discharge zone and exhaustion zone [68-69]. Time evolution of battery output voltage during charge and discharge phases is given in Figure (2.2).

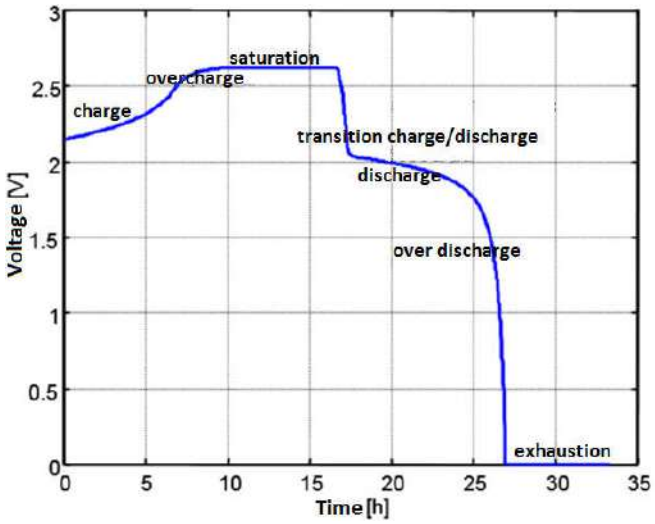


Figure 2.2 Voltage areas variation

2.2.3.1 Charge, Overcharge and Saturation zone

During the phase of charge, the battery receives energy from the source to be stored, which increases its voltage and state of charge. It is considered as the best working zone to prolong the battery lifetime. Equation (2.8) gives the relationship of the output battery voltage as a function of state of charge, battery current and electrolyte temperature.

$$V_c = \left(V_{boc} + K_{boc} SOC(t)\right) + \frac{I(t)}{C_{nominal}}\left(\frac{P_{1c}}{1 + I(t)^{P_{2c}}} + \frac{P_{3c}}{\left(1 - SOC(t)\right)^{P_{4c}}} + P_{5c}\right)\left(1 - \alpha_{rc}\Delta T(t)\right) \quad (2.8)$$

Coulomb efficiency ηc, which denotes charge efficiency and given by equation (2.9), is taken into account in case of charge mode and depends strongly on the charge rate. Its value is close to 1 for low charge currents and low state of charge. However, when a full charge is reached, Coulomb efficiency will decrease to zero.

Where V_{boc}, K_{boc}, a_{cmt}, b_{cmt}, P_{1c} to P_{5c} and α_{rc} are empirical model parameters to be identified, SOC(t) is actual battery's state of charge, I is battery charge current, ΔT is the temperature variation according to the reference of 25 °C.

$$\eta_c = 1 - \exp\left(\frac{a_{cmt}}{\left(\frac{I}{I_{nominal}} + b_{cmt}\right)}\left(SOC(t) - 1\right)\right) \quad (2.9)$$

When the battery reaches gassing voltage level V_g, it can start to saturate, and the charge current starts to decrease. Thus, acceptance of charge decreases due to the effect of gassing electrolyte. This phenomenon appears when battery charge is near to its maximum (95%). This level varies according to the charge current and electrolyte temperature. Expressions (2.10)–(2.14) give equations related to this particular zone:

$$V_g(t) = \left[A_{gas} + B_{gas} ln\left(1 + \frac{I(t)}{C_{nominal}}\right)\right]\left(1 - \alpha_{gas}\Delta T(t)\right) \quad (2.10)$$

$$V_{ec}(t) = \left[A_{fonse} + B_{fonse} ln\left(1 + \frac{I(t)}{C_{nominal}}\right)\right]\left(1 - \alpha_{fc}\Delta T(t)\right) \quad (2.11)$$

$$V_{sc}(t) = V_g(t) + \left(V_{ec}(t) - V_g(t)\right).\left[1 - \exp\left[\frac{-\left(SOC(t)C(t) - SOC_{V_g}(t)C(t)\right)}{I(t)\tau(t)}\right]\right] \quad (2.12)$$

$$\tau(t) = \frac{A_{\tau sc}}{1 + B_{\tau sc}\left(\frac{I(t)}{C_{nominal}}\right)^{C_{\tau sc}}} \quad (2.13)$$

$$SOC_{V_g} = SOC\Big|_{V_c = V_g} \quad (2.14)$$

Where V_g, V_{ec}, V_{sc} are gassing, saturation and overcharge charge voltage respectively. A_{gas}, B_{gas}, A_{fonse}, B_{fonse}, $A_{\tau sc}$, $B_{\tau sc}$ and $C_{\tau sc}$, are model parameters, τ is the time constant in overcharge zone, SOC_{vg} is the battery state of charge when the voltage achieves the gassing level. V_{sc} is the overcharge voltage.

In saturation zone, the battery cannot accept more energy. Nevertheless, terminals voltage reaches the maximum level at this zone and its value varies according to the charge current and the electrolyte temperature as given in Eq. (2.11). State of health is considerably affected in this charge zone. The feeding source must be immediately disconnected [31-32, 63, 69].

2.2.3.2 Discharge zone, Overdischarge zone and Exhaustion zone

In the discharge zone, the battery provides energy to the load. The limits of this zone is while $V_{bat} > 0.9V_N$, with V_N is the nominal voltage of the battery. Equation (2.15) describes the evolution of battery voltage in this zone:

$$V_{dc} = \left(V_{bodc} - K_{bodc}\left(1 - SOC(t)\right)\right) - \frac{|I(t)|}{C_{nominal}}\left(\frac{P_{1dc}}{1 + |I(t)|^{P_{2dc}}} + \frac{P_{3dc}}{SOC(t)^{P_{4dc}}} + P_{5dc}\right)\left(1 - \alpha_{rdc}\Delta T(t)\right) \quad (2.15)$$

V_{bodc}, K_{bodc}, P_{1dc} to P_{5dc} and a_{rdc} are empirical model parameters to be identified, SOC is actual battery's state of charge, I is battery discharge current, ΔT is the temperature variation according to the reference of 25 C.

In the over-discharge zone when the battery voltage reach 90% of nominal voltage, the battery starts to discharge rapidly and it becomes nearly empty. This area affect the battery health, therefore the load must be disconnected. The exhaustion zone is the very dangerous area for the battery. It can damage the battery, when $V_{bat} < 0.7V_N$. A voltage remainder can appear, but there is no extractable energy stored in the battery [31-32, 63, 69].

2.2.3.3 Transition voltage

Due to the battery internal resistance [68, 69], the charge battery voltage V_c and the discharge battery voltage V_{dc} are different as given in expression (2.16). In this transition, the battery presents a voltage drop which causes a discontinuity in the model for the dynamic working mode.

$$V_c\big|_{I=0} \neq V_{dc}\big|_{I=0} \tag{2.16}$$

Battery voltage	**Working zone**		**Zone extremities**	
V_{sc}	Saturation zone	$I > 0$	$V_{bat} = V_{ec}$	$\eta_c \approx 0$
	Overcharge zone		$V_g \leq V_{bat} \leq V_{ec}$	$0<\eta_c<1$
V_c	Charge zone		$V_{bat}<V_g$	
V_{cdc}	Changing from charge to discharge or from discharge to charge	$I \approx 0$	$V_{dc}\leq V_{bat} \leq V_c$	
V_{dc}	Discharge zone	$I < 0$	$V_{bat}> 0.9V_N$	$\eta_c \approx 1$
	Overdischarge		$0.7V_N \leq V_{bat} \leq 0.9V_N$	
	Exhaustion		$V_{bat}<0.7V_N$	

Table 2.1.Battery working zone extremities

$C_{nominal}$=110 Ah	P_{1dc} = 4 Vah	P_{1c} = 6 VAh	A_{fonse}=2.45V
n =10 h	P_{2dc} = 1.3	P_{2c} = 0.86	B_{fonse}=2.011Vh
C_{tcoef} =1.67	P_{3dc} = 0.27 V h	P_{3c} = 0.48 VAh	$A_{\tau sc}$ =17.3 h
α_c = 0.005° C^{-1}	P_{4dc} = 1.5	P_{4c} = 1.2	$B_{\tau sc}$ = 852 h
β_c=0° C °	P_{5dc} = 0.02 Vh	P_{5c} = 0.036Vh	$C_{\tau sc}$ = 1.67
A_{cap}=0.67	a_{cmd}=20.73	A_{gas}=2.24 V	α_{rdc} = 0.007° C^{-1}
B_{cap} = 0.9	b_{cmd}=0.55	B_{gas}=1.970 Vh	α_{rc} = 0.025° C^{-1}
V_{bodc}= 2.085 V	V_{boc} = 2V	α_{gas} = 0.002° C^{-1}	I_δ =0.0001 A
K_{bodc}= 0.12 V	K_{boc}= 0.16 V	α_{fc} = 0.002° C^{-1}	

Table 2.2 Values of the CIEMAT model parameters

If the current I_δ is sufficiently small (Table 2.1, 2.2), which define a transition band when $I_{bat}<|I_\delta|$, we can avoid the discontinuity at this transition by a linear function represented in the equation (2.17). The voltage model at this limit is taken as linear transition [32, 69].

$$V_{cdc} = \frac{V_{c|I_\delta} - V_{dc|I_\delta}}{2I_\delta} I + \frac{V_{c|I_\delta} + V_{dc|I_\delta}}{2} \tag{2.17}$$

Table (2.1) resumes the working zone thresholds and transition conditions of battery output voltage. The parameters given by CIEMAT are given in Table (2.2)

According to the description mentioned previously, we note that the control and the monitoring based on the accurate estimation of the battery voltage areas leads to extending its lifetime by avoiding of the dangerous zones.

2.2.4 Static simulation

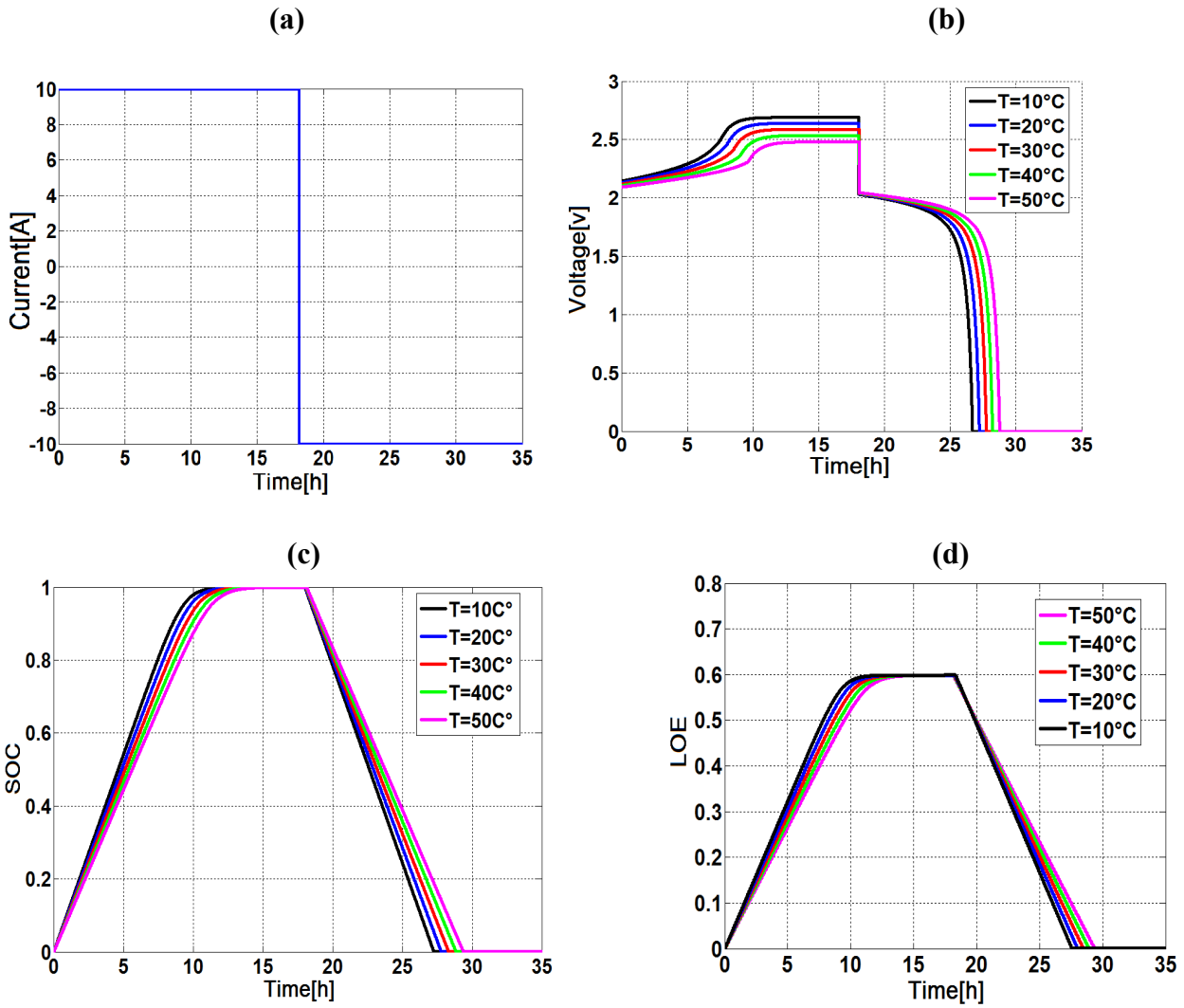
A simulation of lead-acid battery model in Matlab/Simulink environment in static mode for constant current charge and discharge is given. This simulation is running for battery capacity of 110 Ah and +10A/-10 A charge and discharge current.

For each battery's output variation, different temperatures were provided, where T= 10° 20° 30° 40° 50°. The results are given in figures (2.4). Where, (a) is the charge and discharge current, (b) is the variation of the battery output voltage, (c) is the variation of the battery' state of charge and battery' level of energy for different temperatures.

The simulation for constant current shows that whenever the temperature increases the battery's output voltage decreases considerably as it is shown in figure 2.4 (b), also for the state of charge and the level of energy. The temperature is an effective factor for the evolution of battery output.

2.3 parameters extraction

In order to improve the accuracy of the model aforementioned, an enhancement of the empirical parameters is proposed in this section by using automatic extraction parameters. At first, we have used Levenberg-Maquart with a toolbox in Matlab/Simulink. After that, we have proposed an improvement by genetic algorithm. This algorithm is suitable in terms of model complexity and large number of parameters in which it is based on stochastic research.



Figures 2.3: (a) the battery' current for charge and discharge. (b) Variation of voltage as functions temperature. (c) Variation of SOC as functions temperature. (d) Variation of LOE as functions temperature.

2.3.1 Model extraction parameters by Levenberg-Marquardt algorithm

In this step, we have used the Levenberg-Maquart algorithm toolbox in Matlab / Simulink. It consists to minimize the cost function that represents the error between the model and the actual measurement. This classical algorithm collects both Gauss-Newton and gradient algorithm developed by Kenneth Levenberg and published by Donald Marquardt.

2.3.1.1 Algorithm process

Taking the cost function given in expression (2.18) that represents the sum of the squares of error between a certain number of real data d and an approximate function *f(P|t)* which contains a certain parameters to be identified [70].

$$S(\mathrm{P}) = \frac{1}{L}\left(\sum_{i=1}^{L}(d - f(P \mid \mathrm{t}))^2\right) \tag{2.18}$$

Where: L is the number of samples and d is the real measurement.

The process of this algorithm starts by an initial value of parameters $P^T=[a_1\ a_2\ \ldots..\ a_n]$, and for each iteration P is replaced by p+q. For determine the q, the functions $f_i(p+q)$ approached being linearized then equation (2.19) is obtained.

$$f(p+q) = f(p) + Jq \tag{2.19}$$

Where, Jq is the Jacobian of *f* in p

For a minimum of the sum of squares S, the gradient of S equal to zero, by derivation of expression (1.18) the following equation is obtained:

$$(J^T J)q = J^T(y - f(p)) \tag{2.20}$$

Where, q is obtained by the inversion of the matrix j^Tj [70].

In our case, the f function represents the battery output voltage and d is the real measurements that are the both current and temperature of the battery.

2.3.1.2 Results

From the model described previously, 20 parameters were included in the identification algorithm, where a simulation has been carried out using Matlab/Simulink. The control and estimation tool manager in Matlab/Simulink used for the extraction parameters is given by figure (2.6)

For the real measurements of four days taking one sample every 1 minute, a stand-alone string composed of solar panel SORALWORLD, Lead-acid stationary battery and 4 DC lamps used in the experimental study with the characteristics given in Table (2.3). An extraction of parameters has been carried out taking the current and the temperature as model

input and the voltage as output. Figures (2.7) show the battery input measurement, where: (a) is the current measure and (b) is the ambient temperature.

Simulation running Levenberg-Maquart algorithm for parameters extraction of the battery model was carried out using the real measurements given previously. The model presents a good agreement with the real measures by applied the new parameters given in table (2.4). Figure (2.8) (a) shows the matching between the estimated and measured voltage and (b) shows the estimated state of charge by applied the new extracted parameters.

2.3.2 Extraction of Model's parameters using the Genetic algorithm

Genetic algorithm (GA) is an inspiration of biological genetic process to find approximate optimal solutions for mathematical problems. As in natural concept, the chromosome is the information holder, which represents the genes that the child can get from his parents. In real optimization problems, genes are the variables of a mathematical function. Basically, GA randomly generates N chromosomes, in where each one is a vector of the variables representing a solution to the suggested optimization problem. GA imitates the process of biological evolution, including selection, crossover, and mutation based on the principle: good individuals survive and breed good individuals [44-45].

Battery model given by the previous mathematical equations has 21 unknown parameters for charge and discharge zones, which are extracted by GA based adjustment in order to get best matching of the model with experimental measurements. These parameters are divided into two groups. First group as given in Table (2.6) contains temperature independent parameters and the second group as depicted in Table (2.7) contains temperature dependent parameters. Thus, parameters of the first group are identified for a fixed temperature. However, parameters of the second group are identified separately. Equation (2.21), given bellow, is a measure of the mean error between measured and evaluated output battery voltage.

$$Mean\ error = \frac{1}{L}\left(\sum_{i=1}^{L}\frac{\left|V_m - V_s\right|}{V_m}\right) \tag{2.21}$$

Where, V_m and V_s are the measured and evaluated battery voltage respectively and L is number of samples.

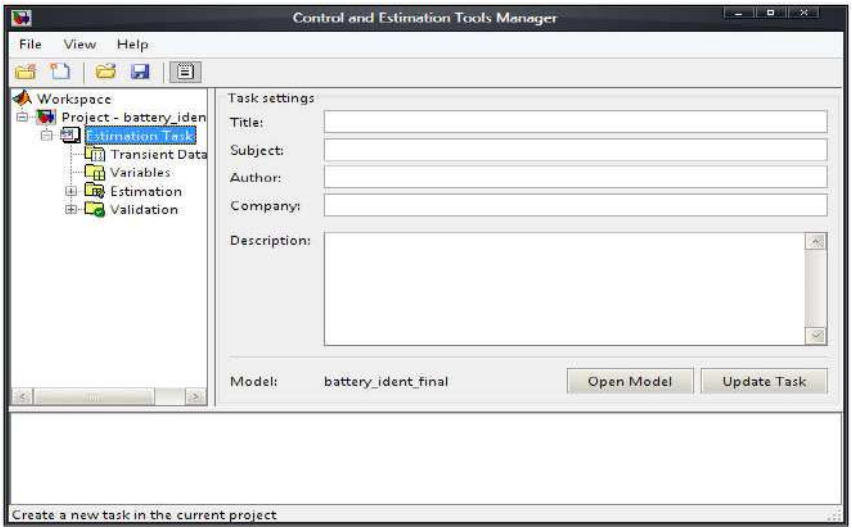
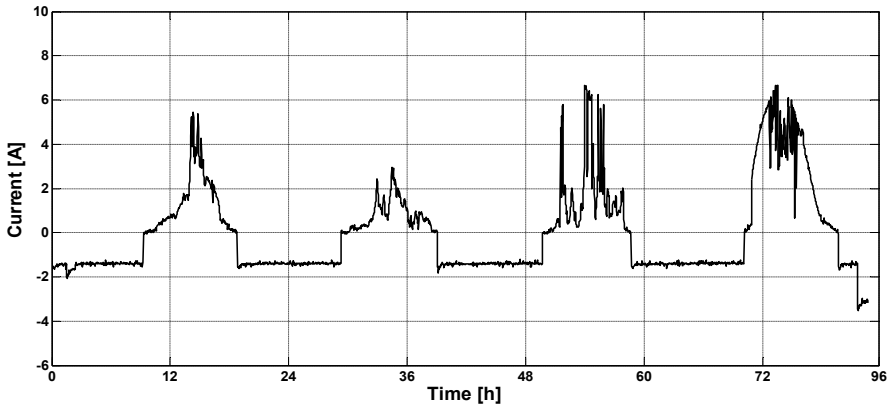
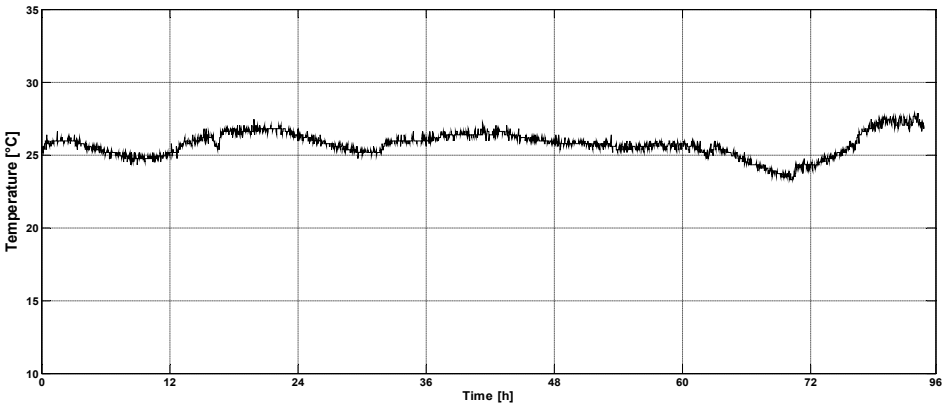


Figure 2.4 Control and estimation tools manager

(a)



(b)



Figures 2.5 Battery input measurements. (a) The battery current. (b) The ambient temperature.

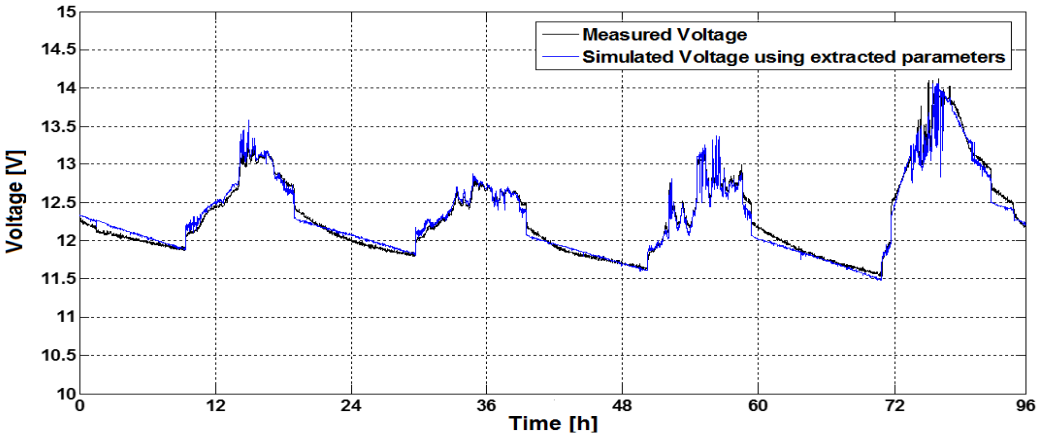
PV module characteristics		Battery's nominal parameter	DC Lamps
V_{oc}= 21.8 V	I_{mpp}=7.67 A	V_{bat} = 12V	V = 12V
I_{sc}= 8.17 A	P_{mpp}=135 W	C_{10} = 110Ah	P = 30 W
V_{mpp}=17.7 V			

Table 2.3 PV module, battery and the load characteristics

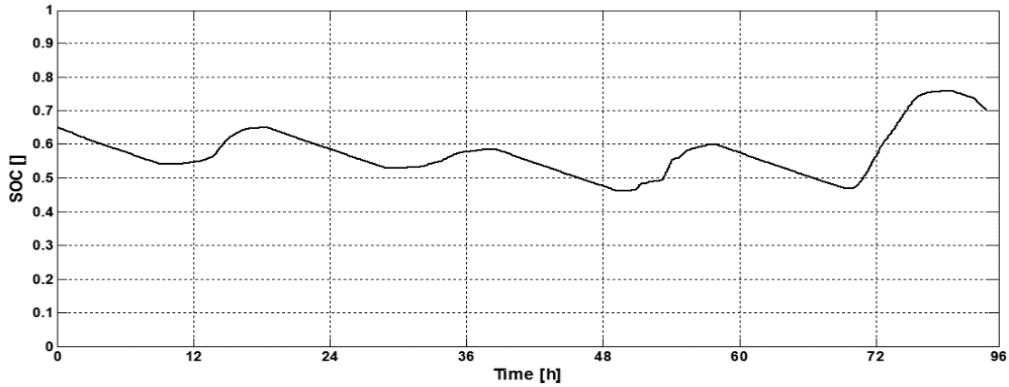
$C_{nominal}$=110 Ah	P_{1dc} = 9.5044 VAh	P_{1c} = 6.0809 VAh	K_{bodc}= 0.2190 V
C_{tcoef} =0.5361	P_{2dc} = 4.9361	P_{2c} = 1.6701	α_{rdc} = 0.0167° C^{-1}
α_c = 0.1320 °C^{-1}	P_{3dc} = 0.9311 V h	P_{3c} = 0.3375 VAh	K_{boc}= 0.16 V
β_c=0 °C	P_{4dc} = 0.037	P_{4c} = 0.9853	V_{bodc} = 2.1612 V
A_{cap}= 0.3031	P_{5dc} = 1.8837 Vh	P_{5c}= 1.7838Vh	
B_{cap} = 0.5027	V_{boc} = 1.9016 V	α_{rc} = 0.01° C^{-1}	

Table 2.4 Extracted parameter values by Levenberg–Marquardt algorithm

(a)



(b)



Figures 2.6 Battery output: (a) battery voltage. (b) Battery state of charge

2.3.2.1 Generation of initial population

GA program starts with a randomly generation of N chromosomes coded in binary in where each chromosome contains a group of parameters. The length of chromosome string M is given by Equation (2.22), where n is the number of parameters and N_b is the length of the sub-string, which represents a number of bits for each parameter in our case ($\alpha_0\ \alpha_1 \ldots . \alpha_{Nb-1}$). The length of integer part n of the vector Conv limits the search domain of GA in the decoding process as expressed in Equations (2.23, 2.24), where Pi is a parameter. The string of individual contains the parameters as shown in the Figure (2.9).a.

$$M = n \times N_b \tag{2.22}$$

$$Conv = \left[2^{n_i}\ 2^{n_i - 1} \ldots 2^0\ 2^{-1} \ldots 2^{(n_i - N_b + 1)} \right] \tag{2.23}$$

$$P_i = \left[\ a_0\ a_1 \ldots a_{N_b - 1} \right] \times Conv^T \tag{2.24}$$

2.3.2.2 Fitness

After decoding of the strings on parameters randomly generated in the precedent step, they will be placed in the model to calculate the mean error, which represents the cost function. The fitness value of each string is the solution of the parameters in the cost function f(x) to be optimized. Its value is mathematically expressed in Equation. (2.25); where f(x) is the mean error calculated by Equation (2.21).

$$Fitness(x) = \frac{1}{1 + f(x)} \tag{2.25}$$

2.3.2.3 Selection

In this process, the algorithm chooses the chromosomes that participate as a parent in the reproduction to give birth to a child in the next generation. All chromosomes of the population can be chosen, but that corresponds to the good fitness has strongest probability. The roulette wheel selection method, presented in Figure (2.9).b, is used. This method calculates the selection probability P_s of each chromosome. It is obtained by the cumulative

sum of the fitness orderly relative to the sum of all fitness S as shown in Equation. (2.26). P_r is a probability randomly generated for drawing [44-45]. The first chromosome corresponds to $P_r < P_s$ is selected for the next generation (Crossover, Mutation).

$$P_s(i) = \frac{\sum_{k=1}^{i} Fitness(k)}{\sum_{j=1}^{N} Fitness(j)} \tag{2.26}$$

Where: j is a counter varies from 1 to N (number of population) and k is a counter that varies from 1 to the current individual.

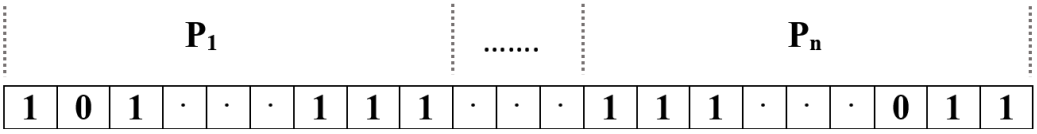
2.3.2.4 Crossover

In this step, the algorithm generates a children from the chromosomes selected as parents in the precedent step by performing a crossover two by two. To draw chromosomes for crossover, P_r is a probability randomly generated. If the parent have a probability $P_r < P_c$, it will be chosen for the crossover. P_c is the probability of crossover. Otherwise, it keeps the same bits for the next generation. The method used is the crossover by point. It consists of randomly choosing one point in the string, then the part after these points are simply swapped as illustrated in Figure (2.9).c.

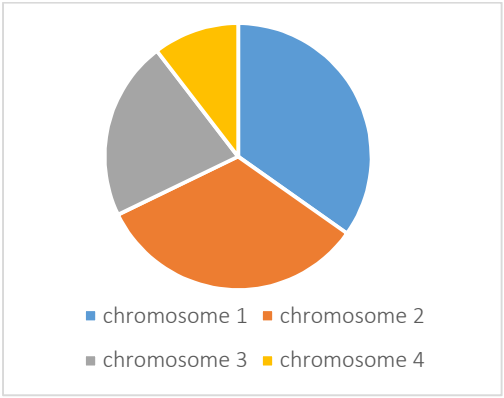
2.3.2.5 Mutation

In a random manner and with a low probability P_m, this operator introduces a change in some characters of the chromosome namely mutation. This change explores all of the search space and made another change if the initial generation does not fall in the global optimum. For a binary code of chromosomes, the bit changes from 0 to 1, and vice versa. To draw the character that will be affected by the mutation, we generate randomly a probability P_r for each character. Then, the one, that corresponds to $P_r < P_m$, is selected. When P_m is the probability of mutation taken by experience. Figure (2.9).d illustrates the processing of this operator.

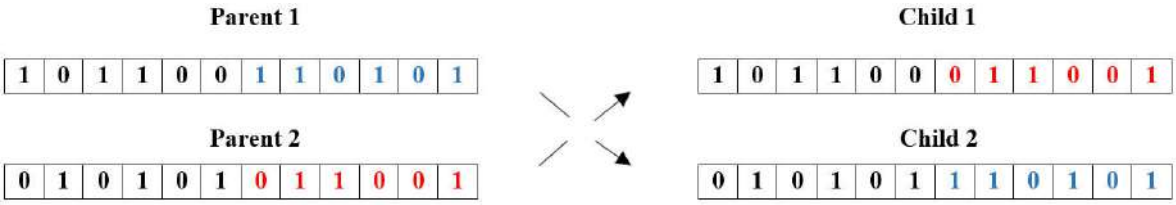
The developed identification process for the battery model parameters is given in the organogram of Figure (2.10).



a. Individual string



b. Example of the roulette wheel



c. Crossover operation



d. Mutation operation

Figure 2.7: Genetic algorithm steps

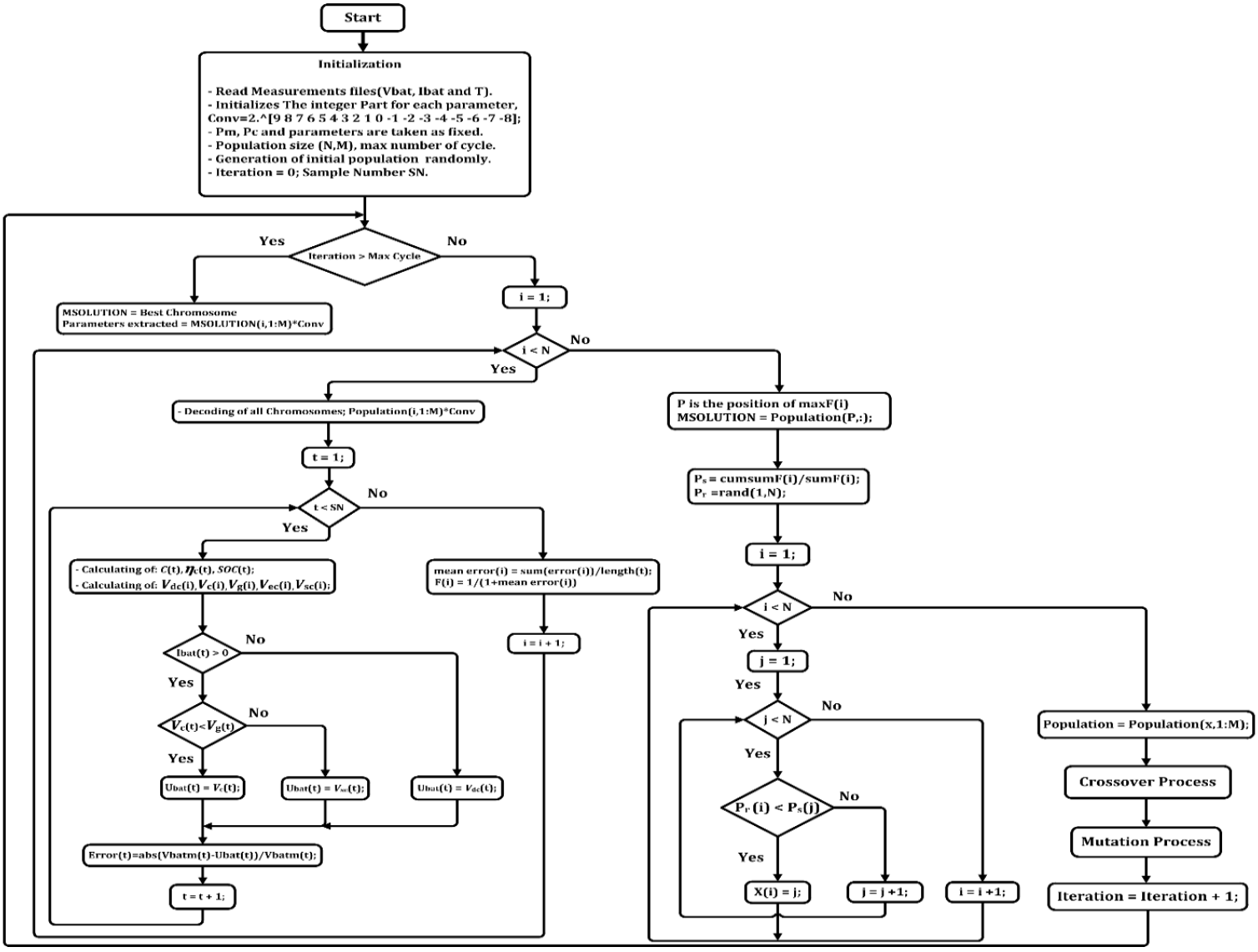


Figure 2.8. Flowchart of GA applied for parameters extraction process

GA parameters	Value
Number of cycle	100
Population length	500
Crossover probability	0.7
Mutation probability	0.2

Table 2.5. The GA parameters taken in program

2.3.2.6 Simulation results

The Simulation study has been carried out with the algorithm parameters given in Table (2.5). The characteristics of both PV module and battery used in the experiment are illustrated in Table (2.3). The parameters of the battery model proposed by CIEMAT used in the comparison study are given in Table (2.2).

Simulation running GA for parameters extraction of the battery model was carried out using real measurements for 2 days taking one sample every 1 minute. After 100 cycles (Table (2.5) and figure (2.11)) we get the following results. The figure (2.12) shows respectively the current provided by PV panel, the ambient temperature, the matching error and the mean error between the simulated model results and real measurements.

The new parameters extracted by GA are shown in Table (2.6), for those which are temperature independent and Table (2.7) for dependent temperature parameters.

Parameters	**Extracted value**	**Parameters**	**Extracted value**
SOC_0	0.7597	P_{1dc}	0.406 VAh
P_{1c}	7.234 Vah	P_{2dc}	3.041
P_{2c}	0.667	P_{3dc}	1.218 Vh
P_{3c}	0.078 VAh	P_{4dc}	0.7812
P_{4c}	0.492	P_{5dc}	0.484 Vh
P_{5c}	0.7421 Vh	V_{bodc}	2.148 V
V_{boc}	1.781 V	K_{bodc}	0.1270 V
K_{boc}	0.5313V	B_{cap}	0.513
A_{cap}	3.351		

Table 2.6: Extracted Temperature Independent Parameters

Parameters	**Extracted value**
α_c	0.0081 C^{-1}
C_{tcoef}	1.7871
α_{rdc}	0.0197C^{-1}
α_{rc}	0.43 $^{-1}$

Table 2.7: Extracted Temperature Dependent Parameters

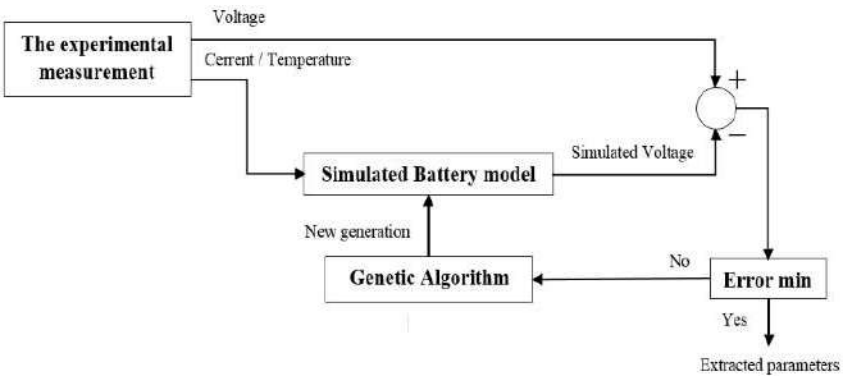


Figure 2.9. Parameters extraction process by GA

In order to validate the developed model in real conditions, different measurements provided by PV modules (Current and Temperature) for different days are taken as battery input to compare the measured terminal battery voltage with that given by both the developed and the former CIEMAT models. A simulation was done with the lead-acid battery model taking the new extracted parameters after applying a GA, and for a real current and temperature measure provided by the PV panel in different regimes (charge and discharge). We note that the energy provided by the PV system varies randomly due to the continuous change of radiation and temperature which gives a validation of the model in real condition. Figures (2.13) show both the current provided by PV model that passes through battery and ambient temperature for three measurements in different days.

Figures (2.14) show the simulation provided by the improved battery model with extracted parameters using GA, compared with the experimental measurement and the simulation model with parameters given by CIEMAT in Table (2.6) and (2.7). It is visible that the improved model with new extracted parameters presents a good matching with the measurement according to the model with the former parameters and gives a lowest mean error as depicted in Table (2.8). Furthermore, Table (2.8) presents a comparison between the mean errors obtained by simulation with parameters extracted using GA and simulation results from nominal parameters.

Simulation	**1**	**2**	**3**
Mean error with parameters given by CIEMAT	1.54 %	1.84 %	1.52%
Mean error with parameters extracted by GA	0.50 %	0.48 %	0.46 %

Table 2.8 Mean error simulated vs measured Voltage

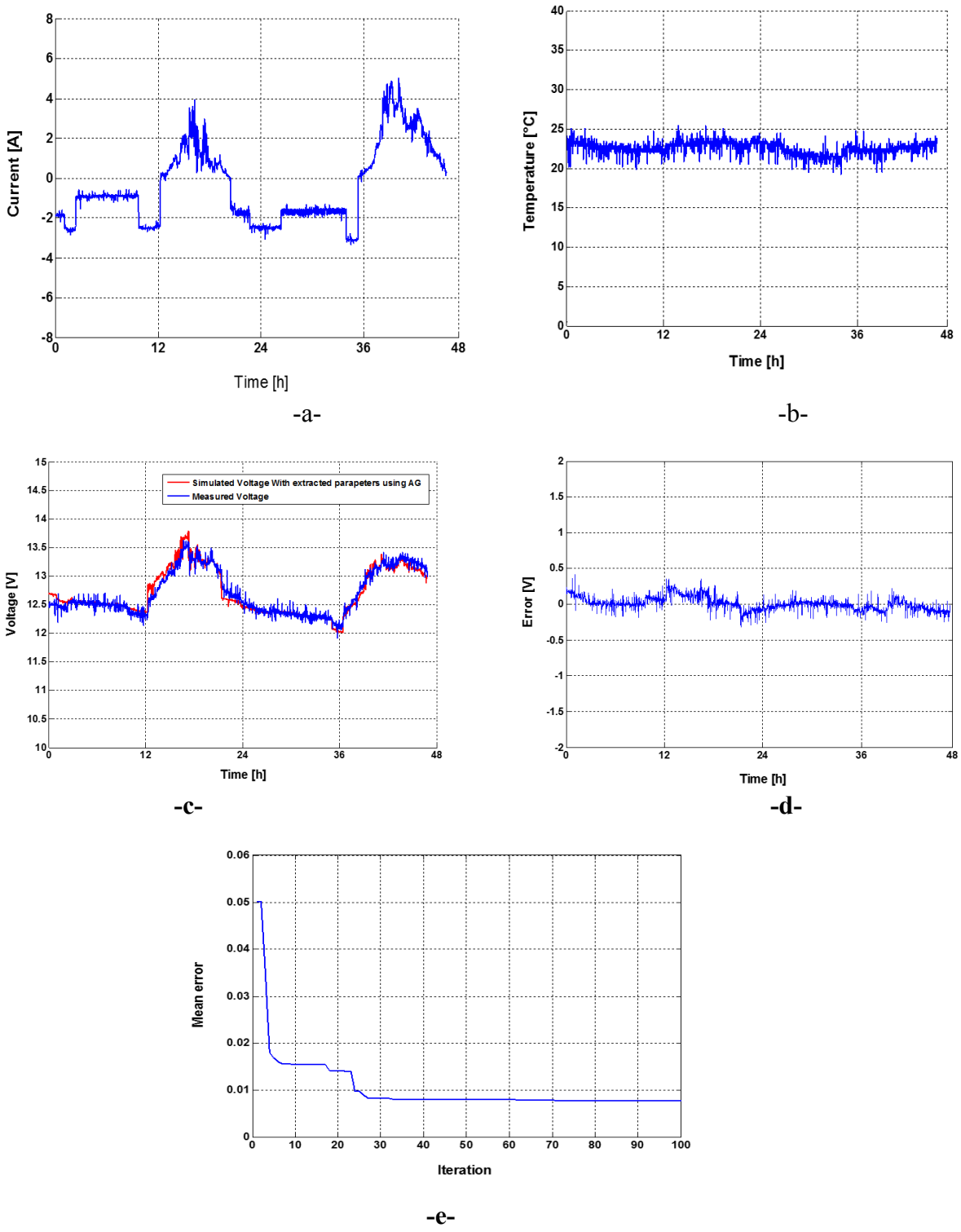


Figure 2.10. Simulation and experimental results: -a- Battery current measurement provided by PV module **-b-** Ambient Battery Temperature measurement **-c-** Measured and Simulated Battery Voltage **-d-** Error between Measured and Simulated Battery Voltage **-e-** The evolution of Mean Error.

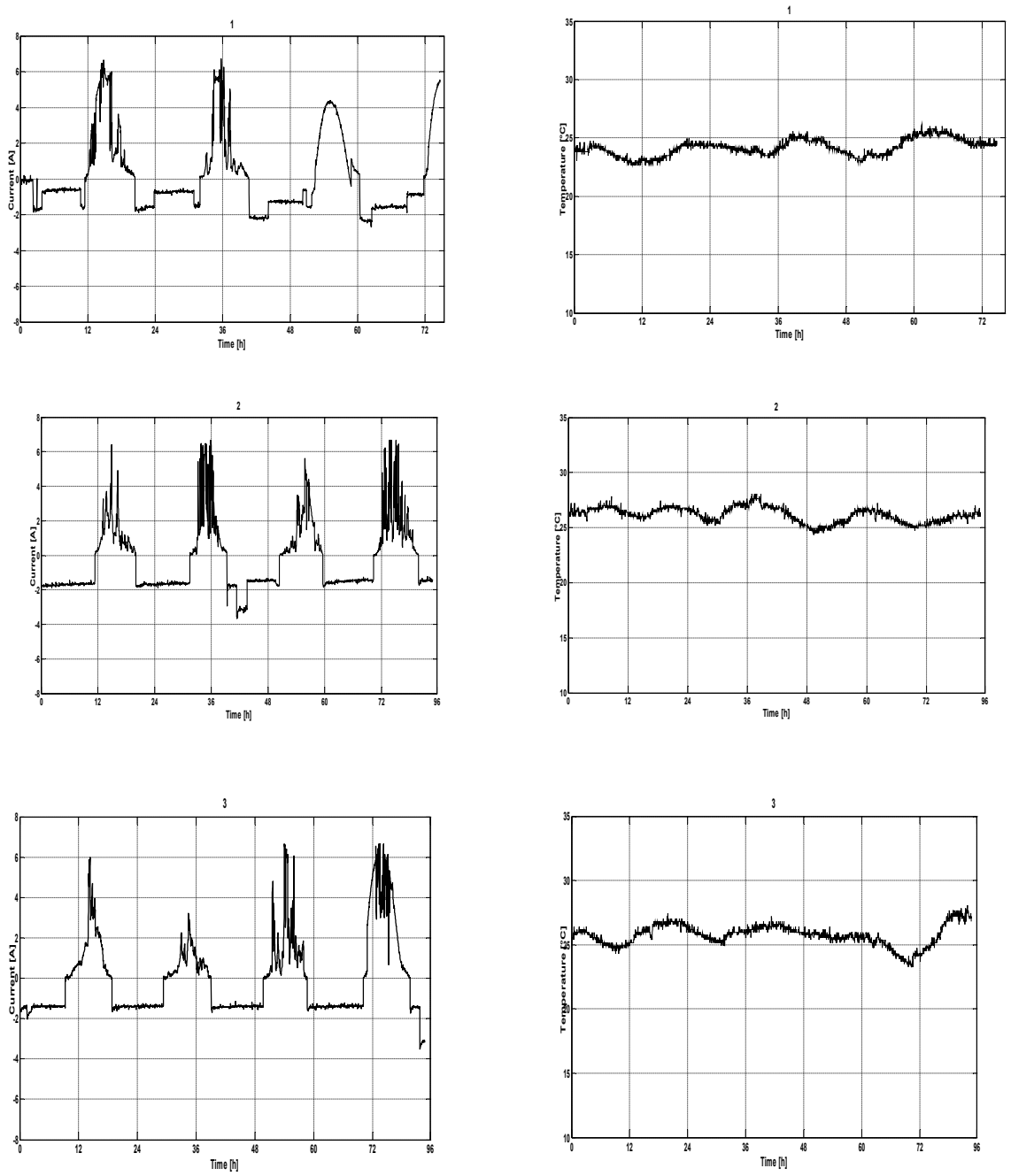
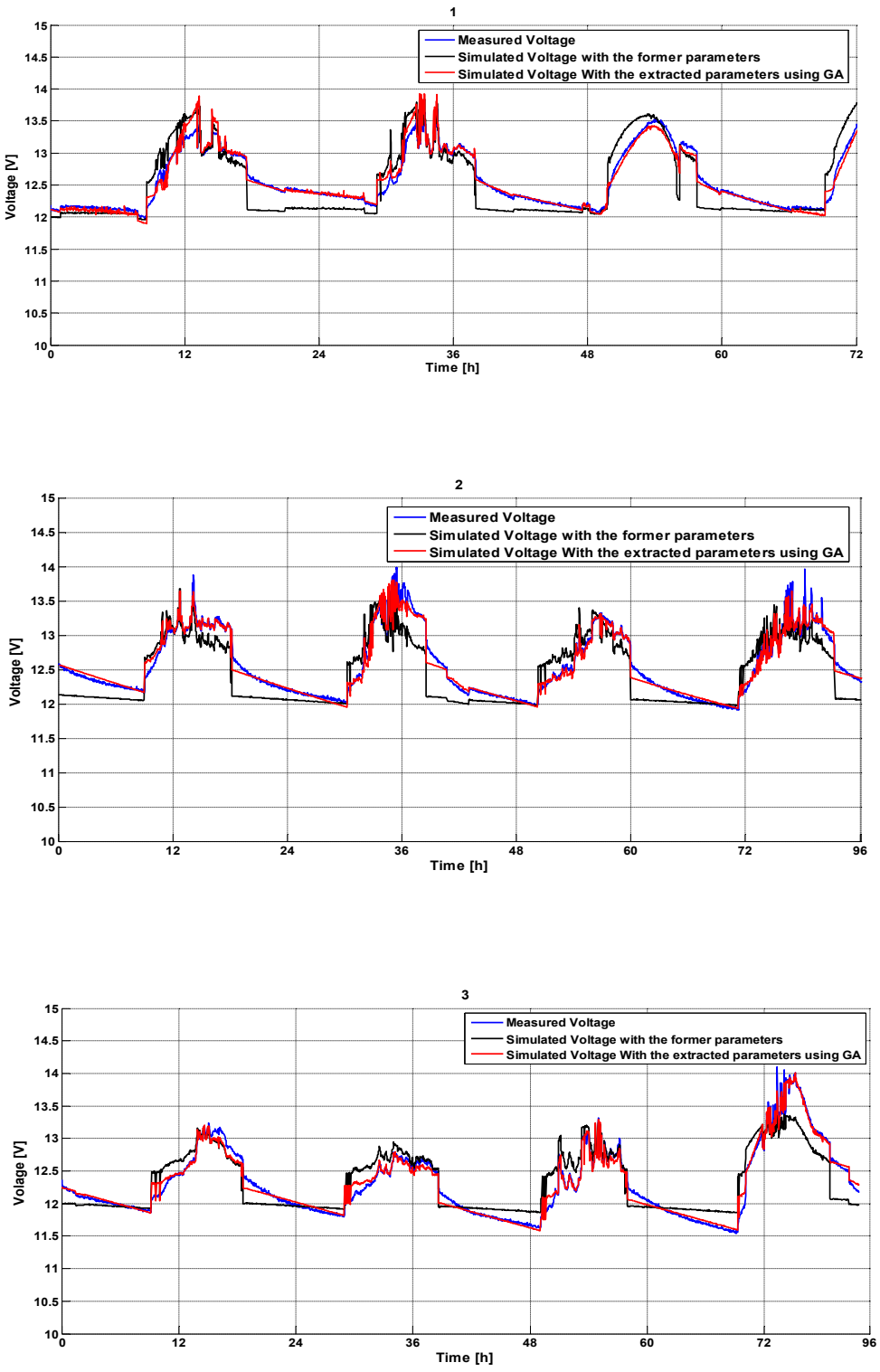


Figure 2.11. Battery current and Ambient Temperature measurements provided by PV modules

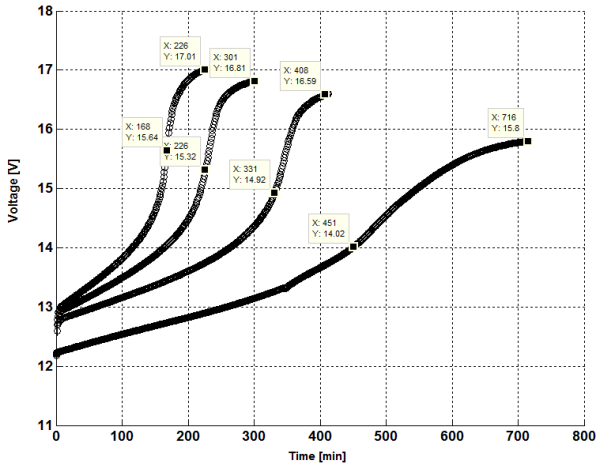
Test 1: three days Test 2: four days Test 3: four days



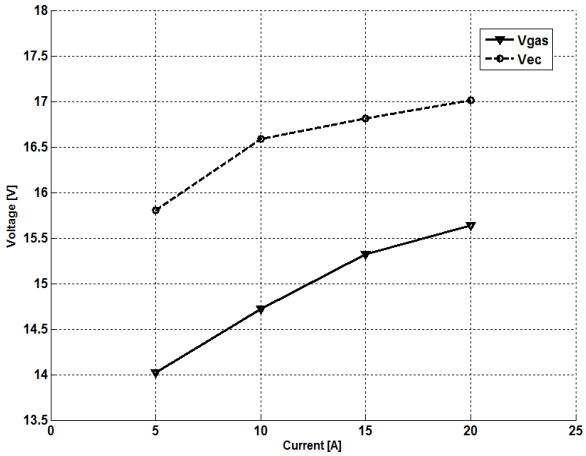
Figures 2.12. Battery voltage measurements of three experiments and simulation results obtained by genetic algorithm extracted parameters and by former parameters

2.4 Extraction of gassing and saturation voltage parameters

As is described above in Equations (2.10, 2.11), the gassing and saturation voltage level varies strongly as function to the charge current, therefore, in these steps, we considered the variation of gassing and saturation voltage according to the Current in the charge and overcharge zones. From the static practice test illustrated in Figures (2.15) (a) and (b) where the battery was charged by different constant currents for 5, 10, 15, 20 A, we identified approximately the parameters of voltage equation in these areas (gassing and saturation) using GA. This approach allows estimating this dangerous area (Overcharge) in order to avoid it in the real time control and monitoring.



-a-



b-

Figures 2.13 battery gassing and saturation level. –a- Battery charge Voltage for different Current. –b- Variation of the gassing and saturation voltage as function to charge current.

After applying the GA in the static approach, we arrived to identify an approximate four parameters of the gassing and saturation voltage zones in Equations (2.10) and (2.11). Table (2.9) illustrates the new parameters in this area.

Parameters	Extracted value
A_{gas}	2.3101 V
B_{gas}	1.8902 Vh
A_{fonse}	2.5102 V
B_{fonse}	2.1103 Vh

Table 2.9: Extracted parameters of overcharge area

The improvement of CIEMAT model using parameters extraction by GA gives a high ability to represent the battery behavior with the continuous variation of the Current (charge and discharge) and temperature. The matching with real measurements is considerably checked if we compare the mean error calculated for different experiences according to the former parameters. This makes model accurate and satisfactory, which will solve many problems of simulation or management in the PVS especially in stand-alone systems.

2.5 Conclusion

In this chapter we have proposed an enhancement of CIEMAT model by automatic extraction parameters, in the first step an improvement of 21 parameters by Levenberg-Maquart using toolbox in Matlab/ Simulink have been done, in the second step an enhancement of this model have been done by using genetic algorithm. Furthermore, we have proposed an improvement of 4 parameters to estimate approximately both gassing and saturation levels through the use of new static method. The improved model has been validated by comparing with both real measurements and the former CIEMAT model. The new model shows a good agreement and low mean error comparing with previous model.

CHAPITRE III

BATTERY MONITORING, MANAGEMENT AND REAL TIME ACQUISITION

CHAPITRE III

BATTERY MONITORING, MANAGEMENT AND REAL TIME ACQUISITION

3.1 Introduction

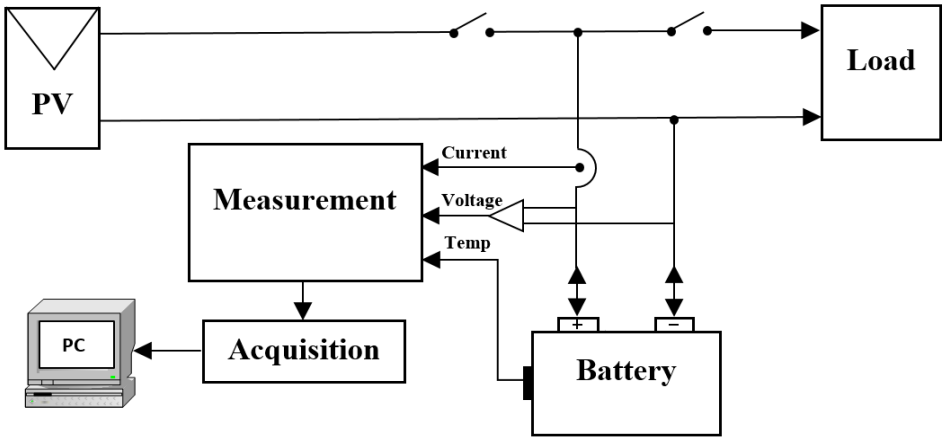
As described previously, the working condition of the battery affects its behavior and its robustness; where the areas that the battery is employed as storage device is still a critical issue. Furthermore, the battery has a limited lifetime in which it cannot offer sufficient power/energy after its capacity degradation, where it should be replaced after a certain time. Therefore, the management and the monitoring based on the good estimation of its state of charge, leads to extend the battery lifetime and benefit to its full capacity. For this purpose, we propose in this chapter a real time monitoring interface using LabVIEW software, as well as real time validation of the improved model by acquisition of real input measurements (Current, temperature) for comparing the output model with real measured voltage .

3.2 System description and test bench

As depicted in Figure (3.1) –a-, the system used in the proposed modeling and monitoring is formed of: simple stand-alone PV chain composed of one solar panel of 135 Watt power, battery of 110 Ah and DC lamps used as load. The monitoring has been carried out by using a simple computer, acquisition system for measuring of the current, temperature and voltage. For showing the evolution of all battery' characteristics in real time manner, LabVIEW language has been used for simulation and validation of the developed model taking real time measurement of current, temperature and voltage as input. Figure (3.1).-b- illustrates the experimental test-bench.

3.2.1 Measurement and acquisition

For the real time validation and monitoring of the battery behavior, three necessary variables are considered to be measured. Current and ambient temperature have been measured as inputs of the model implemented in LabVIEW language; hence they are used to calculate the battery state of charge (SOC) and the instantaneous capacity. Moreover, the battery voltage has been measured for the comparison with the output given by the improved model. The NI_USB 6008 acquisition card is used for associated with the PC (Figure 3.2).



-a-



-b-

Figure 3.1 –a- System description. –b- The test bench

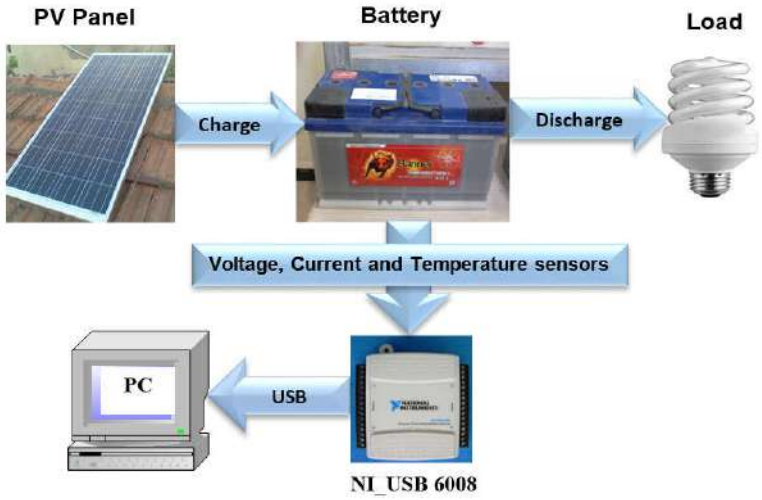


Figure 3.2 PV system and data acquisition

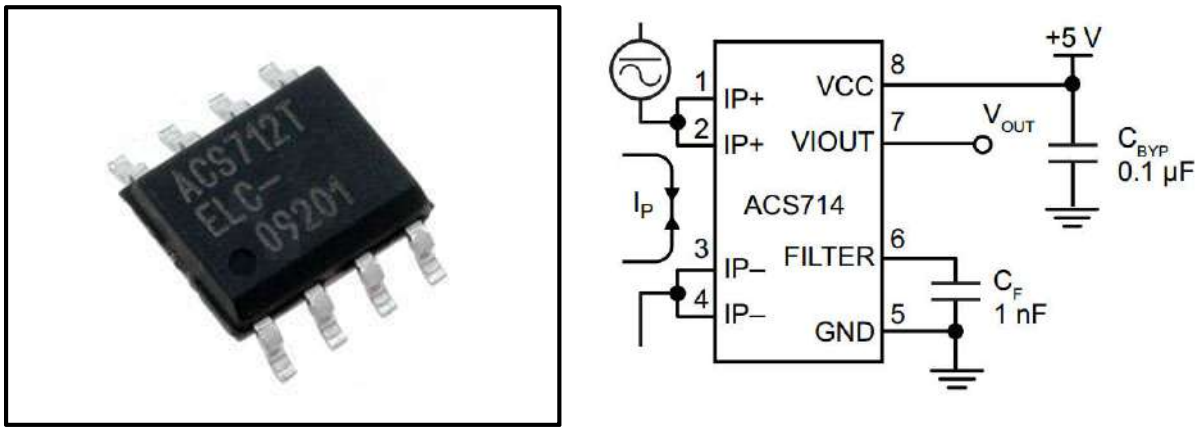
3.2.2 The sensors

In the acquisition board, three sensors have been used; for the measuring of the battery voltage, the LEM LV 25-P sensor is used. The Hall e ect ACS 712 sensor and the LM335 sensor have been used for the measurements of the current and the temperature respectively. For each measure, a signal conditioning circuit based on operational amplifier is used for making the signals compatible associated with the PC.

3.2.2.1. Current measuring

For the measurement of current that passes from and to the battery, the ACS 712 Hall effect sensor is used. This linear sensor provides a good precision and low-offset. In addition to its low cost, the ACS712 contains a signal conditioner that allows to avoid the addition of other circuit. Figures (3.3) shows the simple pinout where this sensor requires only a 5 volt supply voltage and capacitor as filter.

As is described in figure (3.4), the sensor used accepts -20/+20 A as maximum current and provides a positive output voltage contains an offset in the range of [0, 4.5] volt with a linear characteristic. For more details the datasheet of this sensor is given in [76].



-a- **-b-**

Figures 3.3 ACS712 sensor: -a- the sensor design. -b- the sensor pinout

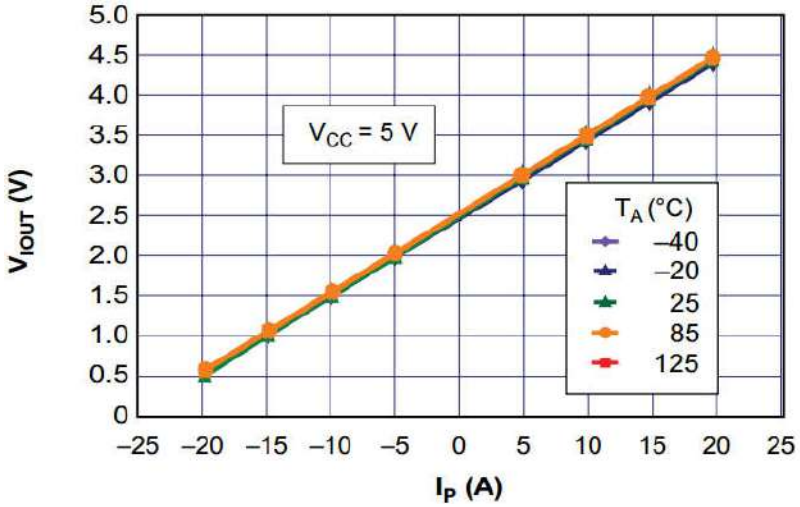
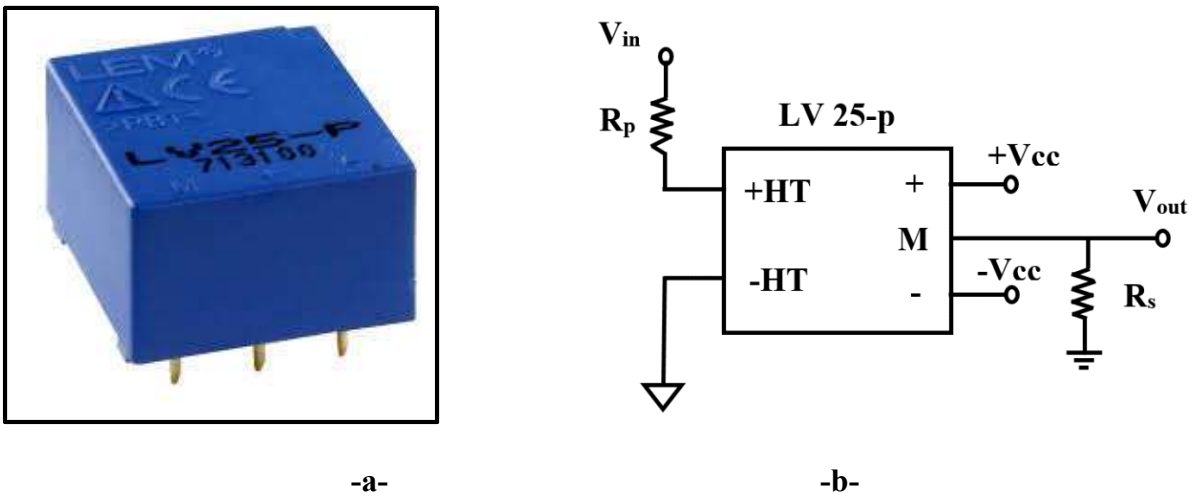


Figure 3.4 Input output characteristic.

3.2.2.2. Voltage measuring

For the measurement of the battery voltage, the LEM LV 25-P sensor is used. This sensor provides an excellent accuracy, good linearity, optimized response time and wide frequency bandwidth. The LEM LV 25-P accepts a primary current less than 10 mA, therefore an adequate primary resistance should be chosen according to the maximum measured voltage. Also, this sensor requires a +/-12 V or +/-15 V supply voltage. Figures (3.5) (a) and (b) show the design and the out pin of this sensor respectively. For more details the datasheet of this sensor is given [77].



-a- -b-

Figures 3.5 LEM LV 25-P sensor. -a- the sensor design. -b- the sensor pinout

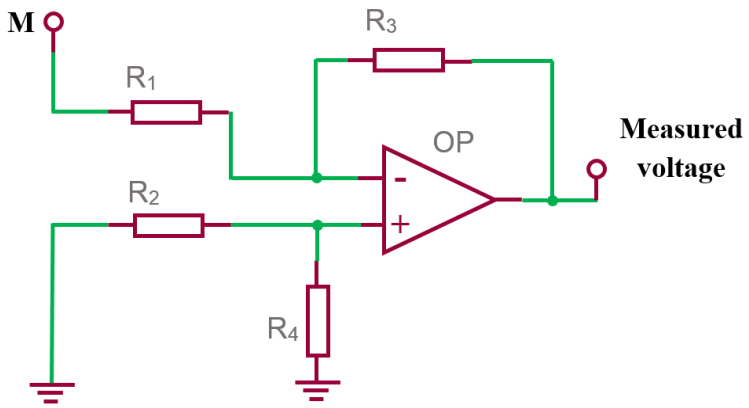


Figure 3.6: the differential amplifier

In order to amplify the measured voltage provided by the sensor and obtain a real potential difference, a classical differential amplifier circuit is added in the output of the voltage sensor based on operational amplifier and resistor. The figure (3.6) shows the used signal conditioning circuit.

3.2.2.3 Temperature measuring

For the ambient temperature the LM335 sensor is used. This sensor is an accurate sensor and can be easily calibrated. This linear sensor provides a low voltage proportional with the temperature with a factor of +10 mV/K. It can works from -40°C to 150 °C under current vary from 400 µA to 5 mA and provides 2.28 V voltage at 25°C. The most common broaching used with this sensor as given in figure (3.7) (b). Figure (3.7) (a) shows the design of this sensor. At 25°C and for a current of 1mA, the typical value of the voltage is 2.98V. Then, the resistance R1 should be calculated according to the V_{cc} supply in which the sensor is traversed by a current of 1 mA. Therefore, the resistance R1 is given by the following expression:

$$R_1 = (\mathrm{Vcc} - 2.98) / 1\mathrm{mA} \tag{3.1}$$

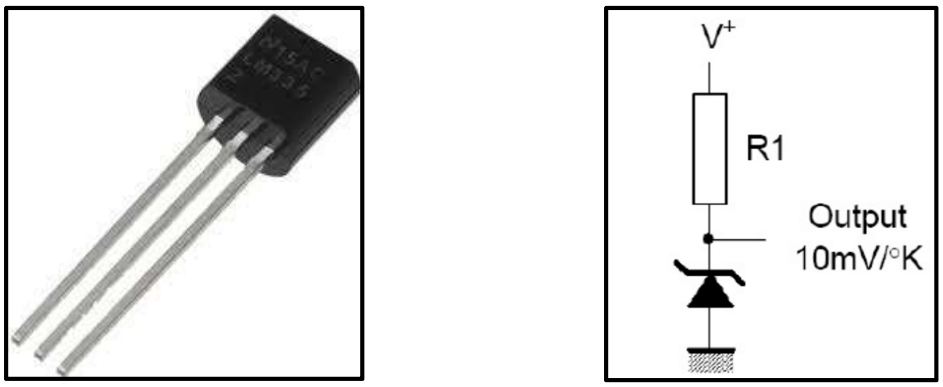
The relationship between the voltage and temperature is given in the following equation (3.2):

$$V(T) = V(T_0) + 0.01 \times (T - T_0) \tag{3.2}$$

Where: V(T) is the voltage provided by the sensor, T is the ambient temperature and $V(T_0)$ is the voltage reference for temperature T_0=25°C, $V(T_0)$= 2.98V. Then the temperature is given by the expression (3.3). For more details about this sensor the datasheet is given in [78].

$$T(°C) = 100 \times V(T) - 273.15 \quad (3.3)$$

For amplifying the measured voltage provided by the sensor and obtaining more accuracy, a classical differential amplifier circuit is added in the output of the voltage sensor. It is the same differential amplifier given in the figure (3.6).



-a- **-b-**

Figures 3.7 -a- the LM335 design. -b- the LM335 broaching used.

3.2.3 Supply circuit

In order to provide the supply voltage for the used sensors, a supply circuit has been realized that is composed of 220/24V transformer, rectifier and regulators. This supply provides +/-12 Volt for the LEM LV 25-P voltage sensor and also for the polarization of the operational amplifier used in the signal conditioning circuits. Supply of 5 volt is provided also for the V_{cc} of the ACS712 current sensor and the LM335 temperature sensor. The figure (3.8) shows the circuit of the realized supply. The measurement board of current, voltage, temperature and the supply circuit is shown in the figure (3.9).

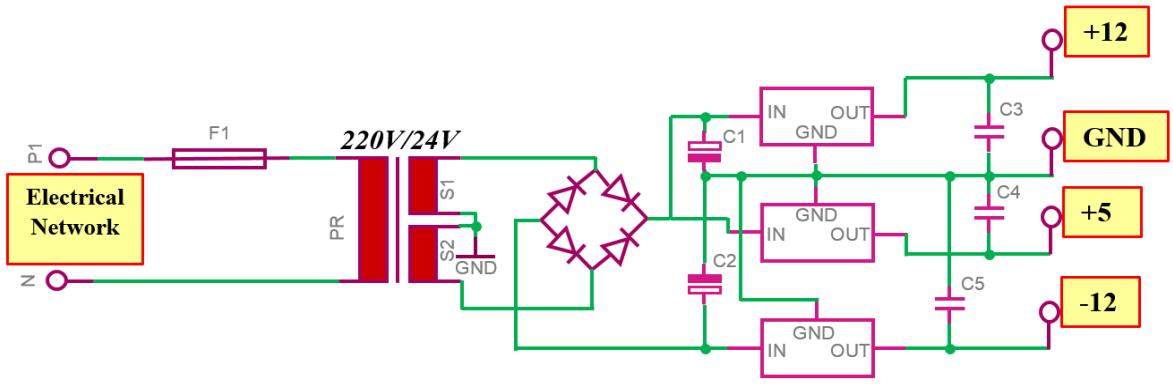


Figure 3.8 Supply circuit design.

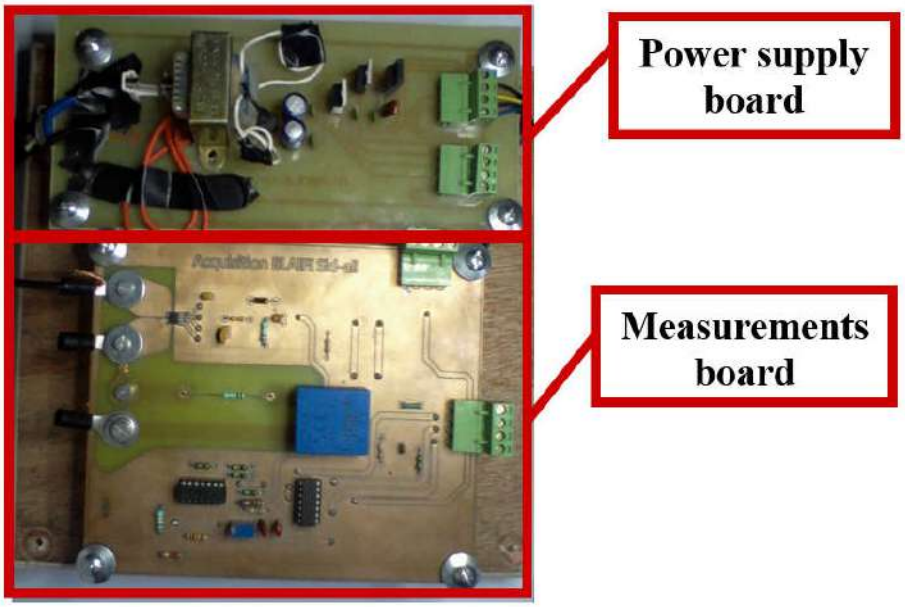


Figure 3.9 Measurements and power supply boards

3.2.4 Acquisition

The acquisition of data has been carried out by using NI-USB 6008 multiplexer manufactured by National Instruments. This module contains eight Single-Ended signal channels and four Differential input in which the interfacing with the PC was done by using LabVIEW Language through USB. The Figure (3.10) shows the NI-USB 6008 multiplexer used for the data acquisition. For more details about this card, the datasheet is provided in [79].

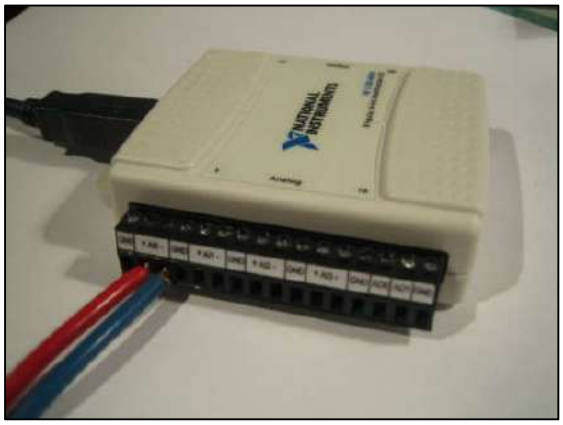


Figure 3.10 NI-USB 6008 multiplexer data acquisition.

3.2.4.1 Acquisition and calibration in LabVIEW language

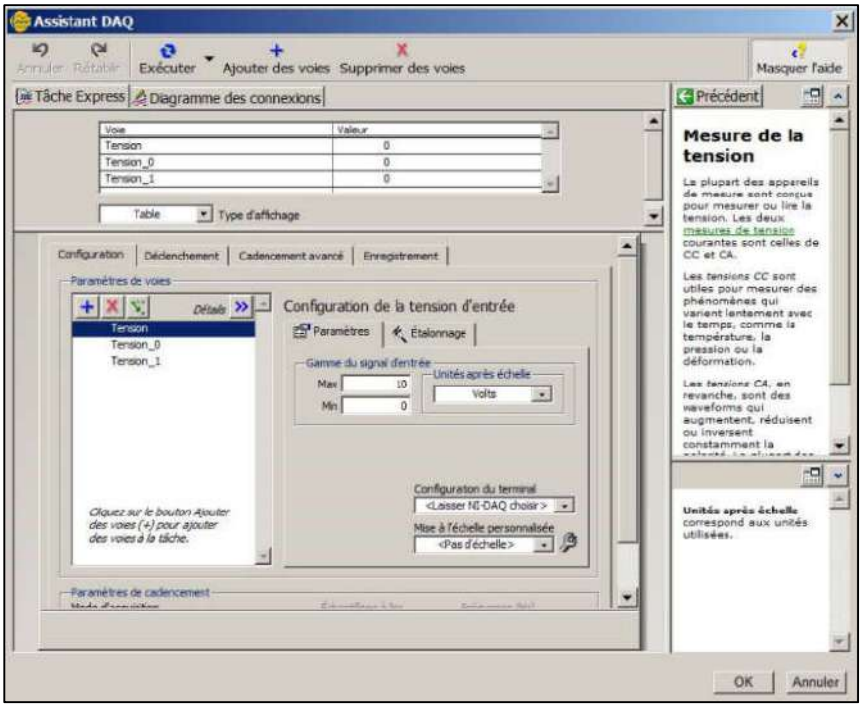
The software acquisition has been carried out with LabVIEW language using DAQ assistant tool. This tool is adaptable with the NI-USB 6008 multiplexer to provide the analogue signal given by the input of this multiplexer as measurements. By the window of DAQ assistant tool shown in figure (3.11) (a) the type of reading and the input used are selected. Once the measurement signals is ready to read in the LabVIEW language, the calibration is done to make the measurements signal in their real values using simple calculating box. The screen shot in figure (3.11) (b) shows the VI program of the data acquisition.

3.2.4.2 Model implementation in LABVIEW

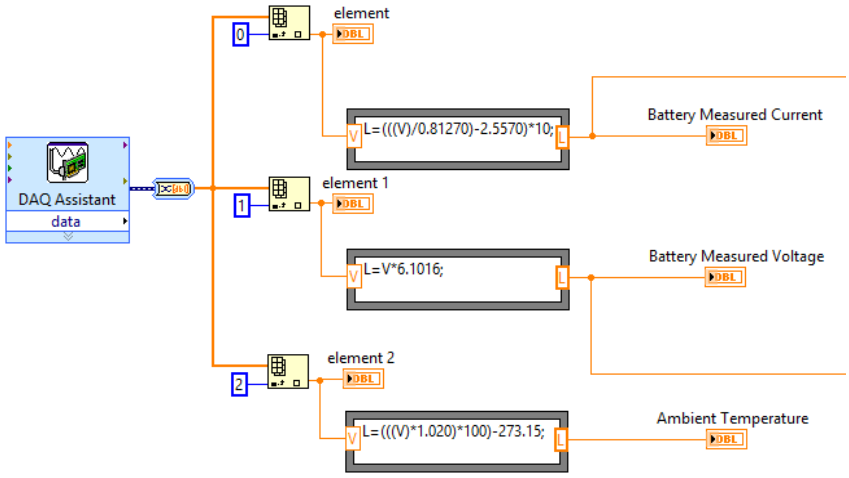
For the model validation in short term (without integration of the capacity degradation) and the setting up of supervision interface, the improved battery model has been implemented in the VI interface in LABVIEW using the calculating box as shown in figure 3.12 (a) . The diagram of Figure 3.12 (b) shows the simulation process which is used to predict and estimate of all battery characteristics behavior and its performance in real time. The acquisition provides the measurements of current, voltage and temperature to use them as model inputs and outputs. Furthermore, the estimation provides the whole battery variables such as: state of charge (SOC), Level of energy (LOE), instantaneous capacity (C) and gassing voltage level in the real time manner.

3.3 Model validation

For the validation of model, the real time comparison has been done between the output voltage or the model with the new extracted parameters Table (2-6) and the measured battery voltage in the charge and discharge mode using a new healthy battery. In dynamic manner, the model provides the charge and discharge equations according to the current direction. The obtained result presents a good matching and lowest absolute error between simulated and measured voltage as is shown in the Figures (3.13) (a) and (b) respectively. The gassing voltage is also estimated in order to provide approximately information for the voltage working when the battery crosses this dangerous area. We note that the gassing voltage is considered only in the charge mode.

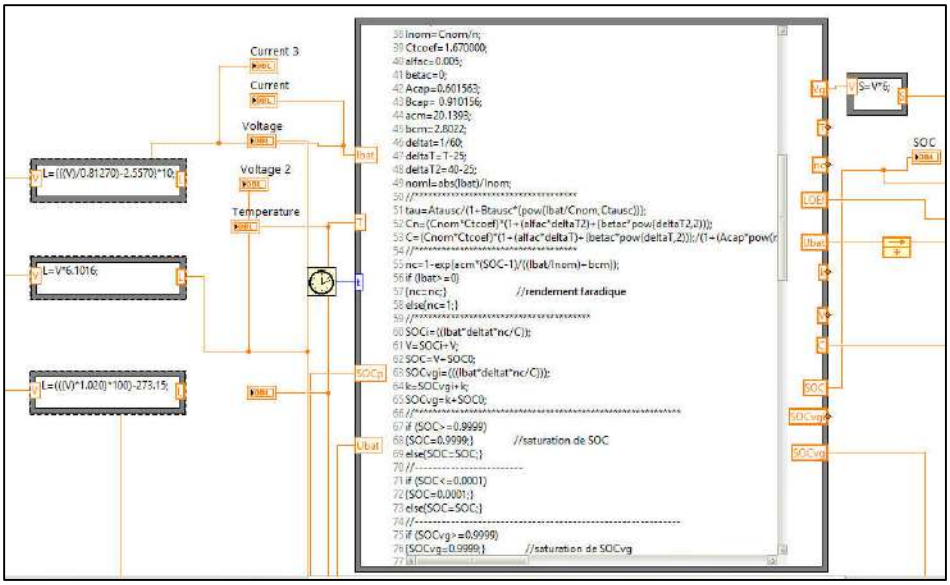


-a-

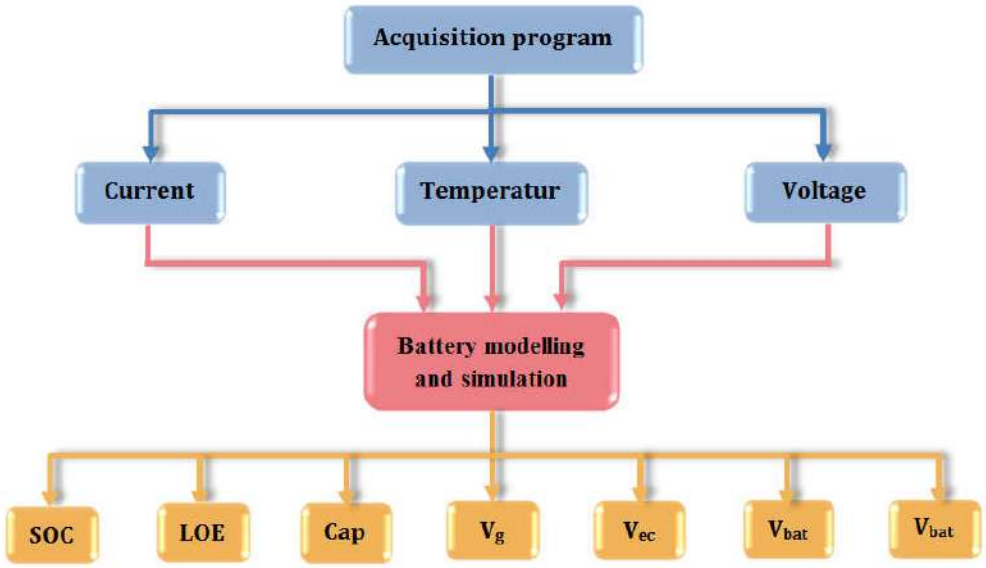


-b-

Figures 3.11: -a- DAQ assistant tool window. -b- VI diagram for acquisition

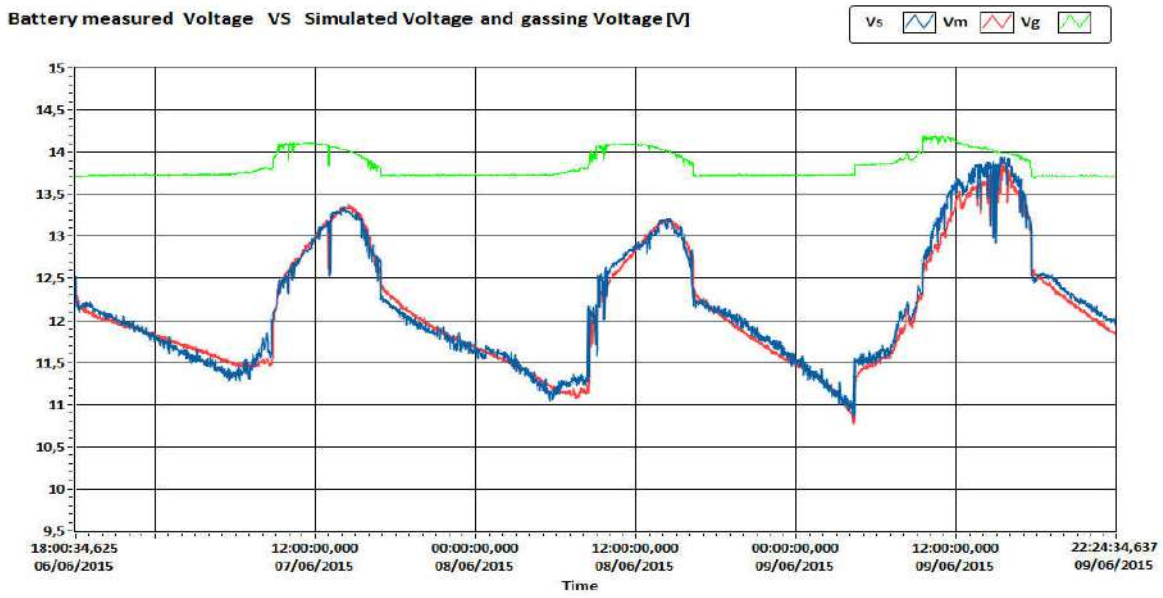


-a-

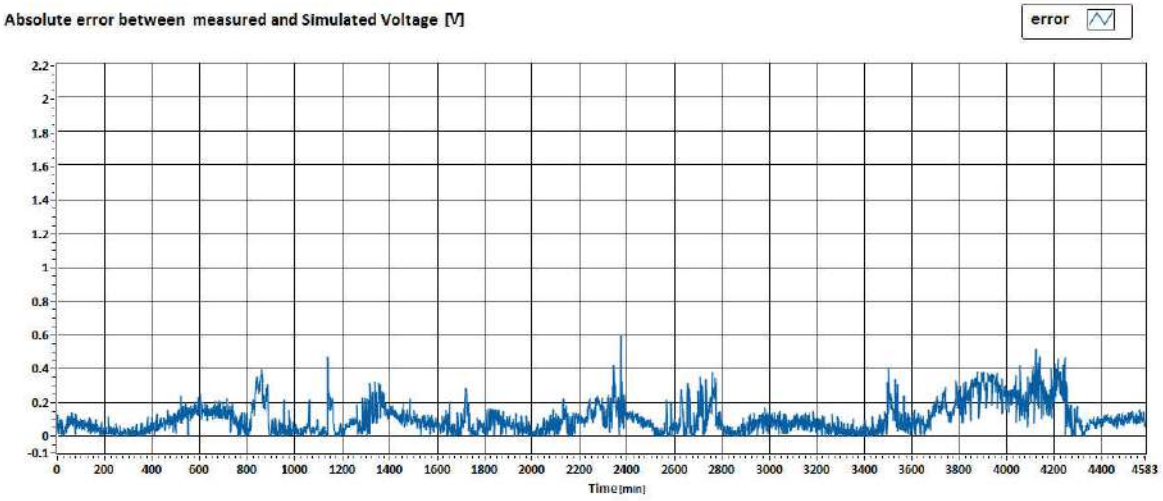


-b-

Figures 3.12: -a- VI diagram for the model implementation. -b- Synoptic Diagram of Simulation process



-a-



-b-

Figures 3.13: -a- Measured vs simulated voltage and representation of gassing voltage.
-b- Absolute error of measured vs simulated voltage

3.4 Monitoring and Simulation LabVIEW interface

In the following front panel, the implementation of the model provides an interface which gives information for different battery variables and characteristics. As is illustrated in Figure

(3.14) taking by a screen shot, the window provides much information for the battery working in real time. The user can observe and control the characteristics of battery such as: the battery current provided by PV panel, battery state of charge estimated by model, ambient temperature, and battery measured voltage and the instantaneous capacity estimated by the model as is shown in Figures (3.15).

3.5 Conclusion

In this chapter, we have proposed a real time monitoring by simulation of the developed model using LabVIEW language. Thus provides online estimation and measurements of all battery data and characteristics in stand-alone photovoltaic system by real time interface. Furthermore, a validation of the model has been proposed in this section. Moreover, the proposed robust and low-cost method of simulation and monitoring can be applied for the study of battery fault detection in photovoltaic systems.

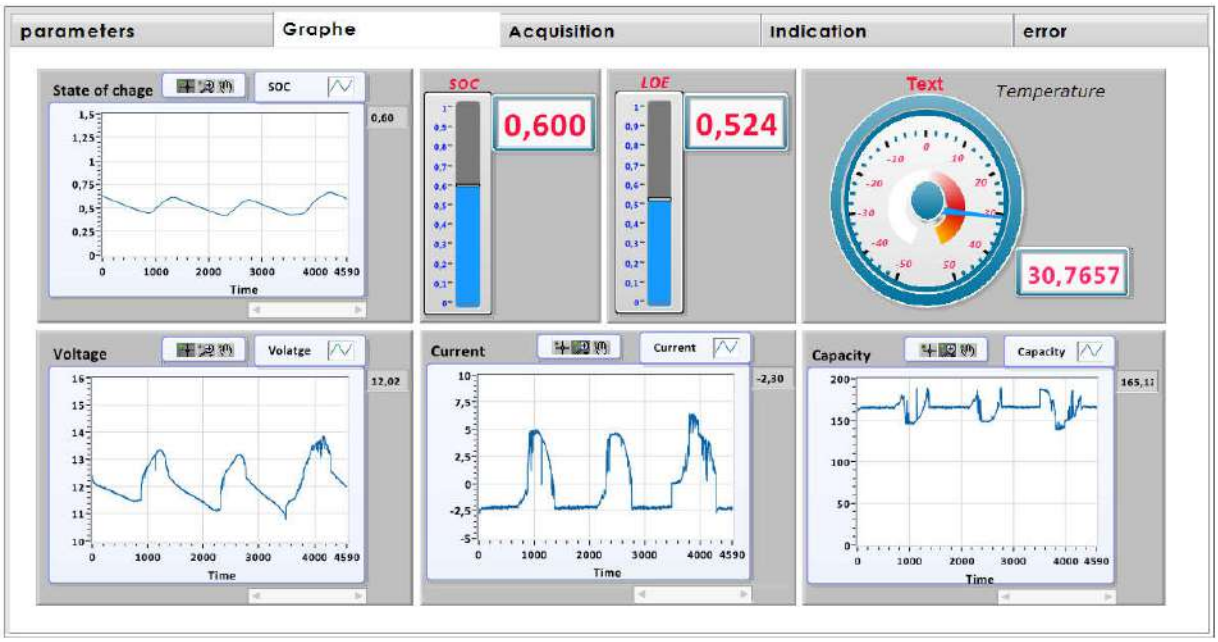
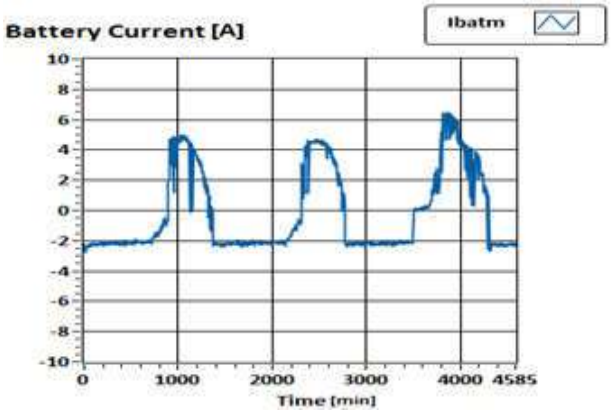
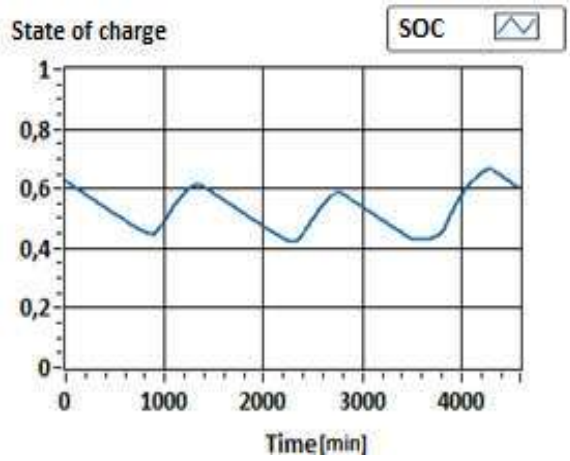
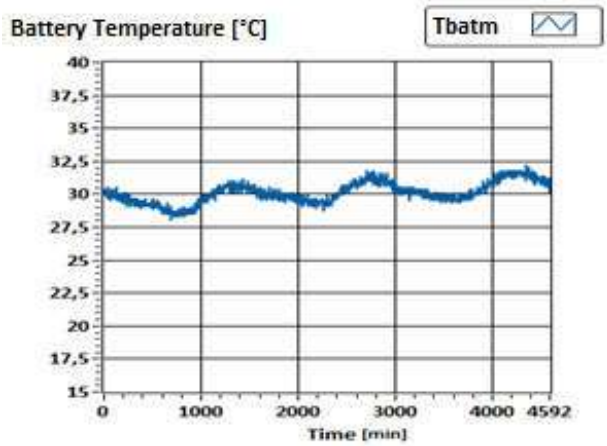


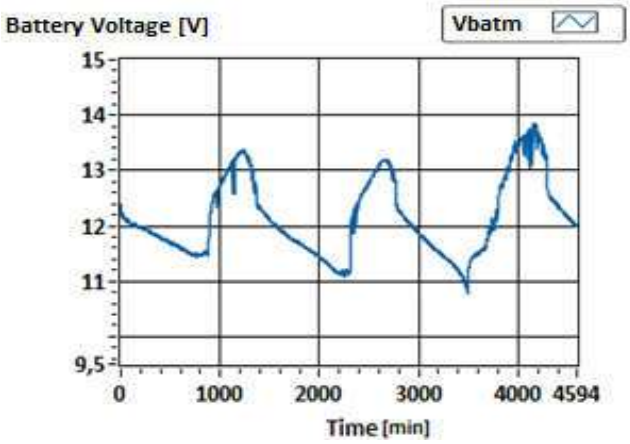
Figure 3.14: LabVIEW monitoring interface.



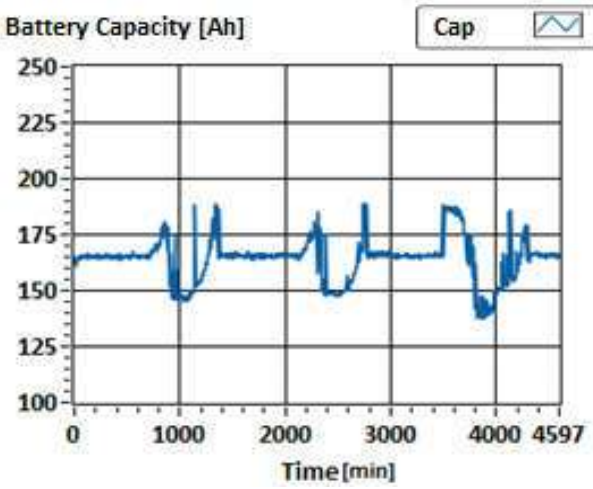


-a- **-b-**





-c- **-d-**



(e)

Figure 3.15 LabVIEW monitoring experimental curves: (a) The measured battery current, (b) Battery state of charge estimated by model, (c) ambient battery temperature measurement, (d) Battery measured voltage, (e) instantaneous Capacity estimated by the model.

CHAPTER IV
DEVELOPMENT OF NOVEL MPPT AND BATTERY CHARGE CONTROLLER

CHAPTER IV

DEVELOPMENT OF NOVEL MPPT AND BATTERY CHARGE CONTROLLER

4.1 Introduction

In addition to its low energy conversion efficiency, the photovoltaic modules in any configuration present a nonlinear power characteristic depending strongly on the continuous change of irradiation and temperature, where the load must be adapted in which the module working in the maximum power point (MPP). Therefore, in this chapter we propose a new fast maximum power point tracker (MPPT) by modeling of the fuzzy logic algorithm using M5P model tree. Furthermore, in the second section we propose a novel battery charge controller integrates the new MPPT.

4.2 The proposed algorithm for the MPPT

In the purpose to develop a fast and robust maximum power point tracker (MPPT) algorithm, we propose a novel modeling of fuzzy MPPT by M5P algorithm. Thus it gives simplicity and high speed progress in the implementation. Based on the input and the output data given by fuzzy MPPT algorithm, a non-parametric model is extracted by the M5P algorithm. This allows minimizing the algorithm complexity and improving the speed of the algorithm. The training of the model has been carried out by using Weka software. The dataset used to train the model is based on the fuzzy logic algorithm as shown in Figure (4.1). To create this dataset, we firstly run the simulation of control algorithm for tracking the maximum power point for a solar panel which is based on the use of the fuzzy logic and save the data collected in 20 milliseconds. The selected attributes are the error, the variation of the error and the target that represents the output of the fuzzy logic. The dataset contains 20000 samples directed for the training and testing the model. 66% of the dataset used for training of the model, means that 13200 are used for the training phase and the remaining data are used for test of the model. The phase of data preprocessing in this case is passed because the data set are obtained by the simulation.

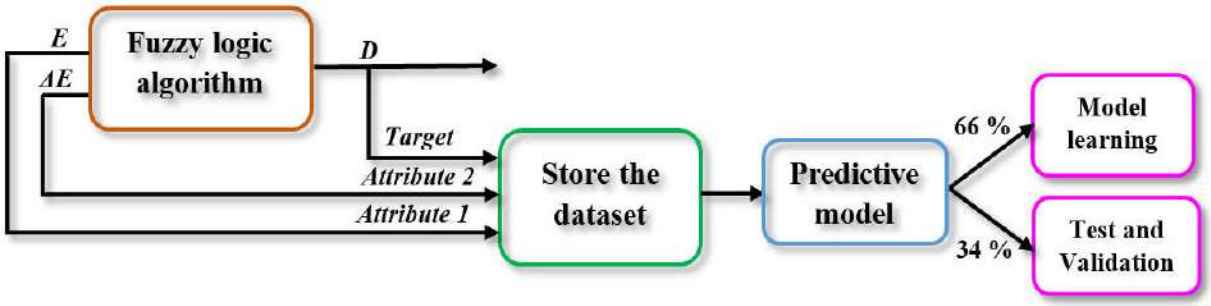


Figure 4.1 The dataset stored for modelling

As shown in figure (4.2), the system is composed of PV panel with the characteristics given in the table (4.1), single DC/DC boost converter as an interface between the PV panel and the proposed algorithm that provides the duty cycle D for the control of the IGBT by PWM signal. The DC/DC parameters are given in the table (4.2). Equation (4.1) expresses the input voltage V_{in} of the DC/DC converter as function the output voltage V_{out}.

$$V_{out} = \frac{1}{1-D} V_{in} \tag{4.1}$$

PV module characteristics	Value
V_{oc}	43.5 V
I_{sc}	4.75 A
V_{mpp}	34.5 V
I_{mpp}	4.35 A
P_{mpp}	150 W

Table 4.1 PV module characteristics

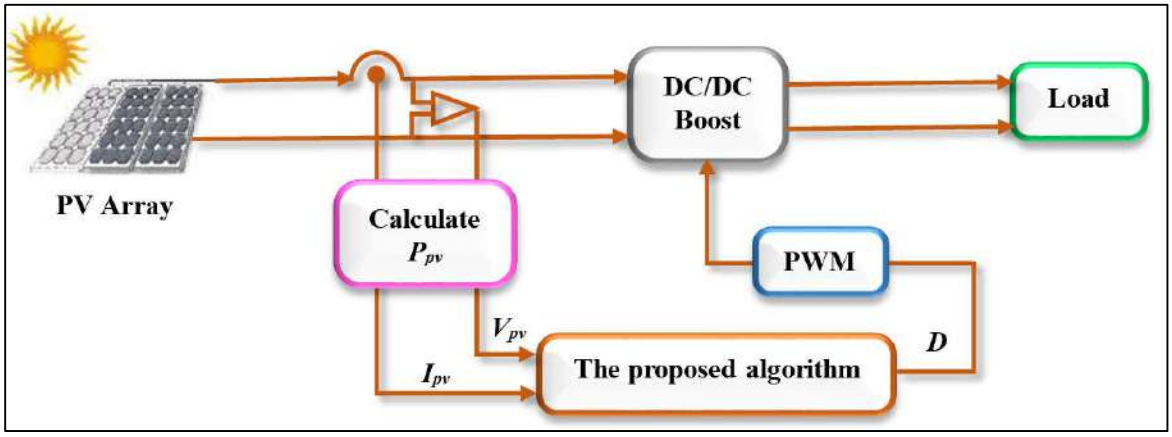


Figure 4.2 the block diagram of the system

DC/DC boost converter parameters	Value
Output Capacitor C_{out}	470µF
Input Capacitor C_{in}	220µF
Inductance L	5 mH
Switch frequency	20kHZ

Table 4.2 DC/DC boost converter parameters

4.2.1 Fuzzy MPPT algorithm

The role of the fuzzy MPPT is the control of the current and the voltage provided from the PV panel by the DC/DC converter in order to extract the maximum of power. While the inference (min-max) model chosen is Mamdani type, the fuzzy MPPT has as input *E* and *ΔE* that are the error and the variation of the error respectively as is described in the equations (4.2-4.5) [71].

$$\Delta P_{pv}(n) = P_{pv}(n) - P_{pv}(n-1) \quad (4.2)$$

$$\Delta V_{pv}(n) = V_{pv}(n) - V_{pv}(n-1) \quad (4.3)$$

$$E(n) = \frac{\Delta P_{pv}(n)}{\Delta V_{pv}(n)} \quad (4.4)$$

$$\Delta E(n) = E(n) - E(n-1) \quad (4.5)$$

As shown in the flowchart given in the figure 4.3, the fuzzy algorithm has three main steps: fuzzification, Inference and defuzzification. In the fuzzification step, the algorithm replaces the numerical input in the linguistic variables presented as memberships function. The inference rules is the most important step, it provides the output that corresponds to the current input. In the defuzzification, the algorithm transforms the output to numerical value.

For a good precision, five triangular and trapezoidal membership functions have been taken for each input in the Fuzzification step also for the output duty cycle. NS (negative Strong), NL (negative low), ZE (zero), PL (positive low) and PS (positive strong). After applying the min-max rules the fuzzy MPPT provides the duty cycle signal in the Defuzzification by using center of gravity method. Figures (4.4) (a), (b) and (c) show the membership function for E, ΔE and the output respectively. Where the range of the error is (-50 to +30 W/V), whereas the range of the variation of the error is (-50 to +50 W/V) and the range of the duty cycle is in the range (-3 to +3).

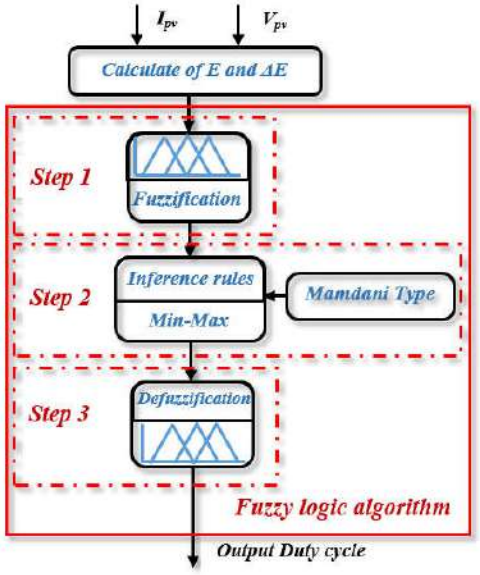
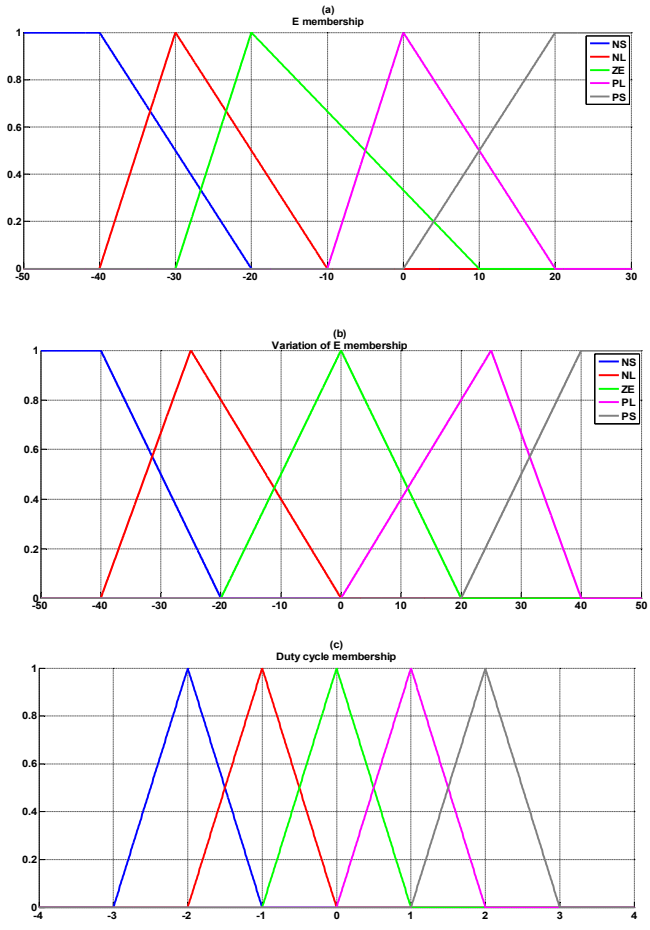


Figure 4.3 Fuzzy logic algorithm steps.



Figures 4.4 (a) Error membership; (b) Variation of error membership; (c) Duty cycle membership.

The inference step is the most important in which the decision is making, the correspondence between the input and the output is given in inference table (table (4.3)) by linguistic variables. The fuzzy algorithm reverses the input for make the error tends to zero. Where, for the error equal to strong negative (NS) and the variation of error equal to strong negative (NS) that mean the error in negative and decrease rapidly, in this case the decision is positive strong and so on.

E\ ΔE	***NS***	***NL***	***ZE***	***PL***	***PS***
NS	***PS***	***PS***	***PL***	***PS***	***PS***
NL	***PS***	***PL***	***PL***	***PL***	***PS***
ZE	***NL***	***NL***	***ZE***	***PL***	***PL***
PL	***NS***	***NL***	***NL***	***NL***	***NS***
PS	***NS***	***NS***	***NL***	***NS***	***NS***

Table 4.3 Inference table [71]

4.2.2 M5P model tree

The proposed algorithm is based on the training of a non-parametric model called model tree. This model is trained from the numerical dataset namely the attributes and target [72]. Basically, the model tree is composed of two algorithms, the first is the decision tree that gives a representation of the model in a tree form. This tree is formed of three parts: the Root node, the internal node and the leaves, where the nodes are interconnected between them by the branches. The second is the multi linear regression (MLR) that represents the algorithm applied to the leaves of the tree [17, 18]. The assembly of these two algorithms makes the model tree algorithm more powerful, efficient and provides a good accurate prediction. Moreover, the model builded by M5P algorithm is converted to a simple rules based on <if ... else> which make it easy for the real time implementation. The aim of this approach is to build a simple model by modeling the fuzzy logic MPPT algorithm data [73].

4.2.2.1 Decision tree

Decision tree is a classification in form of a tree structure. It is consist of building a tree branches by training through a dataset that composed of the attributes and the target. The decision tree is split into three principal nodes: roots node, internal nodes and the leaves. The building passes by the reduction of the dataset into smaller subset in the standard deviation reduction (SDR) process after calculating the standard deviation (SD) of each attribute with the target. The attribute that has the maximum SDR is considered as roots node [17].

Standard deviation: The criterion of top-down splitting for the building of decision tree passes through the calculation of the SD of the target before the SD of each attribute with the target. For determining which attribute can be considered as roots node, its SD is treated as measures of error at this node and it is tested by calculating the reduction in error. The following equations (4.6-4.7) expresses the value of the SD for one attribute that applied to the target.

$$SD(T) = \sqrt{\frac{\sum (T-\mu)^2}{N}} \tag{4.6}$$

$$\mu = \frac{\sum_{i=1}^{N} X_i}{N} \tag{4.7}$$

Where, $\boldsymbol{T}$ is the target instance, $\boldsymbol{\mu}$ is the average of the instances and N is the number of samples.

The calculation of SD between the attribute and the target is taken as sum of product of probability of each class in the attribute with the SD of the target values corresponds to this class. Equation (4.8) describes the calculation of this value.

$$SD(X,T) = \sum P(x).SD(x,T) \tag{4.8}$$

Where, x is the class of the attribute, $P(x)$ is the probability of each class in the attribute and $SD(x, T)$ is the standard deviation of the target values corresponds to each class.

Standard deviation reduction: For choosing the attribute that has been taken as roots node, the expected error reduction is calculated by standard deviation reduction (SDR). The attribute that have maximum SDR is placed in the beginning of splitting. The SDR of each attribute is described by equation (4.9) which consists of subtraction between the SD of the target and SD of each attribute with the target.

$$SDR = SD(T) - SD(X,T) \tag{4.9}$$

Let's the example given in table (4.4) that contains two attributes

Attribute 1	Attribute 2	Target
True	*Cool*	*10*
True	*Medium*	*30*
False	*Medium*	*21,5*
False	*Cool*	*5*
True	*Medium*	*15*

Table 4.4 example of dataset

First step: the calculation of the SD of the target:

$$SD(T)=\sqrt{\frac{(10-16.3)^2+(30-16.3)^2+(21.5-16.3)^2+(5-16.3)^2+(15-16.3)^2}{5}}=\sqrt{\frac{383.8}{5}}=8.76$$

Second step: the calculation of the SD between each attributes and the target:

a) Between Attribute 1 and Target table (4.5)

Attribute 1	Target
True	*10*
True	*30*
True	*15*
False	*21,5*
False	*5*

Table 4.5 Attribute 1 and Target

$$SD\left(T,Attribute1\right)=\frac{3}{5}\times SD\left(T,True\right)+\frac{2}{5}\times SD\left(T,False\right)=\frac{3}{5}\times 8.49+\frac{2}{5}\times 8.25$$

$$SD\left(T,Attribute1\right)=8.39$$

b) Between Attribute 2 and Target table (4.6)

Attribute 2	Target
Cool	*10*
Medium	*30*
Medium	*21,5*
Cool	*5*
Medium	*15*

Table 4.6 Attribute 2 and Target

$$SD(T, Attribute2) = \frac{3}{5} \times sd(T, Medium) + \frac{2}{5} \times sd(T, Cool) = \frac{3}{5} \times 2.5 + \frac{2}{5} \times 6.14$$

$$SD(T, Attribute2) = 3.96$$

Third step: The calculation of the SDR for the two attributes

a) For Attribute 1:

$$SDR(T, Attribute1) = 8.76 - 8.39 = 0.37$$

a) For Attribute 2:

$$SDR(T, Attribute2) = 8.76 - 3.96 = 4.8$$

Fourth step: Choose the attribute that maximizes the SDR

In this example the Attribute 2 has a maximum of SDR, then it is taken as roots node in the decision tree.

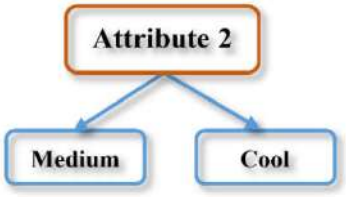


Figure 4.5 decision tree

In our case, all attributes are numeric with continuous values, therefore, the method used for calculating the standard deviation reduction passes by one more step. Before the previous steps, another method is proposed by Brieman [74] for more accuracy. It consists of the conversation of numeric attribute to synthetic binary for the possibility to treating these attributes. For *K* values of attribute, the algorithm creates *K-1* synthetic binary attributes or thresholds after arranging ascending of these values. Thus, each two successive values v_n and v_{n+1} are replaced by S_n that is calculated by equation (4.10), where the thresholds are the average of two successive values.

$$s_n = \frac{v_n + v_{n+1}}{2} \qquad 4.10$$

However, the synthetic value corresponds to the $S_n \leq a_n$ takes the binary outcome true, otherwise false [74]. Consequently, the SDR is calculated for each outcome, then the outcomes have the biggest SDR are taken as roots nodes by the same approach of nominal values.

4.2.2.2 Multi-linear regression model (MLR)

One of the advantages of M5P algorithm is the utilization of a linear regression algorithm at the leaves that make the final model small, simple and more accurate [72]. Basically, the MLR is an introduction of linear prediction model in each leaf. Equation (4.11) describes the general form of the linear model at the leaves for independents numerical attributes. In order to calculate the weights of the MLR model, the algorithm minimizes the least square error between the predicted and the real values of the training data as expressed in Equation (4.12), where T and T' are the real and the predicted target values respectively. The vector of the weights corresponds to the minimal error is given in equation (4.13), where A is the attribute values vector.

$$LM = \omega_0 + \omega_1 a_1 + \omega_1 a_1 + \ldots + \omega_k a_k \qquad (4.11)$$

Where: $a_1 to a_k$ are the attribute values and w_0 to w_k are the weights of the Multi-linear model.

$$Min \sum (T - T')^2 \qquad (4.12)$$

$$W = (A'A)^{-1} A'T \qquad (4.13)$$

Figure (4.6) shows an example of the linear regression approximation of a nonlinear function for one dimension.

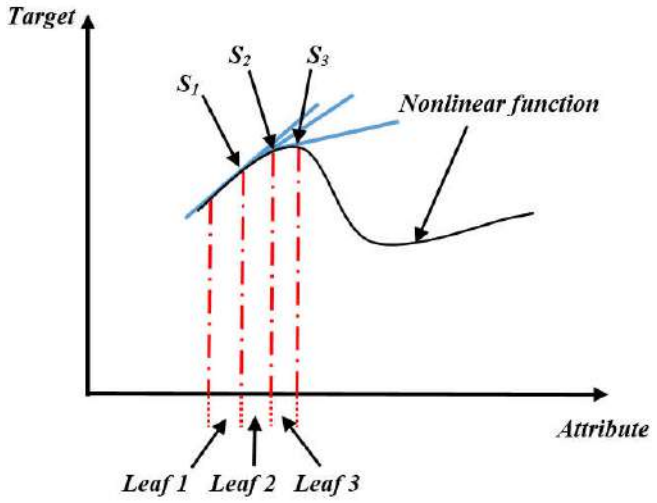


Figure 4.6 Example illustrates the linear regression

Pruning the tree: The pruning of the initial model is an important phase in order to increase the accuracy of prediction model and decreases the size of the tree. Basically, in this phase the

algorithm compares between unpruned and the pruned model by the comparison of the estimated mean absolute error (MAE) between the predicted and the real values that reaching this node using the equation (4.14). The initial model obtained by M5P algorithm might have unnecessary sub-trees nodes that must be replaced by leaf node in order to minimize the size of the tree, this processes is called pruning.

$$MAE = \frac{1}{N}\sum_{i=1}^{N}\left|T - T'\right| \tag{4.14}$$

N is the number of samples.

For each internal node, the algorithm applies the MLR for the unpruned tree in order to estimate the MAE based only on the attributes includes in the subtree tested until reach a minimal MAE, otherwise, the algorithm continuous to divides the tree into other internal nodes. Also, the MAE is calculated to underestimate the anticipated error of unseen samples. A compensation process used to minimize the estimated error based on the multiplication by the factor $(n+c)/(n-c)$, where n is the number of learning samples that arrived to the node and c is the number of weight in the linear model obtained in the same node that predicts the target values [18].

Smoothing: The third fundamental process in the M5P algorithm is the smoothing. The approximation of the leaves by the linear model presents a discontinuity between each two adjacent linear models. In this step the algorithm improve the accuracy of the model by avoiding this discontinuity in the leaves of pruned tree by the introduction of the smoothing factor p' expressed in equation (4.15). In particular case, some linear models are builded from few number of instances in the training data, in this case the smoothing is recommended. Also the smoothing is most affect where the training data contains instances widely different in terms of scenarios.

$$p' = \frac{np + kq}{n + k} \tag{4.15}$$

Where p is the prediction passed the current node from below, q is the model predicted value in the current node, n is the number of learning samples that arrived to the node and k is a constant used by smoothing taken as default value 15 [18].

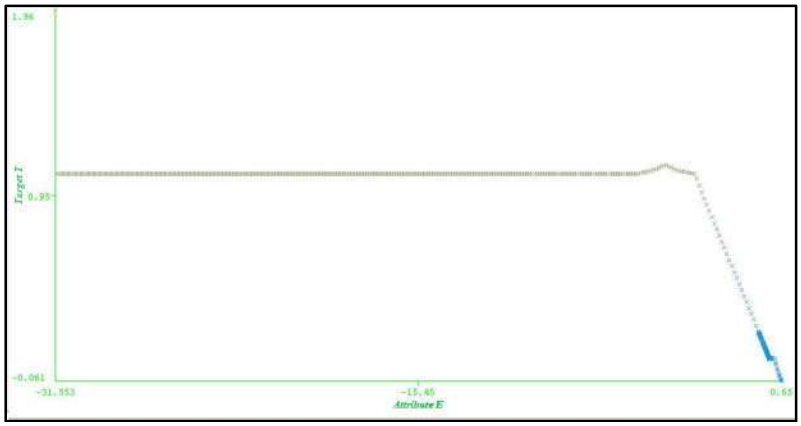
4.3 Training model results

After running of the fuzzy logic MPPT algorithm for 500 W/m^2 irradiation, its input that consist of the error E and the variation of the error ΔE, and output that consist of the duty cycle was recorded in order to use them as attributes and target respectively for the training and the test. Where 66% of the data are used for the training and the remainder of data are used for the test. The building phase of the new model is done by using M5P algorithm before the evaluation of this model by unseen dataset. The construction of the model was carried out by using the Weka software for 20000 data samples.

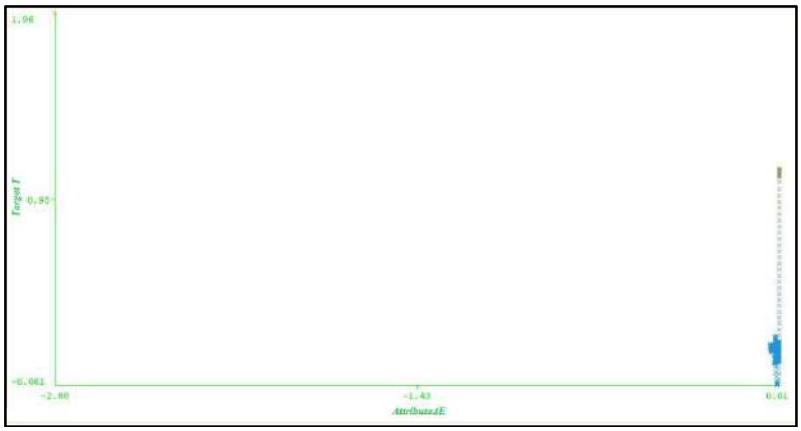
4.3.1 Modeling results

After running of the training process using Weka software, a simple model tree is obtained that composed of nodes which will be translated to <if...else> instructions program. That's make the model easy to implemented for the real time MPPT. Figures (4.7) illustrates the correspondence input/output of the dataset, where figure (4.7)-(a) shows the variation of the target as function the error E; as is clearly highlighted the model obtained from the target(E) is linear. Also the data based on E provides a good information about the target. However, from the figure (4.7)-(b) it is visible that the variation of the error ΔE data is not widely significant in the progress of the algorithm, therefore, it has not been appears widely in the decision tree. As shown in figure (4.8), the algorithm gives simple model tree that is composed of nodes and leaves that will be translated to <if…else> program.

As is shown in table (4.7), the training and testing algorithm gives good results in terms of the rapidity and the accuracy. The algorithm takes low time to build the model, which allows us also to use it for the on line modeling for other applications. In other hand, good precision matching between the fuzzy and the new model is given as is highlighted from the different parameters as: correlation coefficient, mean absolute error, root mean squared error, relative absolute error and root relative squared error.



(a)



(b)

Figures 4.7 Training model results: (a) Target as function the Error *E*, (b) Target as function the variation of Error ΔE

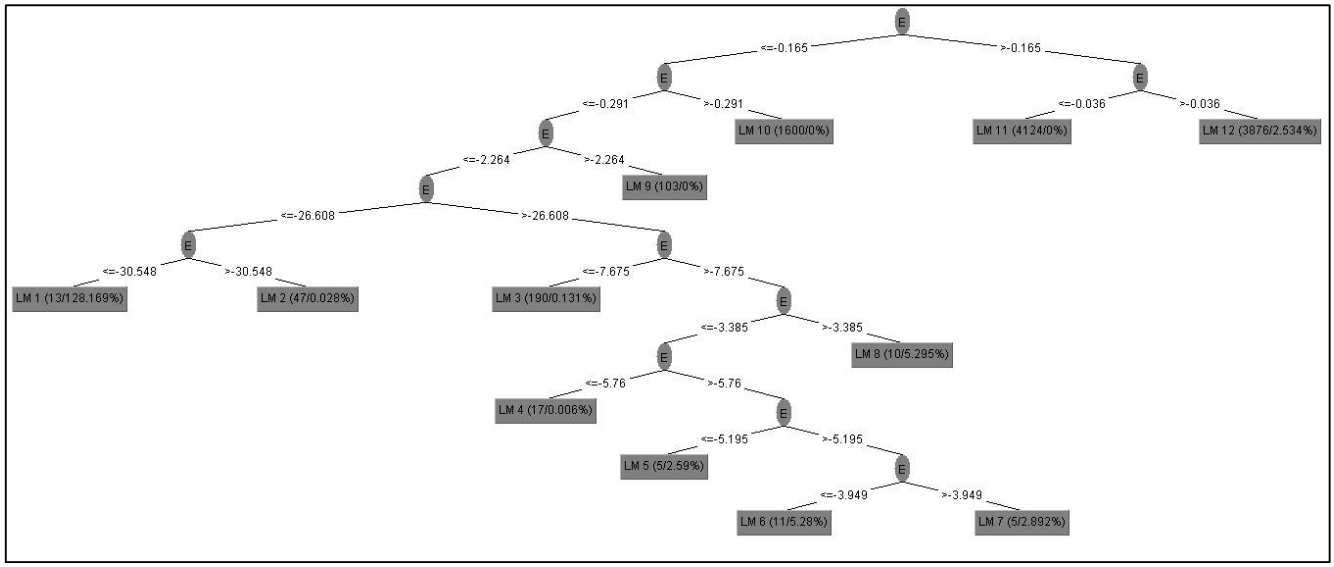


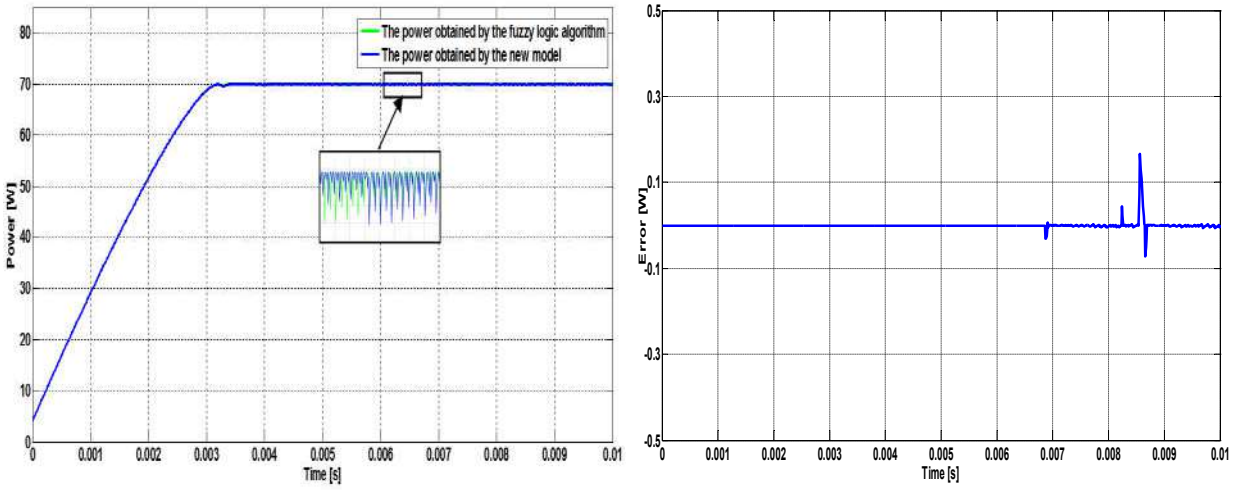
Figure 4.8: The model tree for MPPT obtained by the M5P algorithm

Parameters	Value
Time taken to test model on training split	10.4 seconds
Time taken to build model	20.1 seconds
Correlation coefficient	0.9977
Mean absolute error	0.0029
Root mean squared error	0.0109
Relative absolute error	4.8084 %
Root relative squared error	6.9359 %
Total Number of Instances	3400

Table 4.7: Result of training and testing of the final model:

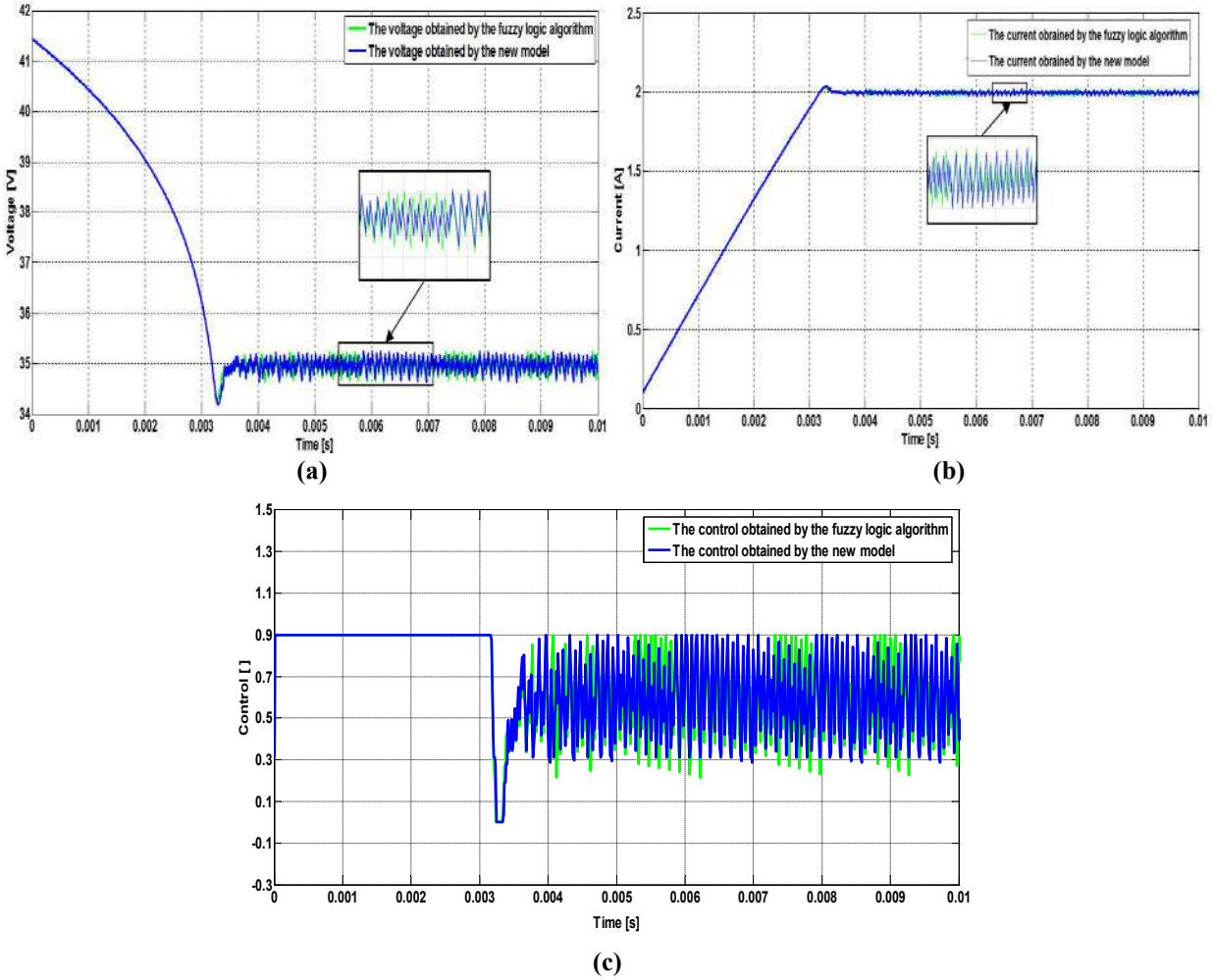
4.3.2 Modeling robustness results

After running the two model simultaneously, the new model is implemented with the fuzzy algorithm, the new model presents a good matching with the former fuzzy model on the power variation as illustrated in figure (4.9) (a). Figure 9 (b) shows the error between the new model and the former fuzzy model. Furthermore, the matching between the two models in the voltage, current, and the duty control is highlighted in figures (4.10) (a), (b) and (c) respectively.



(a) **(b)**

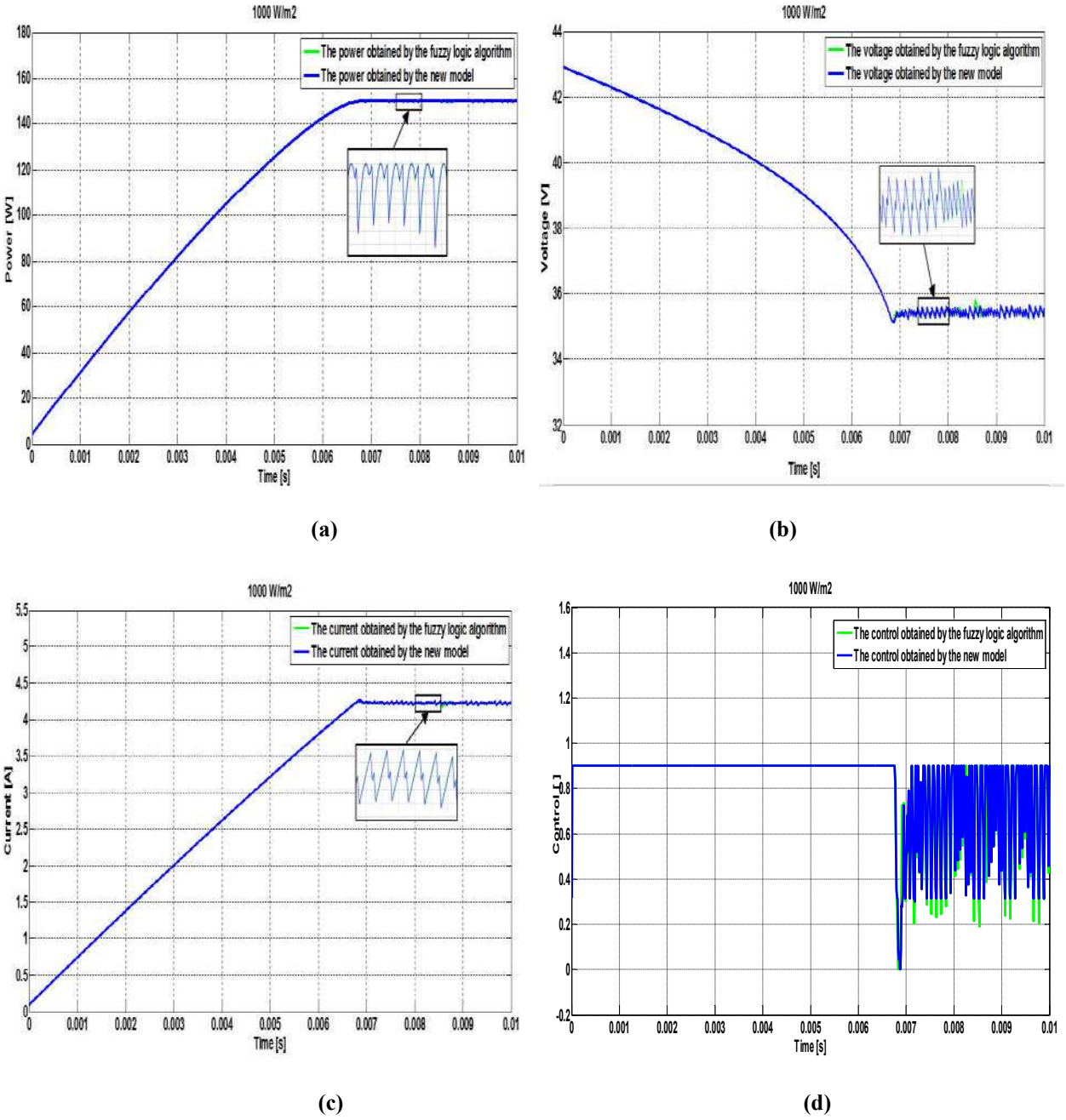
Figures 4.9: Power obtained from fuzzy algorithm vs Power obtained the new model: (a) fuzzy algorithm VS new model. (b) The error between fuzzy algorithm and new model



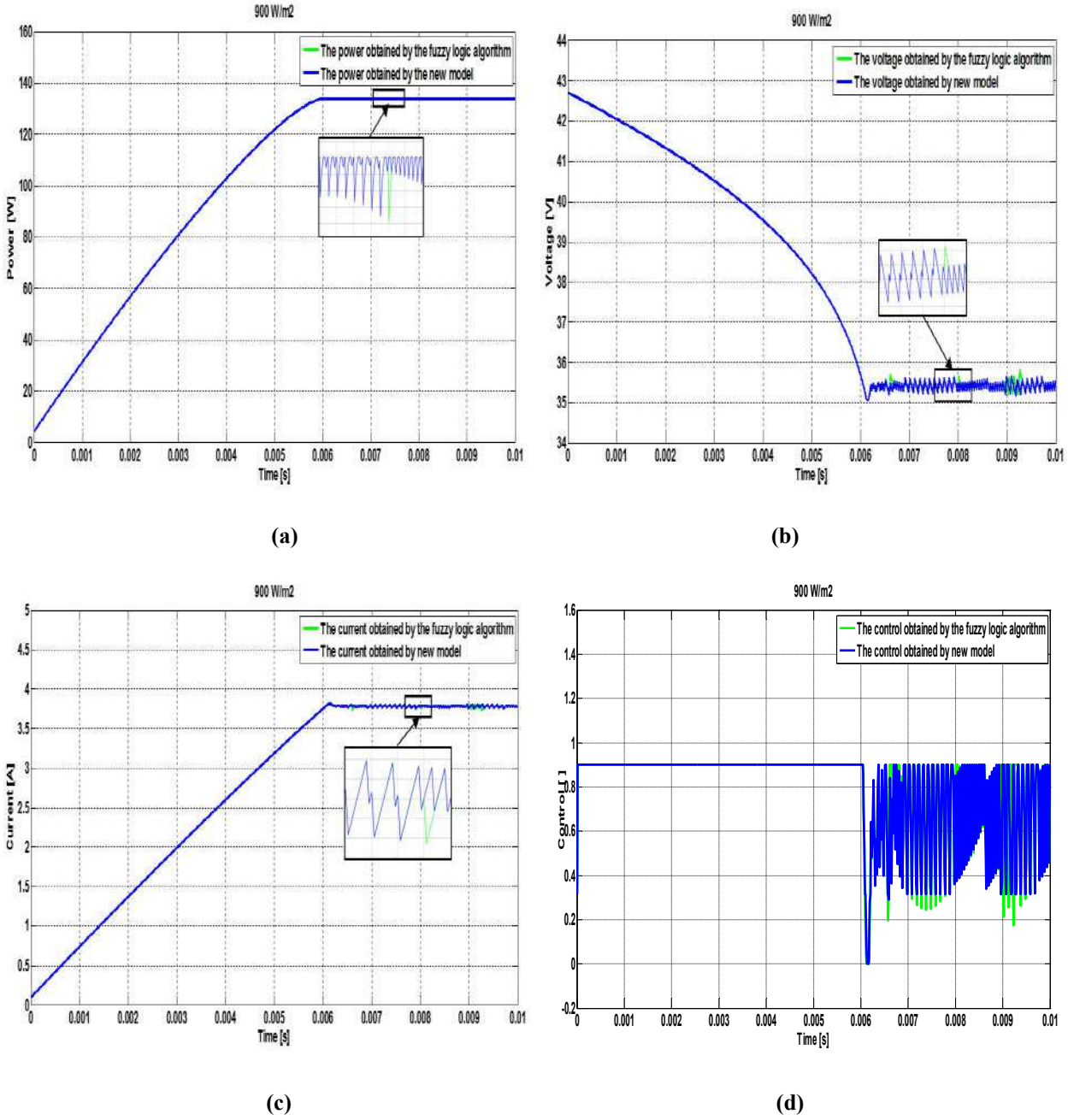
Figures 4.10: Results obtained from fuzzy algorithm vs new model:
(a) The voltage (b) the current (c) the control

4.4 Simulation results and discussion

In this section, we propose to test of the new model with an unseen data obtained for different irradiation. As it's known, the training of the model has been carried out for the irradiation 500 W/m^2, also has been tested with 34 % for this data. Moreover, now we propose to test this model for different unseen irradiation, therefore, a simulation of this model was done with an invariant irradiation for 1000 W/m^2, 900 W/m^2, 800 W/m^2, 700 W/m^2, 600 W/m^2, 400 W/m^2 and 300 W/m^2 in which also the two models has been simulated simultaneously. It's noticed that the two model present a good matching for the power, voltage, current and the control as is shown in figures (4.11-4.17) where (a), (b), (c) and (d) are the power, the voltage, the current and the control respectively.



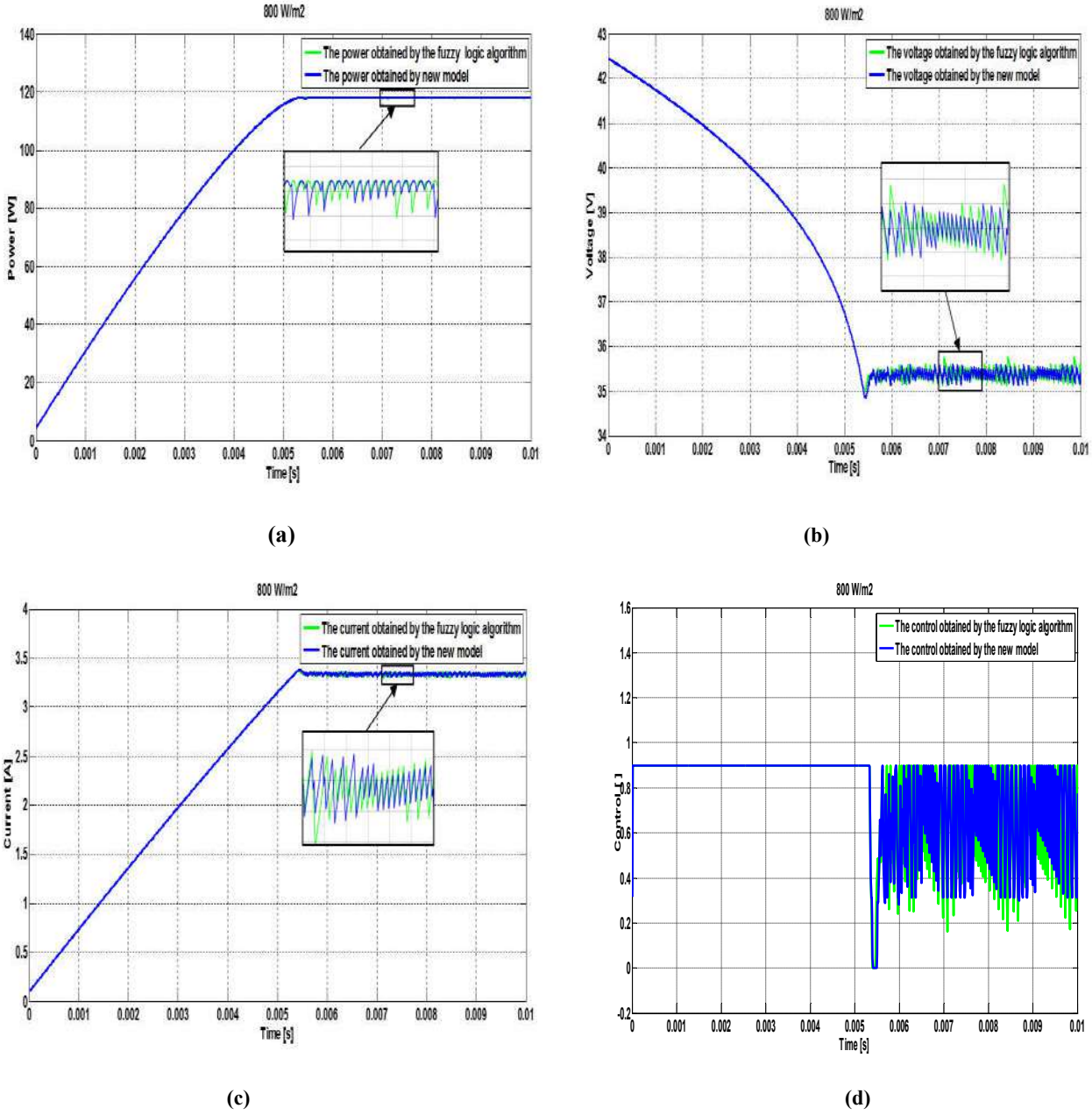
Figures 4.11: Results for irradiation 1000 W/m2: fuzzy logic algorithm vs new model (a) power (b) voltage (c) current (d) control



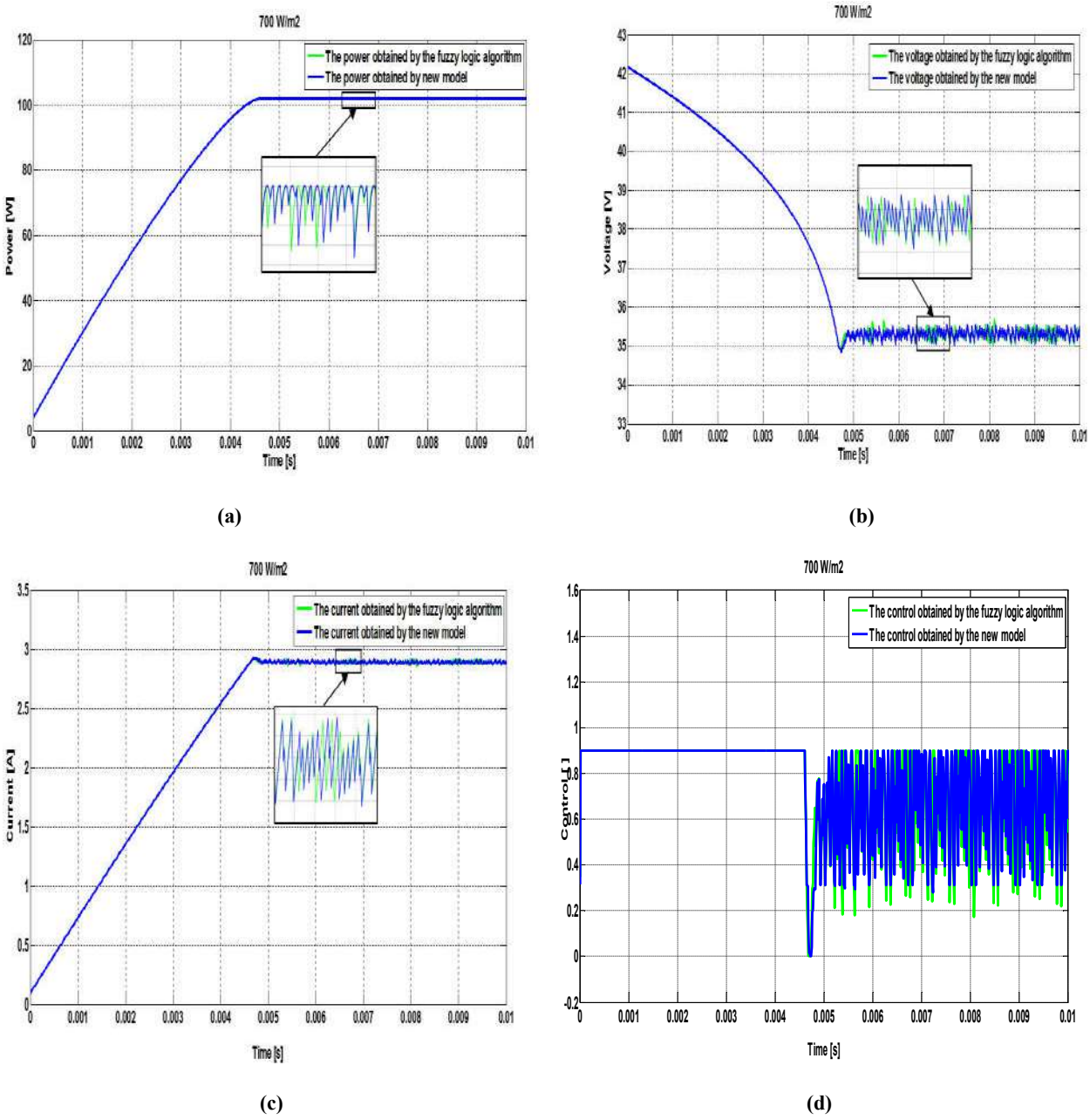
(a) **(b)**

(c) **(d)**

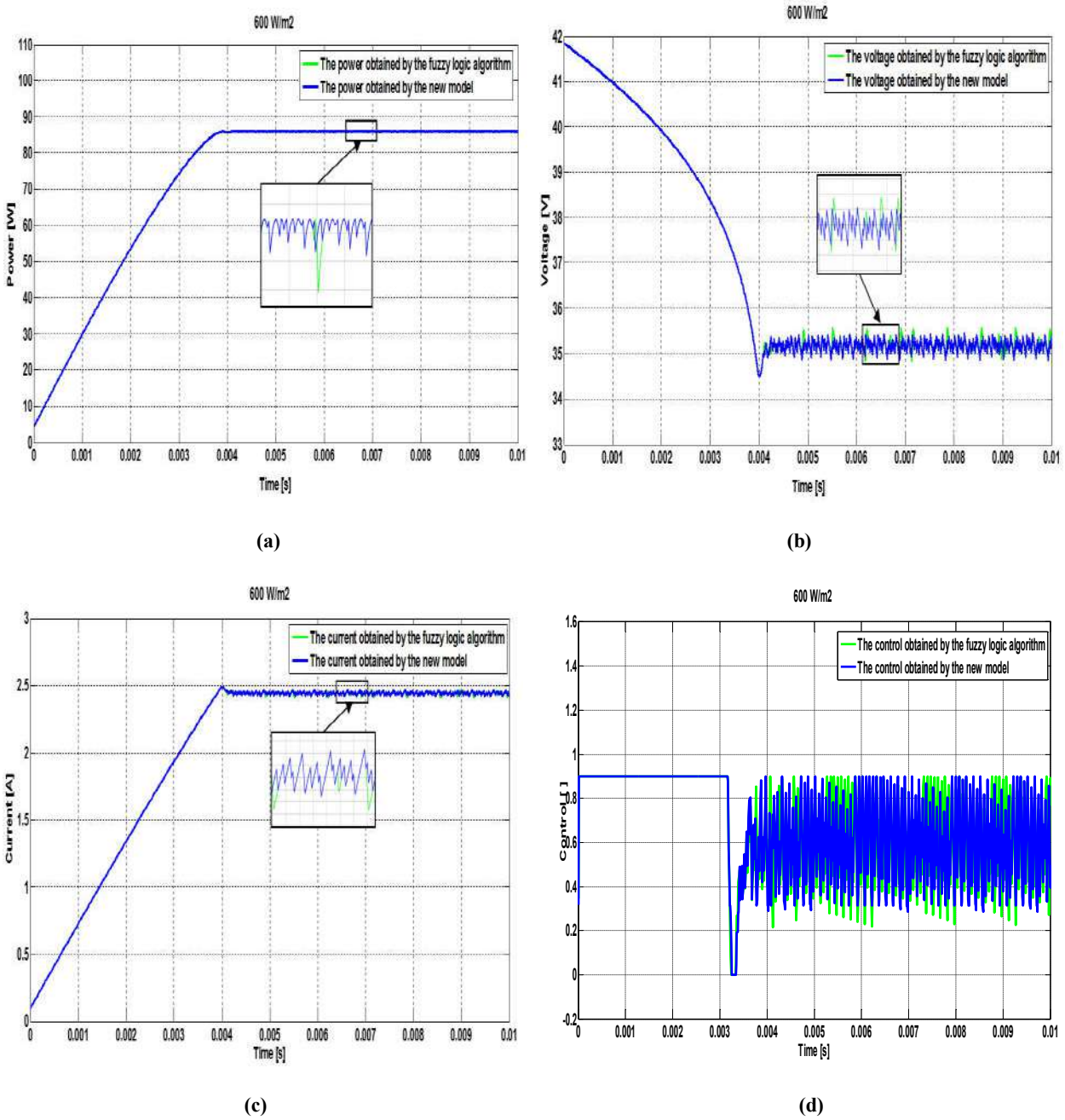
Figures 4.12: Results for irradiation 900 W/m2: fuzzy logic algorithm vs new model (a) power (b) voltage (c) current (d) control



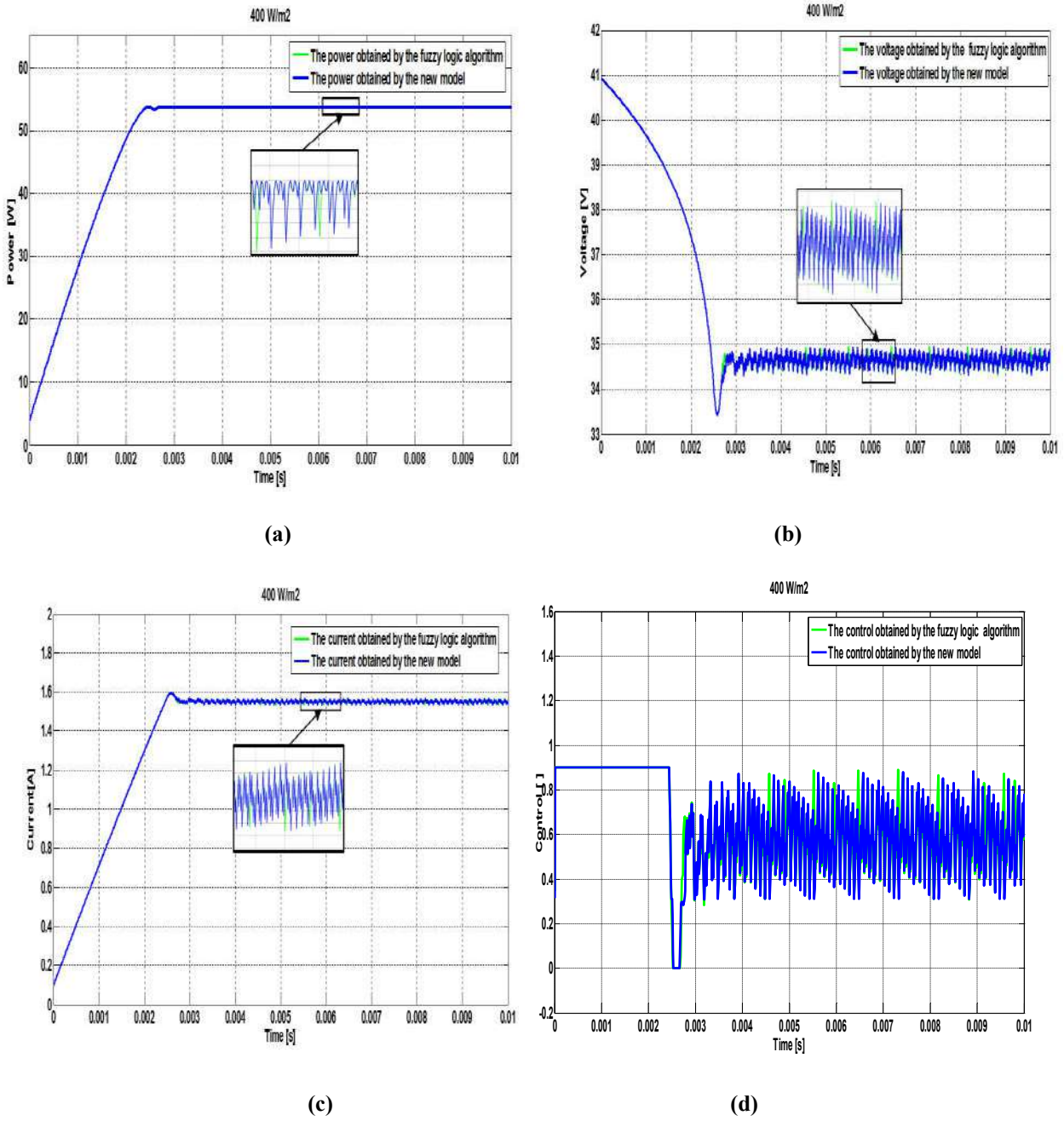
Figures 4.13: Results for irradiation 800 W/m2: fuzzy logic algorithm vs new model (a) power (b) voltage (c) current (d) control



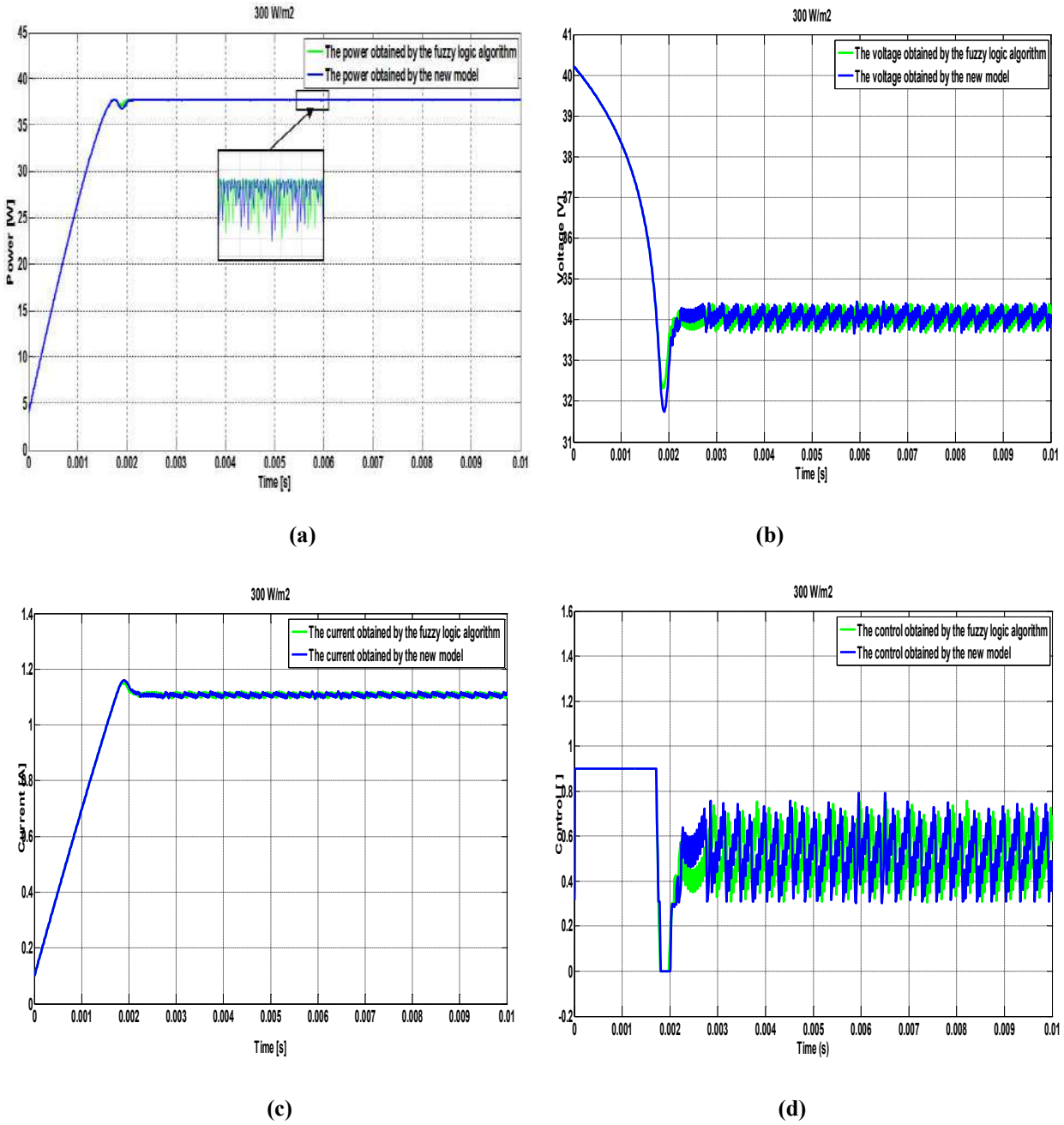
Figures 4.14: Results for irradiation 700 W/m2: fuzzy logic algorithm vs new model
(a) power (b) voltage (c) current (d) control



Figures 4.15: Results for irradiation 600 W/m2: fuzzy logic algorithm vs new model (a) power (b) voltage (c) current (d) control

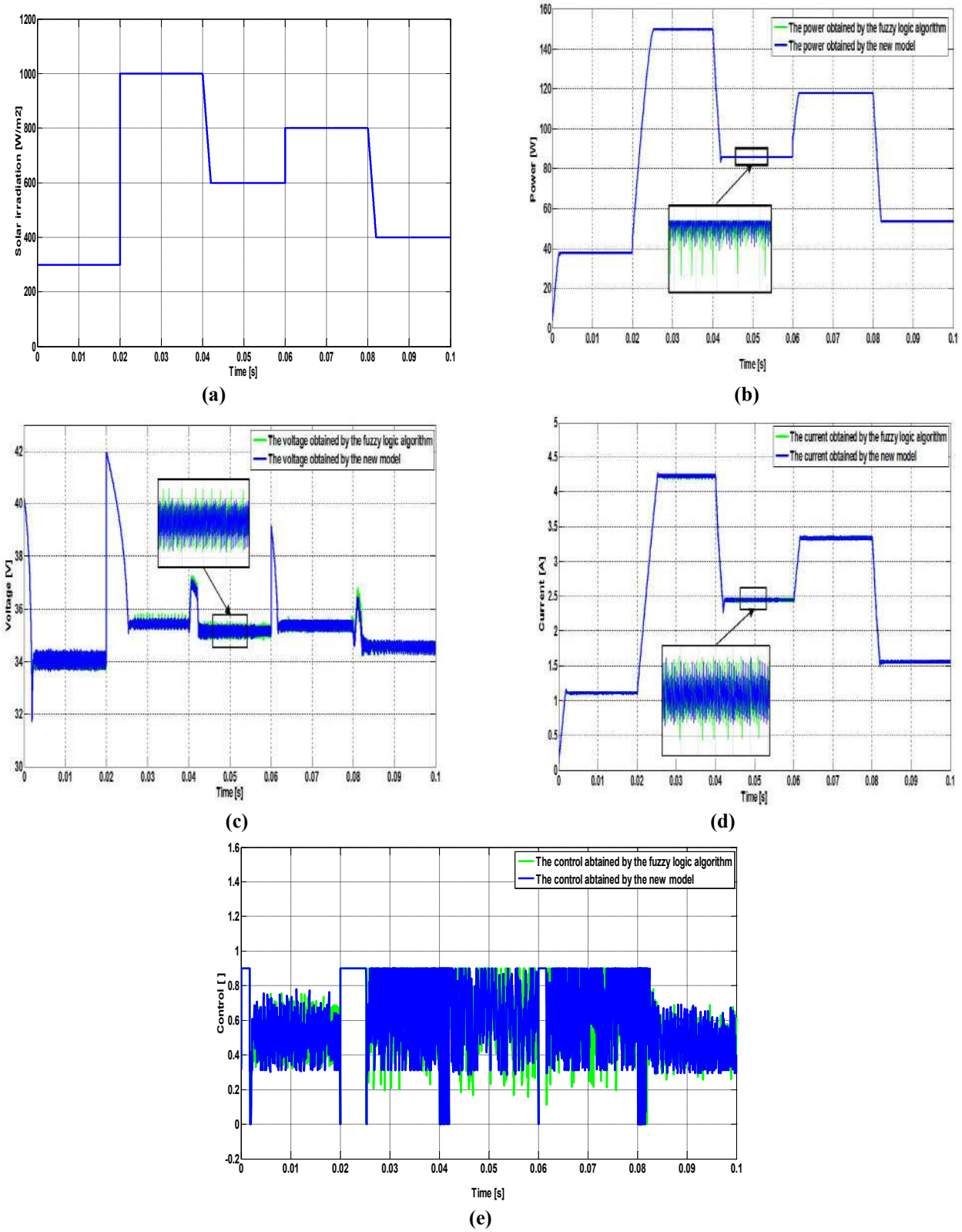


Figures 4.16: Results for irradiation 400 W/m2: fuzzy logic algorithm vs new model (a) power (b) voltage (c) current (d) control



Figures 4.17: Results for irradiation 300 W/m2: fuzzy logic algorithm vs new model (a) power (b) voltage (c) current (d) control

The new algorithm gives also a good agreement with the former model under the fast variation of the irradiation. In the fellow results the algorithm was tested also for different unseen data under a variation from 300 W/m^2 to 1000 W/m^2, 600 W/m^2, 800 W/m^2 and 400 W/m^2 where it presents a good response as shown in figures (4.18) where (a), (b), (c), (d) and (e) are the solar irradiation profile, power, the voltage, current and the control respectively.



Figures 4.18: Results for irradiation variation from 300 W/m^2 to 1000 W/m^2, 600 W/m^2, 800 W/m^2 and 400 W/m^2: (a) solar irradiation (b) Power (c) Voltage (d) Current (e) control

4.5 The battery charge controller

In this section, we propose a PWM battery charge controller that based on the battery state of charge estimated mathematically from the equation (2.3). This controller used the constant voltage charging method where the voltage is kept in its value when the estimated battery state of charge achieves 95%. Furthermore, the new MPPT algorithm is integrated in the proposed controller. Only one DC/DC buck converter is used for both the MPPT and the regulation of the voltage. The figure (4.19) shows the description of the control system.

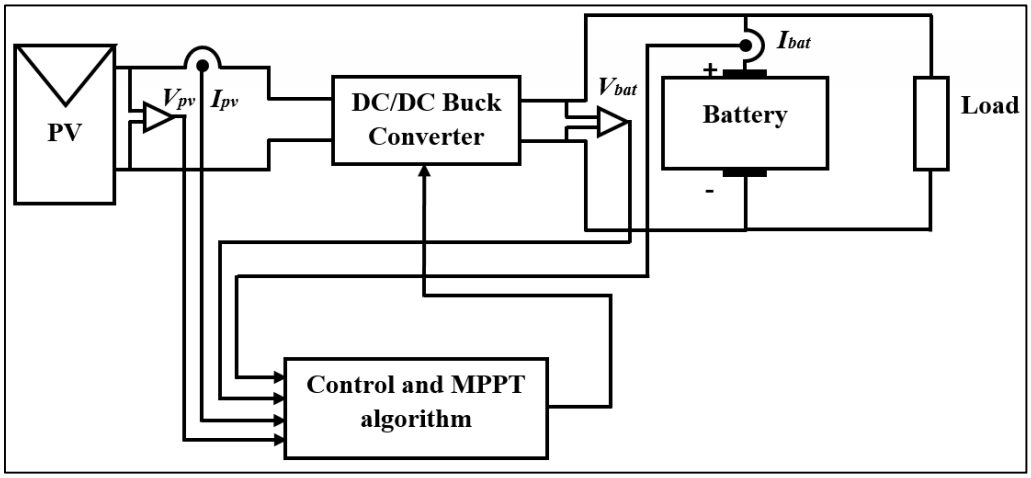


Figure 4.19: the control system description.

4.5.1 Description of the controller

In the charging phase, the system works as MPPT in order to extract the maximum of power from the PV panel. When the estimated SOC reaches the 95% the system works as a regulator to fix the voltage in the reference value correspond to maximum SOC reached by using PI controller. When the voltage is fixed, the current starts to decrease until zero value. In the discharging phase, the system works with on-off mode. The discharge process is stopped when the battery SOC reach 40% and resume the discharge at 60% in order to minimize the switching frequency. Figures 4.24 and 4.25 describe the progress of the regulator for the charging and discharging process.

4.5.2 Design and implementation

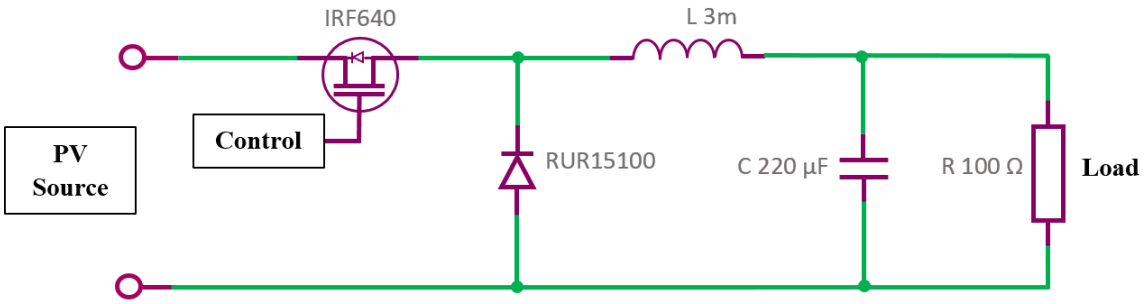
4.5.2.1 Design

For the required variables measurement for the MPPT and the charging control, two boards that described in the chapter III are used. Two voltage sensors are needed for the measure of the

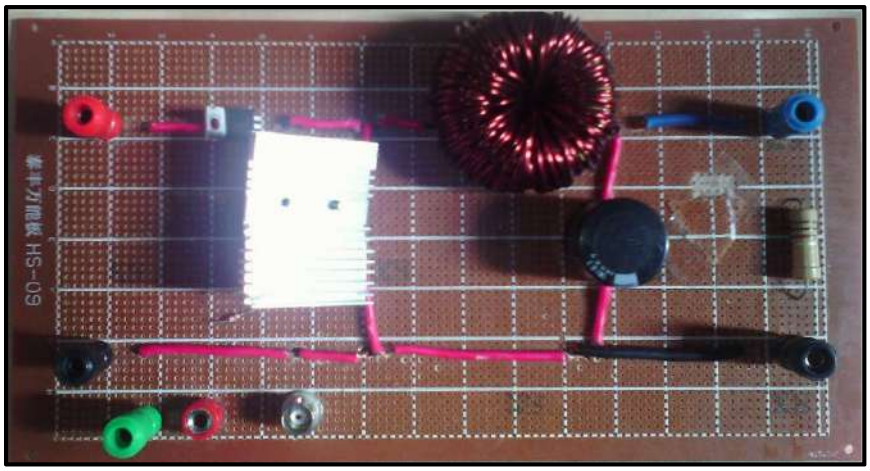
PV voltage V_{pv} and the battery voltage V_{bat}. Two current sensors are needed for the measure of the PV current I_{pv} and the battery current I_{bat}. For the temperature compensation the measurement of the ambient temperature is required in the calculation of SOC.

A simple DC/DC buck converter shown in Figures (4.20) (a) and (b) has been realized for both the MPPT and the charging control with parameters and the characteristics given in the table (4.8). The TLP 250 isolator and driver given in figure (4.21) is used for the control of the MOSFET IRF640.

(a)



(b)



Figures 4.20: realized DC/DC buck converter.

DC/DC buck converter parameters	Value
Output Capacitor C_{out}	470µF
Inductance L	3 mH
Switch frequency	20kHZ

Table 4.8. DC/DC buck converter parameters

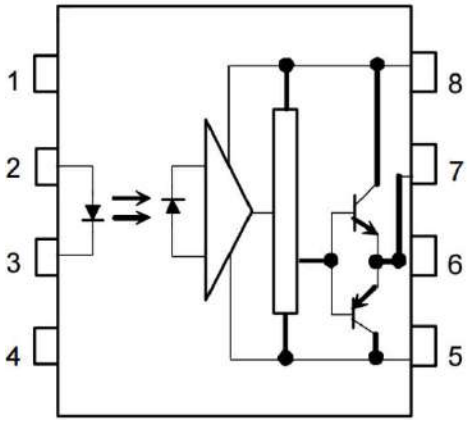


Figure 4.21: TLP 250 driver.

4.5.2.2 Implementation of the controller

For the control of both MPPT and the charge regulation the STM32F407 kit shown in figure (4.22) is used. This kit contains high performance microcontrollers with an internal register of 168 MHZ clock frequency, 32 bit, 1-Mbyte Flash memory and 192-Kbyte RAM. Also this device provides 16 analogs input multiplexed with ADC resolution of 12 bits, 2 DAC for the analog output and 6 PWM numerical outputs.

The most important advantage of this board is the library provided by Matlab/Simulink that allows to programing it easily. As shown in figure (4.23) the control program has been implemented in STM32F407 through the Matlab/Simulink environment

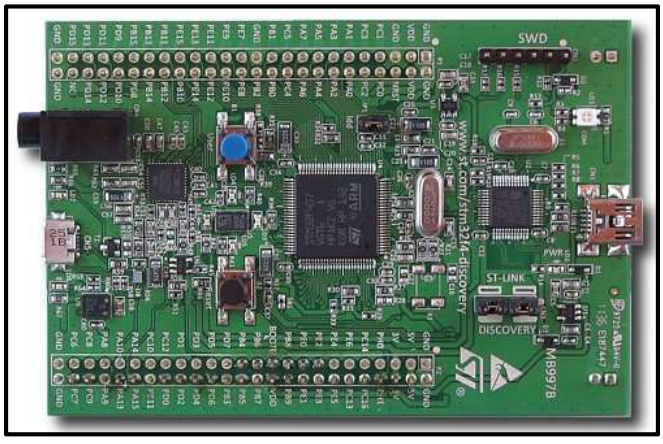


Figure 4.22: STM32F407 kit.

.

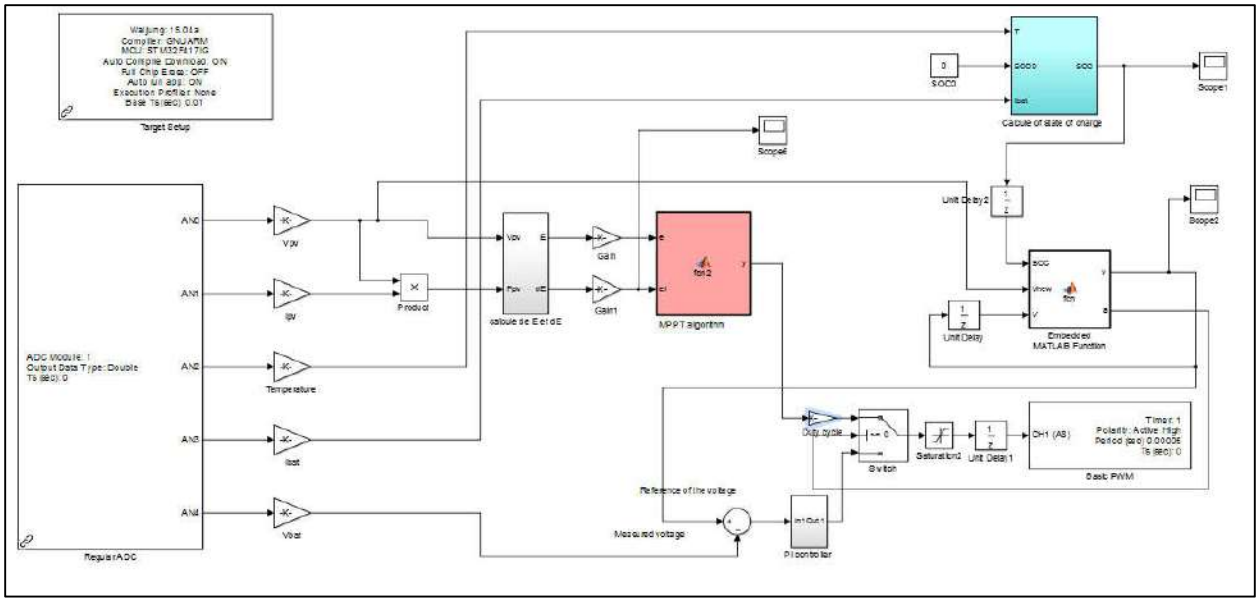


Figure 4.23: The MPPT and the charge regulation control program in Matlab/Simulink

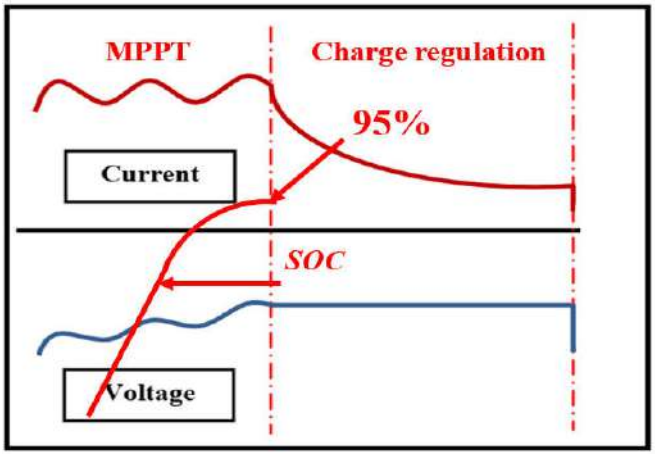


Figure 4.24: Charging mode progress

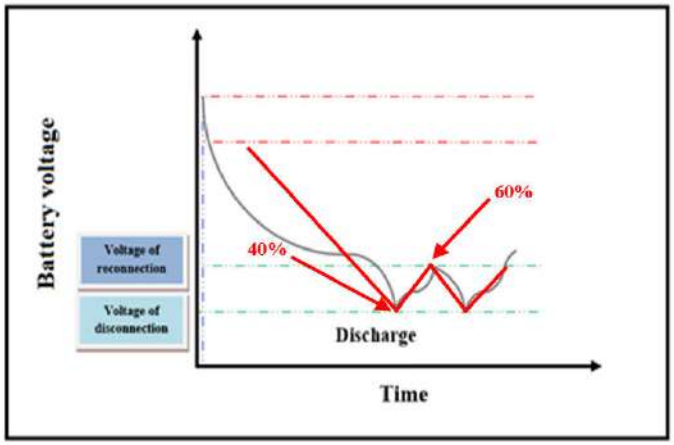


Figure 4.25: Discharging mode progress

4.6 Conclusion

In this chapter we have proposed the contributions that will be introduced in the enhanced charge controller. Firstly, a novel fast MPPT has been proposed by the new modeling of the fuzzy MPPT by using the M5P model tree. This allows obtaining a more advantages such as the ease of implementation and the less computational time with keeping the advantages of the former fuzzy algorithm such as the speed of convergence and the accuracy the steady-state. In other hand, we have proposed a novel method of battery regulation that's based on constant voltage charging mode from the estimation of the battery state of charge SOC.

Conclusion

Conclusion

The aim of this doctoral thesis is to provide an optimal management of the stand-alone photovoltaic systems that meets the future challenges, and to provide solutions some problems encountered in these systems.

The optimal efficiency of the photovoltaic systems is based on the good management that start by the optimization in the solar panel level. This can be obtained by the introduction of the good strategy of the maximum power point tracker (MPPT). The trade-off among the speed of convergence, the calculating time, the stability in the steady state and the ease of implementation is still widely appears. Therefore, we have proposed a new fast MPPT by modelling the Fuzzy logic algorithm using M5P model tree. The purpose has been to take advantages of the fuzzy logic algorithm such as the speed of convergence and the stability in the steady state regime to improve it by elimination of its disadvantages such as the complexity and large calculating time. This has been realized by using simple if/else code of M5P model tree. This method gives good results in terms of the matching of the new model with the former Fuzzy logic algorithm. Also, the proposed MPPT has been tested with an unseen data for different solar irradiation and for the fast variation of the weather conditions. We believe that this new algorithm can be much recommended for the real time applications. Furthermore, while the algorithm is based on a simple if/else code can be also used for the embedded systems applications such as the FPGA.

Because of its electrochemical complexity, the battery in the stand-alone photovoltaic systems has always been a major issue either in the purpose to its management or to the prediction of its characteristic. The modeling of the lead-acid battery is still the major problem in the recent researches. Therefore, many models have been proposed for different approaches. In this context, we are interested to the CIEMAT model. This model takes into account all phenomena's of the lead-acid battery in addition to its suitability with photovoltaic working. Our proposition has been the improvement of this model by the extraction of its parameters to give it more usefulness and accuracy. As a first step, we have proposed automatic extraction parameters with Levenberg-Marquardt algorithm. This gives good results in terms of the matching with the real measurements. After that, in order to provide a method that can be implemented easily, we have proposed an enhancement of 21 parameters by using the genetic algorithm. This method

presents good results in terms of the good matching and lower error between the real measurement and the enhanced model. Furthermore, by using static measurement method, we have proposed an improvement of this model for predicts approximately the gassing and the saturation areas. It is recommended to introduce the battery degradation capacity in this model as future works

A real time monitoring interface using LabVIEW has been proposed also to provide usefulness to the improved battery model. This robust and low-cost simulation method provides all battery characteristic to the user. Also, it is can be used for the data acquisition and for the battery fault detection in the future.

In order to extend its lifetime, it is necessary to provide the adequate management of the battery. After a long study about the battery behavior, it is clearly visible that the good estimation of its states leads to extend considerably its lifetime by avoiding to achieve the dangerous charging zones. We conclude that the best indicator of the charge of the battery is the state of charge (SOC) highlighted in chapter 2. From this, we have proposed a robust PWM charge regulator based on the SOC indicator. The new MPPT algorithm developed is also integrated in this regulator.

REFERENCES

REFERENCES

[1] S. Saravanan, Ramesh Babu N. RBFN based MPPT algorithm for PV system with high step up converter. Energy Conversion and Management 122 (2016) 239–251.

[2] Hadjer Bounechba, Aissa Bouzid, Hamza Snani, Abderrazak Lashab. Real time simulation of MPPT algorithms for PV energy system. Electrical Power and Energy Systems 83 (2016) 67–78.

[3] Mustafa Engin Başoğlu, Bekir Çakır. Comparisons of MPPT performances of isolated and non-isolated DC–DC converters by using a new approach. Renewable and Sustainable Energy Reviews 60 (2016) 1100–1113.

[4] Abdelhamid Loukriz, Mourad Haddadi, Sabir Messalti. Simulation and experimental design of a new advanced variable step size Incremental Conductance MPPT algorithm for PV systems. ISA Transactions 62 (2016) 30–38.

[5] Mohammed A. Elgendy, Bashar Zahawi, Senior Member, IEEE, and David J. Atkinson. Assessment of Perturb and Observe MPPT Algorithm Implementation Techniques for PV Pumping Applications. IEEE Transactions on Sustainable Energy, vol. 3, no. 1, January 2012.

[6] Trishan Esram and Patrick L. Chapman. Comparison of Photovoltaic Array Maximum Power Point Tracking Techniques. IEEE Transactions on Energy Conversion, vol. 22, no. 2, June 2007.

[7] Bader N. Alajmi, Khaled H. Ahmed, Stephen J. Finney, and Barry W. Williams. Fuzzy-Logic-Control Approach of a Modified Hill-Climbing Method for Maximum Power Point in Micro-grid Standalone Photovoltaic System. IEEE Transactions on Power Electronics, vol. 26, no. 4, April 2011.

[8] G. Carannante, Ciro Fraddanno, Mario Pagano, and Luigi Piegari. Experimental Performance of MPPT Algorithm for photovoltaic sources subject to inhomogeneous insolation. IEEE Transactions on Industrial Electronics, vol. 56, no. 11, November 2009.

[9] Ahmed K. Abdelsalam, Ahmed M. Massoud, Shehab Ahmed, and Prasad N. Enjeti. High-Performance Adaptive Perturb and Observe MPPT Technique for Photovoltaic-Based Microgrids. IEEE Transactions on Power Electronics, vol. 26, no. 4, April 2011.

[10] Dezso Sera, Remus Teodorescu, Jochen Hantschel, and Michael Knoll. Optimized Maximum Power Point Tracker for Fast-Changing Environmental Conditions. IEEE Transactions on Industrial Electronics, vol. 55, no. 7, July 2008.

[11] Rosa A. Mastromauro, Marco Liserre, and Antonio Dell'Aquila. Control Issues in Single-Stage Photovoltaic Systems: MPPT, Current and Voltage Control. IEEE Transactions on Industrial Informatics, vol. 8, no. 2, may 2012.

[12] Wu-Shun Jwo, Chia-Chang Tong, Chi-Jui Chao. Firmware Implementation of an Adaptive Solar Cell Maximum Power Point Tracking Based on PSOC. In: Proceedings of the IEEE photovoltaic Specialists conference; 2010. p. 000407–11.

[13] Dezso Sera, Laszlo Mathe, Tamas Kerekes, Sergiu Viorel Spataru, and Remus Teodorescu. On the Perturb-andObserve and Incremental Conductance MPPT Methods for PV Systems. IEEE Journal of Photovoltaics, vol. 3, no. 3, July 2013.

[14] Chian-Song Chiu. T-S Fuzzy Maximum Power Point Tracking Control of Solar Power Generation Systems. IEEE Transactions on Energy Conversion, vol. 25, no. 4, December 2010.

[15] S. Mishra, Senior and P. C. Sekhar. TS Fuzzy Based Adaptive Perturb algorithm for MPPT of a Grid Connected Single Stage Three Phase VSC Interfaced PV Generating System. In: Proceedings of the IEEE Power and energy Society General meeting; 2012. p. 1–7.

[16] Chian-Song Chiu, and Ya-Lun Ouyang. Robust Maximum Power Tracking Control of Uncertain Photovoltaic Systems: A Unified T-S Fuzzy Model-Based Approach. IEEE Transactions on Control Systems Technology, vol. 19, No. 6, November 2011.

[17] Ross J. Quinlan: Learning with Continuous Classes. In: 5th Australian Joint Conference on Artificial Intelligence, Singapore, 343-348, 1992.

[18] Y. Wang, I. H. Witten: Induction of model trees for predicting continuous classes. In: Poster papers of the 9th European Conference on Machine Learning, 1997.

[19] D. Malerba, F. Esposito, M. Ceci, A. Appice, Top-down induction of model trees with regression and splitting nodes, IEEE Transactions on Pattern Analysis and Machine Intelligence 26 (5) (2004) 612–625.

[20] Electrical energy storage: white paper. Technical report. Prepared by electrical energy storage project team. International Electrotechnical Commission (IEC), Published December 2011. <http://www.iec.ch/ whitepaper/pdf/iecWP-energystorage-LR-en.pdf> [accessed 15.05.14].

[21] Succar S, Williams RH. Compressed air energy storage: theory, resources, and applications for wind power. Princeton Environmental Institute. Energy Anal Group; 2008.

[22] Zhou L, Qi ZP. A review of flywheel energy storage system. Proceedings of ISES World Congress 2007 (Vol. I – Vol. V). Berlin, Heidelberg: Springer, Berlin Heidelberg; 2009. p. 2815–19.

[23] Chen H, Cong TN, Yang W, Tan C, Li Y, Ding Y. Progress in electrical energy storage system: a critical review. Prog Nat Sci 2009; 19:291–312.

[24] Earle Waghorne W. Viscosities of electrolyte solutions. Philos Trans Roy Soc A Math Phys Eng Sci 2001; 359:1529–43.

[25] Ryan Ahmed, Mohammed El Sayed, Ienkaran Arasaratnam, Jimi Tjong, and Saeid Habibi. Reduced-Order Electrochemical Model Parameters Identi cation and State of Charge Estimation for Healthy and Aged Li-Ion Batteries—Part II: Aged Battery Model and State of Charge Estimation. IEEE Journal of emerging and selected topics in power electronics, Vol. 2, No. 3, September 2014

[26] Ryan Ahmed, Mohammed El Sayed, Ienkaran Arasaratnam, Jimi Tjong, and Saeid Habibi. Reduced-Order Electrochemical Model Parameters Identi cation and SOC Estimation for Healthy and Aged Li-Ion Batteries Part I: Parameterization Model Development for Healthy Batteries. IEEE Journal of emerging and selected topics in power electronics, Vol. 2, No. 3, September 2014.

[27] Woosuk Sung, Chee Burm Shin. Electrochemical model of a lithium-ion battery implemented into an automotive battery management system. Computers and Chemical Engineering 76 (2015) 87–97.

[28] Jingzhi Xun, Rui Liu, Kui Jiao. Numerical and analytical modeling of lithium ion battery thermal behaviors with different cooling designs. Journal of Power Sources 233 (2013) 47-61.

[29] Ziyad M. Salameh Margaret A. Casacca William A. Lynch. A Mathematical Model for Lead-Acid Batteries. IEEE Transactions on Energy Conversion, Vol. 7, No.1, March 1992.

[30] J. B. Copetti, E. Lorenzo and F. Chenlo. A General Battery Model for PV System Simulation Progress in Photovoltaic: Research end Applications, Vol I, 283-292 (1993).

[31] J.B. Copetti and F. Chenlo. Lead/acid batteries for photovoltaic applications. Test results and modelling. Journal of Power Sources, 47 (1994) 109-118.

[32] D. Guasch and S. Silvestre. Dynamic Battery Model for Photovoltaic Applications. Progress in Photovoltaic: Research end Applications Prog. Photovolt: Res. Appl. 2003; 11:193–206 (DOI: 10.1002/pip.480).

[33] Rafael Illanes, Adolfo De Francisco, Francisco Núñez, Marian De Blas, Almudena García, José Luis Torres. Dynamic simulation and modelling of stand-alone PV systems by using state equations and numerical integration methods. Applied Energy, 135 (2014) 440–449.

[34] Wladislaw Waag, Dirk Uwe Sauer. Adaptive estimation of the electromotive force of the lithium-ion battery after current interruption for an accurate state-of-charge and capacity determination. Applied Energy 111 (2013) 416–427.

[35] Guangming Liu, Minggao Ouyang, Languang Lu, Jianqiu Li, Jianfeng Hua. A highly accurate predictive-adaptive method for lithium-ion battery remaining discharge energy prediction in electric vehicle applications. Applied Energy 149 (2015) 297–314.

[36] Robert L. Fares, Jeremy P. Meyers, Michael E. Webber. A dynamic model-based estimate of the value of a vanadium redox ow battery for frequency regulation in Texas. Applied Energy 113 (2014) 189–198.

[37] Massimo Ceraolo. New Dynamical Models of Lead–Acid Batteries. IEEE Transactions on power systems, Vol. 15, NO. 4, Novenber 2000.

[38] Stefano Barsali and Massimo Ceraolo. Dynamical Models of Lead-Acid Batteries: Implementation Issues. IEEE Transactions on energy conversion, Val. 17, NO. 1, March 2002.

[39] Wenhua H. Zhu, Ying Zhu, Bruce J. Tatarchuk. A simpli ed equivalent circuit model for simulation of Pb–acid batteries at load for energy storage application. Energy Conversion and Management 52 (2011) 2794–2799.

[40] Emmanuel Karlo Nyarko, Rudolf Scitovski. Solving the parameter identi cation problem of mathematical models using genetic algorithms. Applied Mathematics and Computation 153 (2004) 651–658.

[41] B.P.F. William H. Press, Saul A. Teukolsky, William T. Vetterling,, Numerical Recipes in Fortran 77, CAMBRIGE.

[42] Kannan Thirugnanam, Ezhil Reena Joy T. P, Mukesh Singh, and Praveen Kumar. Mathematical Modeling of Li-Ion Battery Using Genetic Algorithm Approach for V2G Applications. IEEE TRANSACTIONS ON ENERGY CONVERSION, VOL. 29, NO. 2, JUNE 2014.

[43] Fardin Ahmadizar, Khabat Soltanian, Fardin AkhlaghianTab, Ioannis Tsoulos. Arti cial neural network development by means of a novel combination of grammatical evolution and genetic algorithm. Engineering Applications of Arti cial Intelligence 39 (2015) 1–13.

[44] Jingang Guo, Junping Wang and Binggang Cao. Application of Genetic Algorithm for Braking Force Distribution of Electric Vehicles. 978-1-4244-2800-7/09/$25.00 ©2009 IEEE.

[45]A .L.S. Chan. Generation of typical meteorological years using genetic algorithm for different energy systems. Renewable Energy 90 (2016) 1-13.

[46] Abele A, Elkind E, Intrator J, Washom B, et al. 2020 Strategic Analysis of Energy Storage in California. University of California, Berkeley School of Law; University of California, Los Angeles; and University of California, San Diego. California Energy Commission; 2011.

[47] Energy storage – packing some power. The Economist. Published 3rd March 2012. <http://www.economist.com/node/21548495> [accessed 08.06.14].

[48] Compressed Air Energy Storage < http://www.thegreenage.co.uk/tech/compressed-air-energy-storage/ >.

[49] Raju M, Kumar Khaitan S. Modeling and simulation of compressed air storage in caverns: a case study of the Huntorf plant. Appl Energy 2012; 89: 474–81.

[50] Finkenrath M, Pazzi S, D'Ercole M. Status and technical challenges of advanced Compressed Air Energy Storage (CAES) technology. In: Int. workshop on environment and alternative energy; 2009.

[51] Pena-Alzola R, Sebastian R, Quesada J, Colmenar A. Review of flywheel based energy storage systems. In: 2011 Int. Conf. Power Eng. Energy Electr. Drives, IEEE; 2011. p. 1–6.

[52] Lin FC, Dai X, Xu ZA, Li J, Zhao ZG. High density capacitors. High Power Laser Part Beams 2003; 1: 94–6.

[53] Capacitors age and capacitors have an end of life: a white paper from the experts in business-critical continuity. Emerson network power. n.d. <http:// www.emersonnetworkpower.com/documentation/en-us/brands/liebert/ documents/white%20papers/sl-24630.pdf> [accessed 27.05.14].

[54] AEA Technology plc. Energy storage and management study. Scottish Government. Published 2nd October 2010. <http://www.scotland.gov.uk/ Publications/2010/10/28091356/0> [accessed 11.06.14].

[55] Ali MH, Dougal RA. An overview of SMES applications in power and energy Systems. IEEE Trans Sust Energy 2010;1:38–47.

[56] Taylor P, Bolton R, Stone D, Zhang XP, Martin C, Upham P, et al. Pathways for energy storage in the UK. Technical report. Centre for low carbon futures. Published 27th March 2012. <http://www.lowcarbonfutures.org/reports/ research-reports?page=1>. [accessed 11.06.14].

[57] Díaz-González F, Sumper A, Gomis-Bellmunt O, Villafáfila-Robles R. A review of energy storage technologies for wind power applications. Renew Sust Energy Rev 2012;16:2154–71.

[58] Battery Reference Book. British Library Cataloguing in Publication Data a catalogue record for this book is available from the British Library. ISBN 07506 4625 X.

[59] Xing Luo, Jihong Wang, Mark Dooner, Jonathan Clarke. Overview of current development in electrical energy storage technologies and the application potential in power system operation. Applied Energy 137 (2015) 511–536.

[60] Shen Guo. The Application of Genetic Algorithms to Parameter Estimation in Lead-Acid Battery Equivalent Circuit Models. Thesis submitted in accordance with the requirements of the University of Birmingham for the degree of Master of Philosophy.

[61] A.M.Humada, M. Hojabri, S. Mekhilef, H.M.Hamada, "Solar cell parameters extraction based on single and double-diode models: A review" Renewable and Sustainable Energy Reviews, vol.56, pp.494–509, 2016.

[62] T.O. Paine, Maximum Power Point Tracker, National Aeronautics and Space Administration, NASA, Patent US3, 566, 143, 1969.

[63] Luis Castaner and Santiago Silvestre. Modelling Photovoltaic Systems using PSpice. John Wiley & Sons, Ltd. ISBN: 0-470-84527-9.

[64] W. Merrouch. Développement d'un régulateur intelligent pour un système PV de faible puissance. Magistral Thesis, Algerie, 2011.

[65] S. Blaifi, S. Moulahoum, I. Colak, W. Merrouche. An enhanced dynamic model of battery using genetic algorithm suitable for photovoltaic applications. Applied Energy 169 (2016) 888–898.

[66] S. Blaifi, S. Moulahoum, N. Kabache, I. Colak. An Improved dynamic battery model suitable for photovoltaic applications. 4th Interntional Conference on Renewable Energy Research and Applications Palenno, Italy, 22-25 Nov 2015.

[67] chen shi, guanghui teng, zhuo li. an approach of pig weight estimation using binocular stereo system based on labview. Computers and electronics in agriculture volume 129, 1 november 2016, pages 37–43.

[68] Copetti JB, Chenlo F, Lorenzo E. Comparison between charge and discharge models and real data for PV applications. Proceedings of the 11th European PV Solar Energy Conference, Montreux, 12–16 October 1992; 1131–1134.

[69] Gergaud GRO, Multon B, Ben Ahmed H. Energy modeling of a lead–acid battery within hybrid wind/ photovoltaic systems. EPE 2003 – Toulouse; 2003.

[70] Algorithme de Levenberg-Marquardt. - Wikipédia. <https://fr.wikipedia.org/wiki/Algorithme_de_Levenberg-Marquardt >.

[71] R. Boukenoui, H. Salhi, R. Bradai, A. Mellit. A new intelligent MPPT method for stand-alone photovoltaic systems operating under fast transient variations of shading patterns. Solar Energy 124 (2016) 124–142.

[72] I. H. Witten and E. Frank, Data Mining: Practical Machine Learning Tools and Techniques: Morgan Kaufmann, 2000.

[73] Sayad, S. (2011). Real time data mining. Canada: Self-Help Publishers.

[74] Breiman, L., J. H. Friedman, J. H. Olshen, C. I. Stone. 1984. Classifi- cation and Regression Trees, Wadsworth, Belmont, California.

[75] Pang-Ning Tan (Auteur), Michael Steinbach (Auteur), Vipin Kumar (Auteur). Introduction to Data Mining. 2 Mai 2005.

[76]http://www.alldatasheet.com/view.jsp?Searchword=Acs712%20datasheet&gclid=EAIaIQobChMIwIilr4b60wIVxJ8bCh2jggPmEAAYASAAEgJBPvD_BwE.

[77]http://www.alldatasheet.com/view.jsp?Searchword=Lv25p&gclid=EAIaIQobChMIoerMwIf60wIVEY0bCh2tRg6mEAAYASAAEgLLHfD_BwE.

[78] http://www.alldatasheet.com/view.jsp?Searchword=Lm335

[79] http://sine.ni.com/psp/app/doc/p/id/psp-117/lang/en

PUBLICATIONS AND CONFERENCES

1- **S. Blaifi**, S. Moulahoum, I. Colak, W. Merrouche. An enhanced dynamic model of battery using genetic algorithm suitable for photovoltaic applications. Applied Energy 169 (2016) 888–898.

Abstract— Modeling of batteries in photovoltaic systems has been a major issue related to the random dynamic regime imposed by the changes of solar irradiation and ambient temperature added to the complexity of battery electrochemical and electrical behaviors. However, various approaches have been proposed to model the battery behavior by predicting from detailed electrochemical, electrical or analytical models to high-level stochastic models. In this paper, an improvement of dynamic electrical battery model is proposed by automatic parameter extraction using genetic algorithm in order to give usefulness and future implementation for practical application. It is highlighted that the enhancement of 21 values of the parameters of CIEMAT model presents a good agreement with real measurements for different modes like charge or discharge and various conditions.

2- **S. Blaifi**, S. Moulahoum, I. Colak, W. Merrouche. Monitoring and enhanced dynamic modeling of battery by genetic algorithm using LabVIEW applied in photovoltaic system. Electrical Engineering Springer. DOI 10.1007/s00202-017-0567-6.

Abstract— the dynamic modeling of batteries used in photovoltaic systems (PVS), exceptionally in stand-alone or micro-grid systems, is considered as an important issue and a major problem for the monitoring and simulation and even for fault detection applications. In this work, we propose as first step an enhancement of CIEMAT model by the improvement of 21 charge and discharge parameters; also we propose an enhancement of 4 parameters for the estimation approximately of the gassing and the saturation levels by a new static method using genetic algorithm. Basically, this method relies on static measurements by charging of the battery with different constant currents to give a more accurate estimation of this area. Furthermore, a real-time interface system using LabVIEW using the improved model was proposed in this work to provide online estimation and measurements of all battery data and characteristics in PVS. The proposed robust and low-cost method of simulation and monitoring can be applied for the study of battery fault detection in PVS.

3- **S. Blaifi**, S. Moulahoum, N. Kabache, I. Colak. An Improved dynamic battery model suitable for photovoltaic applications. 4th International Conference on Renewable Energy Research and Applications Palermo, Italy, 22-25 Nov 2015.

Abstract— Modeling of batteries used in photovoltaic applications has been a real issue for many research groups due to its complex electrochemical and electrical behavior. In this paper, we propose an improvement of the battery model by identification of all parameters in order to estimate the different areas of Battery's output voltage in real conditions for PV systems. For this purpose, we also performed both static and dynamic simulation. Comparison with real measurement has shown good agreement with the simulation.

4- W. Merrouche, D. Ghribi, L. Djellal, M. Trari, **S. Blaifi**, I. Gaci. " Comparison between two Accelerated Test Procedures on Batteries Suitable for Photovoltaic Applications**",** EU PVSEC 2015, du 14 au 18 Septembre 2015, Hamburg, Allemagne.

Abstract— In Photovoltaic Systems PVS, Depending on application and battery quality, Lead-Acid Batteries lifetimes vary from 2 to 15 years. To test this lifetime, the users will not wait 3 years or more to know the real battery lifetime. For this reason, an accelerated test procedure is required to minimize testing time. This paper presents results of two test procedures experienced at the CDER battery test Bench. The first procedure is based on the regulation mode adopted on PVS but at high thresholds to accelerate battery aging. The second procedure takes into account the variation of battery Charge/Discharge rate to reproduce the real